VTT PUBLICATIONS 721

Aku Itälä

Chemical Evolution of Bentonite Buffer in a Final Repository of Spent Nuclear Fuel During the Thermal Phase

VTT PUBLICATIONS 721

Chemical Evolution of Bentonite Buffer in a Final Repository of Spent Nuclear Fuel during the Thermal Phase

Aku Itälä

ISBN 978-951-38-7363-9 (soft back ed.)
ISSN 1235-0621 (soft back ed.)

ISBN 978-951-38-7364-6 (URL: http://www.vtt.fi/publications/index.jsp)
ISSN 1455-0849 (URL: http://www.vtt.fi/publications/index.jsp)

JULKAISIJA – UTGIVARE – PUBLISHER

VTT, Vuorimiehentie 3, PL 1000, 02044 VTT
puh. vaihde 020 722 111, faksi 020 722 4374

VTT, Bergsmansvägen 3, PB 1000, 02044 VTT
tel. växel 020 722 111, fax 020 722 4374

VTT Technical Research Centre of Finland, Vuorimiehentie 3, P. O. Box 1000, FI-02044 VTT, Finland
phone internat. +358 20 722 111, fax + 358 20 722 4374

Technical editing Mirjami Pullinen
Cover picture SKB, Svensk Kärnbränslehantering AB

Edita Prima Oy, Helsinki 2009

Aku Itälä. Chemical Evolution of Bentonite Buffer in a Final Repository of Spent Nuclear Fuel During the Thermal Phase [Bentoniittipuskurin kemiallinen evoluutio käytetyn ydinjätteen loppusijoitustilassa termisen vaiheen aikana]. Espoo 2009. VTT Publications 721. 78 p. + app. 16 p.

Keywords THC, temperature dependence, modelling, cation exchange, heat formation, heat transport, bentonite, porewater, montmorillonite

Abstract

Finnish spent nuclear fuel disposal is planned to be based on the KBS-3V concept. Within this concept, the role of the bentonite buffer has been considered to be central. The aim was to model the evolution of a final repository during the thermal phase (heat-generating period of spent fuel), when the bentonite is partially saturated at the beginning, and the rock matrix surrounding it is fully saturated. It is essential to study how temperature affects saturation and how both of these affect the chemistry of bentonite.

In order to make the modelling more concrete, an experimental case was adopted: the Long Term Test of Buffer Materials (LOT) A2-parcel test at the Äspö Hard Rock Laboratory (HRL) in Sweden. In the A2-parcel the MX-80 bentonite was exposed to adverse (120–150^{o}C) temperature conditions and high-temperature gradients. The test parcel diameter was smaller than in the KBS-3V concept to speed up the saturation. Different kinds of thermodynamic and kinetic properties of minerals cause a redistribution of phases inside the bentonite. For example, according to laboratory tests, gypsum seems to dissolve and anhydrite seems to precipitate near the heater-bentonite interface. Also incoming groundwater affects the bentonite porewater and its properties. These changes may affect the mechanical properties of bentonite and it has to be clarified if these phenomena have to be taken into account in safety assessment.

The applied model is a coupled thermo-hydro-chemical model, which means that all the mechanical alterations and effects are not considered. The purpose of the model was first to obtain similarity to the results compared to the experiment, and thus, the time frame was limited to 10 years (the LOT A-2 parcel test lasted approximately 6 years). The system is simplified to 1-D in order to reduce the computational work, which is significant mostly due to complex chemical calculations. TOUGH and TOUGHREACT was applied to model the reactive unsaturated transport processes in 1-D and the grid was pitched at uniform intervals. The results may be used to gain knowledge of the bentonite evolution during the thermal phase, and after a good match with experiment the modelling can be continued until the end of the thermal phase for thousands of years.

Aku Itälä. Chemical Evolution of Bentonite Buffer in a Final Repository of Spent Nuclear Fuel During the Thermal Phase [Bentoniittipuskurin kemiallinen evoluutio käytetyn ydinjätteen loppusijoitustilassa termisen vaiheen aikana]. Espoo 2009. VTT Publications 721. 78 s. + liitt. 16 s.

Avainsanat THC, temperature dependence, modelling, cation exchange, heat formation, heat transport, bentonite, porewater, montmorillonite

Tiivistelmä

Monet maat Euroopassa, Suomi mukaan lukien, suunnittelevat bentoniitin käyttämistä puskurimateriaalina korkea-aktiivisten ydinjätteiden loppusijoitustilassa. Suomalaisen käytetyn polttoaineen loppusijoituksen on suunniteltu perustuvan KBS-3V-konseptiin. Tässä konseptissa bentoniittipuskurin rooli on keskeinen. Tämän työn tarkoituksena oli mallintaa loppusijoitustilaa termisen vaiheen aikana (polttaineen lämpöä tuottava ajanjakso), jolloin bentoniitti on aluksi osittain kyllästynyt ja kallio sen ympärillä täysin kyllästynyt. On tärkeää tutkia, miten termiset, hydrologiset, mekaaniset ja kemialliset ilmiöt ja prosessit loppusijoitustilassa voivat muokata bentoniitin kemiallisia ja mekaanisia ominaisuuksia. Bentoniitin pitkäaikaiskestävyyden tutkiminen perustuu mallinnukseen, koska kokeellinen tutkimus veisi tuhansia vuosia.

Jotta mallinnuksesta saatiin luotettavampaa, käytettiin vertailupohjana LOT-koetta. Äspön kalliolaboratoriossa Ruotsissa on menossa pitkäaikainen puskurimateriaalin testaus, niin sanottu LOT-koe korkea-aktiivisen ydinjätteen loppusijoitusta varten. Tässä työssä keskitytään yhteen näistä kokeen osista, A2-sylinterikokeeseen. A2-kokeessa suhteellisen pienet testisylinterit altistetaan kohonneelle lämpötilalle. Suunniteltu maksimilämpötila loppusijoitustilassa on 90 ^{o}C, mutta A2-kokeessa se asetettiin 120–150 asteeseen. Noin 5–6 vuoden altistamisen jälkeen testisylinteri nostettiin ja paloiteltiin osiin tutkimuksia varten. Viiden vuoden jakso näissä olosuhteissa kattaa merkittävän osan koko termisestä kuormasta KBS-3V-loppusijoitustilassa.

Malli luotiin käyttämällä PetraSim 4.1.0219 -käyttöliittymää TOUGH2- ja TOUGHREACT-ohjelmille. Sovellettu malli on termo-hydro-kemiallinen (THC) kytketty malli, mikä tarkoittaa sitä, että useat mekaaniset muutokset ja vaikutukset on jätetty huomiotta. Mallin tarkoituksena oli saada aluksi tulokset vastaamaan suhteellisen hyvin kokeellisia tuloksia, joten laskenta-aika rajoitettiin kymmeneen vuoteen. Malli on yksidimensioinen.

Preface

The research work for this thesis was carried out during the period from May 2008 to August 2009 in the Nuclear Waste Management team at the Technical Research Centre of Finland (VTT). I would like to thank my project manager and team leader Kari Rasilainen for the opportunity to work with such a great team.

I would like to express my gratitude to my mentor, Dr. Markus Olin, who has been advising me during this thesis year, Dr. Arto Muurinen for his help with the data and modelling subject and Dr. Kari Rasilainen for the comments on my work. Also my co-workers Ms. Merja-Tanhua Tyrkkö and Mr. Veli-Matti Pulkkanen have been of great help together with M.Sc. (Eng.) Jarmo Lehikoinen from B+Tech.

I would like to thank Patrick Sellin of SKB (Svensk Kärnbränslehantering AB) for allowing me to use the experimental data obtained within the LOT project taking place at the Äspö Hard Rock Laboratory in Sweden.

Thanks to the head of the Laboratory of Chemistry at Tampere University of Technology Prof. Helge Lemmetyinen for being my examiner and for the constructive comments on my work.

I also like to thank my parents for financial and other support, and thanks to my family and friends for being there for me.

This thesis was jointly financed by the Finnish Research Programme on Nuclear Waste Management (KYT) and by VTT.

Helsinki, August 21, 2009

Aku Itälä

Contents

List of symbols

Symbols

c	Concentration [mol/kg]
G	Water/air accumulation term [kg/m^3]
P	Pressure
Q	Water source/sink term
S	Saturation
$\vec{f}$	Water/air mass flux [kgm^{-2}s^{-1}]
k_H	Henry's constant
ϕ	Porosity of a material ($0 < \phi < 1$)
Ω	Arbitrary domain
$\partial\Omega$	Closed surface
$\vec{n}$	Normal vector
$\vec{f}$	Water mass flux [kg·m^{-2}s^{-1}]
X	Mass fraction
$\vec{u}$	Darcy velocity or flow rate of water
$\mathbf{K}$	Hydraulic conductivity tensor [m/s]
$\vec{v}$	Average water velocity
h	Hydraulic head [m]
$\boldsymbol{\kappa}$	Intrinsic permeability tensor
$\mathbf{K}$	Hydraulic conductivity
$\vec{g}$	Vector of gravitational acceleration
κ	Intrinsic permeability [m^2]
μ	Dynamic viscosity [Pa·s]

θ_w	Moisture content
κ_r	Relative permeability
$\boldsymbol{\kappa_a}$	Absolute permeability tensor
λ	Van Genuchten model parameter called pore-size distribution index
S_l	Liquid saturation degree
S_{ls}	Saturation in fully saturated state
S^*	Dimensionless water content
S_{lr}	Liquid residual saturation
z	Depth [m]
ρ	Density [kg/m^3]
g	Gravitational acceleration [m/s^2]
C^i	Accumulation term for chemical components (concentration)
$\overrightarrow{b^i}$	Mass flux for chemical components
s^i	Sink or Source term for chemical components
D_i	Effective diffusion coefficient [m^2/s]
τ	Tortuosity
d	Diffusion coefficient in water
R	Molar gas constant
T	Temperature
N_A	Avogadro's number
d_m	Molecular diameter
M	Molecular weight
k	Coefficient of thermal conductivity
k_H	Henry's constant
C	Specific heat capacity
e	Energy density or energy accumulation term
$\vec{q}$	Heat component or heat flux [Jm^{-2}s^{-1}]
q	General source/sink term
H	Heat source term
u	Specific internal energy
J	Advective flux
g	Diffusive flux

f	Total diffusive flux
G_m	Volume normalized extensive quantity
A	Area
L	Chemical species index
N_C	Total number of primary species
N_R	Number of reactions
ν	Stoichiometric coefficient
γ	Activity coefficient
a	Activity
m	Molal concentration/molality
I	Ionic strength
ω	Born coefficient
η	1.66027 Åcal/mol
$r_{e,j}$	Effective radius of the ion
z_i	Electrical charge of species i
K	Equilibrium constant
k_n	Rate constant
A_n	Specific reactive surface area
Ω_n	Kinetic mineral saturation ratio
E_a	Activation energy
Γ	Gas fugacity
B	Dissolved cationic species
X_ν	Exchange site
w	Activity of the exchanged species
β	Equivalent fraction
d_w	Free water diffusivity

Subscripts

a	Air
β	Phase (liquid, gaseous)
c	Capillary
f	Gas index

g	Gaseous/gas
l	Liquid
R	Rock
r	Reference
v	Vapour
w	Water

Abbreviations

CEC	Cation Exchange Capacity
HRL	Hard Rock Laboratory
IFDM	Integral Finite Difference Method
LOT	Long term buffer Test
THC	Thermal-Hydraulic-Chemical
THCM	Thermal-Hydraulic-Chemical-Mechanical
TOT	Tetrahedral-Octahedral-Tetrahedral
VTT	Technical Research Centre of Finland

1. Introduction

Many countries in Europe including Finland are planning to use bentonite as a buffer material around waste canisters in a high-level radioactive waste disposal, whereupon saturation with groundwater, the bentonite swells thus isolating the canisters from flowing groundwater. However, thermal, hydrological, mechanical and chemical phenomena and processes taking place in the bentonite buffer may change the mechanical and chemical properties of the bentonite. Determination of the long-term stability of bentonite in final repository conditions must be based on modelling, as experimental testing would require millennia to implement. In addition, the disposal system can be studied experimentally only on a subsystem level. This thesis concentrates on modelling the temperature effects on the bentonite buffer in a spent nuclear fuel repository during the thermal phase. However, the complexity of nature and the demands on computing power preclude models that include all the processes. Therefore, we are forced to consider only simplified models of the final repository.

In order to make the modelling more concrete, we use experimental reference, data obtained in the Long-term buffer test (LOT) at the Äspö Hard Rock Laboratory (HRL) in Sweden. The long-term buffer test A-2 lasted approximately five years. The installation was started on October 29, 1999 and the uncovering of rock was started on January 17, 2006. [17]

Differences in thermodynamic properties of minerals cause a redistribution of minerals within the bentonite. For example, laboratory tests indicate gypsum dissolution and anhydrite precipitation near the heater-bentonite interface. Incoming groundwater will also affect the bentonite porewater. As these changes may affect the properties of bentonite, it must be determined whether these phenomena are to be taken into account in the safety assessment of the repository.

The first aim of this thesis was to investigate the thermal phase (heat-generating period of spent fuel) of the final repository and the coupled thermal-

hydraulic-chemical (THC) phenomena affecting the bentonite. The thermal phase will last a few thousand years but most of the phenomena are assumed to occur during the first thousand years [26]. Proper knowledge of the bentonite behaviour during and after the thermal phase is crucial in estimating the long-term safety of a nuclear waste repository. It is important to know how the bentonite is going to function as a buffer and whether it will maintain its properties during the thermal phase, when the bentonite is initially only partially saturated. The phenomena affecting bentonite are viewed and compared to the LOT test case. During first hundred years there is a high temperature gradient in the bentonite. This gradient originates from the high activity nuclear waste. In the A2 test case there are more adverse conditions compared to the final repository site to accelerate the reactions and to compare the thermal load of the A2 test to the KBS-3V concept conditions during thousands of years.

The second aim of the thesis was to improve the modelling capabilities at VTT to understand the bentonite evolution problem and to create a model that could be further employed to model the evolution of the final repository being planned at Olkiluoto.

This thesis is organized in the following way: Chapter 2 introduces the goals of this work. Chapter 3 presents the characteristics of the material and transport phenomena. Chapter 4 describes the experiment. Chapter 5 explains the modelling concept and its limitations. Chapter 6 presents the results. The discussion and conclusions are presented in Chapters 7 and 8.

2. Characterization, chemistry and transport phenomena of bentonite

This chapter describes the materials in question and their phenomena, the calculation methods needed to construct a model with PetraSim, and the methods the program uses to calculate the chemical and physical phenomena.

To understand how PetraSim calculates the solutions, one has to understand the theory behind TOUGH2 and TOUGHREACT and what methods and equations these programs use to solve the problems with partially saturated and saturated porous materials. Thus, understanding the material structure and behaviour is the starting point.

2.1 Materials and phenomena

2.1.1 Bentonite

Research has indicated sodium bentonite to currently be the most viable material for the isolation of radioactive materials owing to its multiple beneficial characteristics [42]:

1. In case of canister failure, the migration of the majority of contaminants (radionuclides) is retarded considerably via sorption to the reactive clay surfaces.
2. Bentonite's ability to swell makes it an efficient barrier against the migration of corroding agents.
3. Bentonite constitutes a mechanical and chemical zone of protection around the canister.
4. Bentonite has a high thermal conductivity, thus serving to efficiently dissipate heat emitted by the waste.

Bentonites (montmorillonite clays) differ by mineralogical composition. The type chosen for final repository planning, MX-80, is extracted for example from Wyoming (USA) and is a commercial material supplied in powder form.

The MX-80 material consists mainly of sodium montmorillonite clay with small amounts of quartz, tridymite, cristobalite, feldspars, muscovite/illite, sulphides and other trace minerals. The mean mineralogical composition of the montmorillonite part is given by

$(Si_{7.92}\,Al_{0.08})(Al_{3.10}Fe^{3+}_{0.4}Fe^{2+}_{0.02}Mg_{0.48})O_{20}(OH)_4\;Na_{0.48}Ca_{0.04}Mg_{0.02}$ [17].

2.1.2 Montmorillonite

Montmorillonite is the main mineral in bentonite structure from 65 to 90%. The properties of bentonite are mainly determined by this clay mineral (see for example [13]). There are many opinions concerning the structure of montmorillonite but the most often used concept is that montmorillonite has a 2:1 layer structure and is formed of an alumina octahedral sheet between two silica tetrahedral sheets [29]. Some of these cations have been replaced by other cations with lesser charge ($Al^{3+} \rightarrow Mg^{2+}$ and $Si^{4+} \rightarrow Al^{3+}$), which causes a negative charge in the montmorillonite layer [8]. Figures 2.1 and 2.2 illustrate the tetrahedral-octahedral-tetrahedral (TOT) layers showing how they combine together to form platelets. These platelets are only a few individual montmorillonite layers thick and bigger clay particles are composed of platelets stacks (3–5 in Na-montmorillonite to 10–20 for a Ca-montmorillonite) [29].

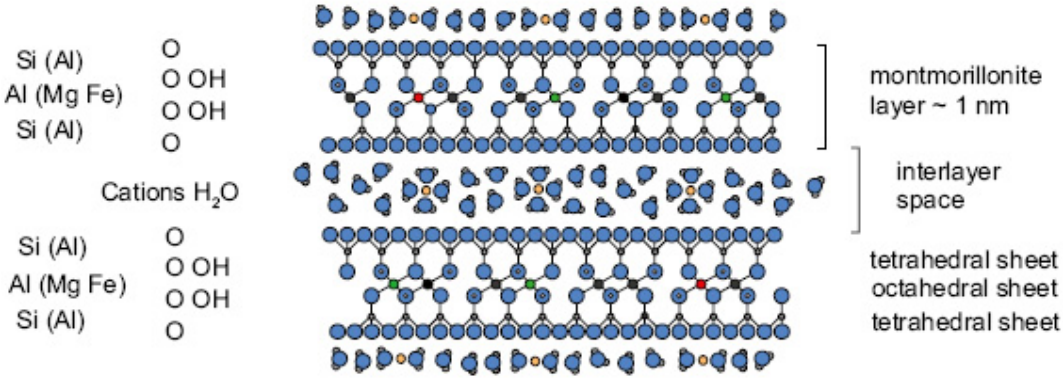

Figure 2.1. A Schematic view of two montmorillonite layers with interlayer cations and water molecules [16].

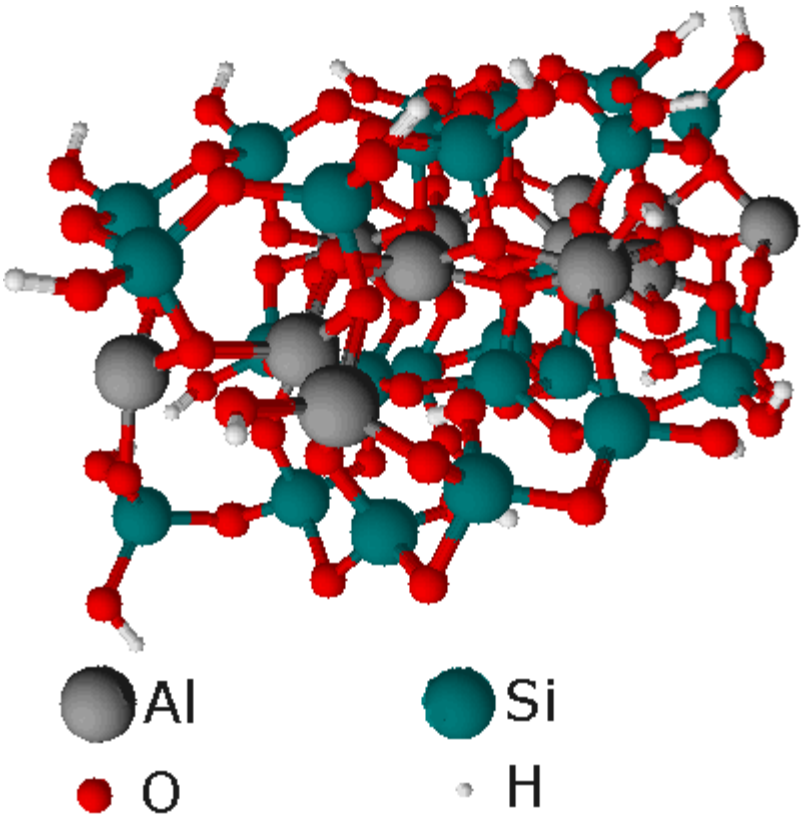

Figure 2.2. A 3-D picture from the TOT layer in montmorillonite.

As stated above, the montmorillonite clay platelet surface carries a permanent negative charge, which is due to substitution of the lattice cation by other cations of lower valency. Compensating cations reside mainly within the area of the interlayer space (see Figure 2.1). These electrostatically bound cations constitute the electrical double layer and can undergo a stoichiometric exchange with the cations in the solution [29, 41]. The cation-exchange capacity (CEC) is the total amount of permanent negative charge. The exchange capacity of montmorillonite is approximately 1 Eq/kg and about 75% of bentonite is montmorillonite, which makes the exchange capacity significant. [29]

In bentonite there is a large amount of montmorillonite and only a little volume of porewater. Thus, the ion-exchange capacity of solids is greater than those in the aqueous phase. The CEC acts as a powerful buffer for the composition of the porewater and thus the montmorillonite determines the porewater components. [8]

Montmorillonite in bentonite can act as an ion exchanger when this solid is in contact with a solution, like water. This process can also occur in other phases such as the solid phase. Real systems can contain many counter-ions in high concentration and many ion exchangers which can all change ions. There can also be other reactions and precipitations with these components. [33]

There is also a second category of reactive sites related to montmorillonite. These are called surface hydroxyl groups (= SOH) and they are located along the edges of the TOT clay platelets (see Figure 3.1) [7]. These sites have only a capacity of about 10% of the CEC and they can protonate and deprotonate as a function of pH, which means that the hydroxyl groups can function as a powerful pH buffer [8].

2.1.3 Bentonite swelling

When bentonite is in contact with water the bentonite swells. Swelling can occur through two processes. The first is the re-hydration of the interlayer cations, which is the main mechanism at close range separation of the montmorillonite layers. Then, after there is enough (3–4) monolayer water between the unit layers of montmorillonite, the hydration effect becomes less important than the electrical double layer repulsion. Swelling pressures in re-hydration can be a thousand bars and in repulsion several tens of bars [8, 41].

When bentonite takes up water and swells it seals the copper canister tightly from the rock matrix and buffers mechanically the canister against the effects of rock movements. Swelling occurs in the vertical direction, according to Figure 3.4. During re-saturation the porosity of the bentonite gets smaller which means that the water monolayers occupy the space that was full of air before [8].

2.1.4 Waters in bentonite

It is a common consensus that there are three different kinds of water inside bentonite. The first is the re-saturation internal water, which resides in the interlayer space between the individual TOT montmorillonite units “interlayer water” (see for example Figures 2.3, 2.4 or [27]). Because of its structured nature it probably has different properties from free water. The second can be called “external water” and can be categorized into two groups. The first can be in the electrical double layers that reside in the external surfaces of the clay stacks called “double layer water”. If the stack surfaces are close together the double layers will over-

lap and they will break and external surface spacing will be of the same order as the TOT layers. The second is the “free water”, which can be on the outside of the clay stacks or as films surrounding the other mineral grains in the bentonite. In this thesis the bentonite porewater refers to this free water. [8] Figure 2.3 illustrates the different kinds of water in bentonite, and comparison with Figure 2.1 shows the similarity.

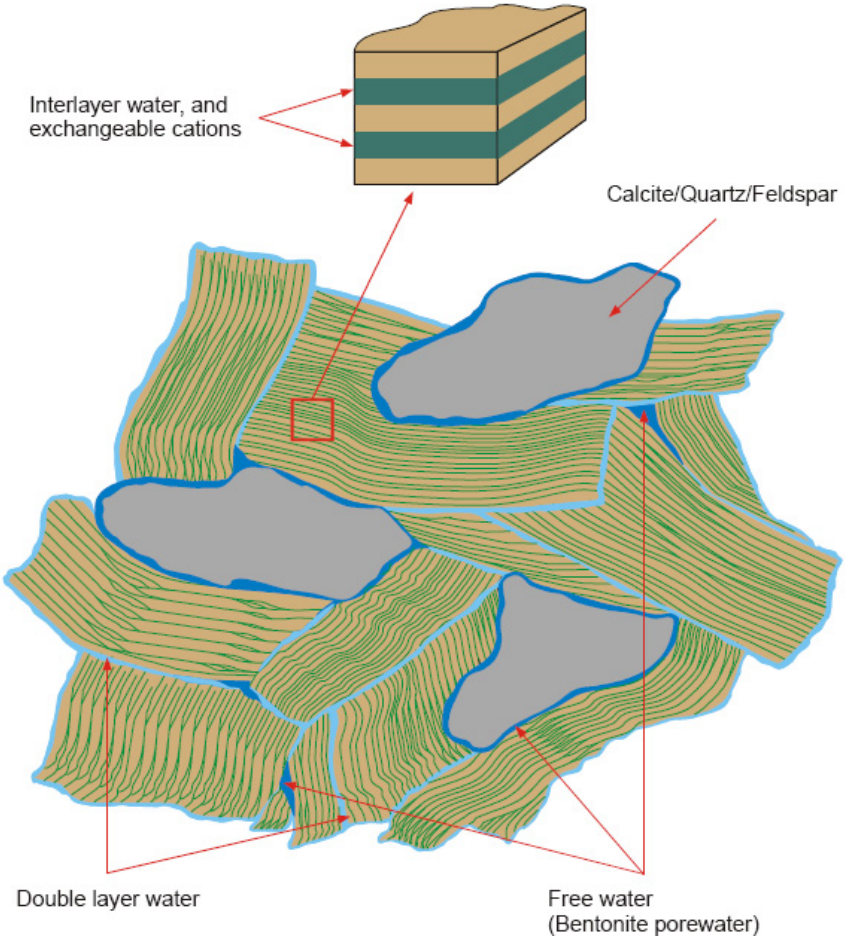

Figure 2.3. A schematic picture of the three waters inside bentonite [8].

2.1.5 Phenomena in bentonite

As discussed in the previous section, bentonite interacts with porewater and groundwater which consist of water flowing along water-carrying fractures and of non-flowing stagnant water in the rock matrix pores. The main mineral interacting with the groundwater is montmorillonite which, with other minerals, defines the composition of the porewater. In the experiment montmorillonite interacts with the free porewater with two reactions, cation exchange and surface site exchange. Figure 2.4 shows how the minerals of the bentonite, groundwater and bentonite interact with each other in one realistic system.

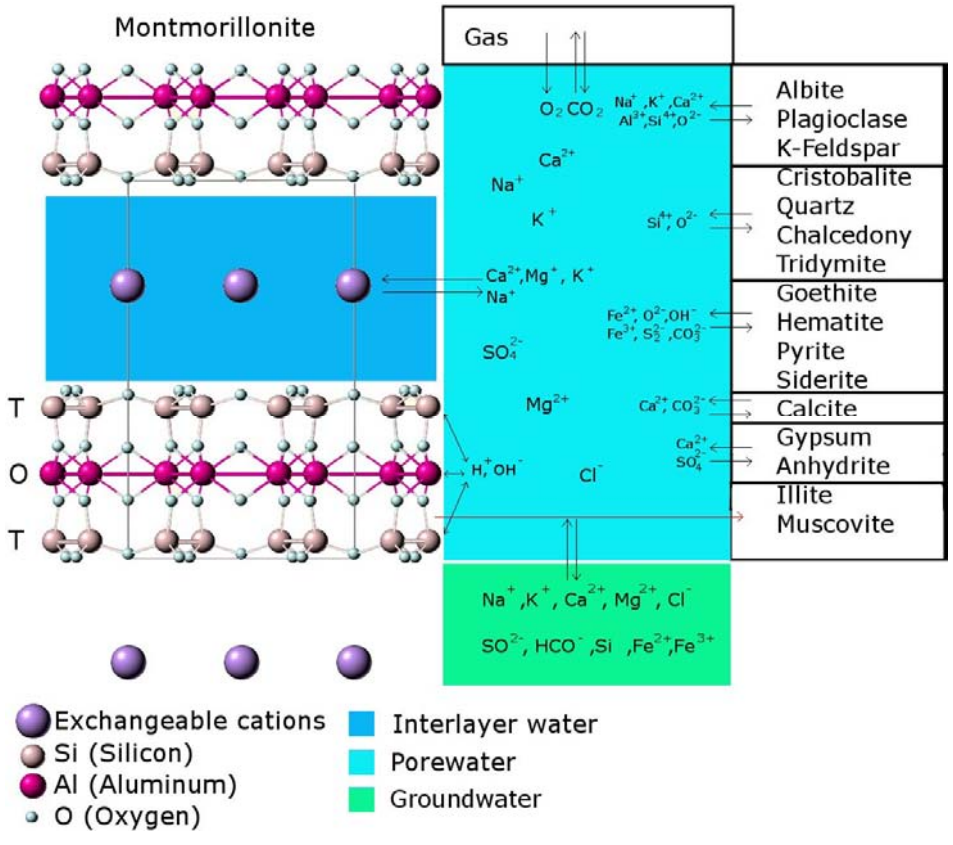

Figure 2.4. Schematic illustration of geochemical equilibrium processes in bentonite-water system in a final repository.

2.2 Flow of water

TOUGH2 implements the assumption that locally all phases are in thermodynamic equilibrium. Deriving the equations in TOUGH2 and TOUGHREACT is done in general for any liquid or gaseous phase, but in this work the fluids in question are water and air. Normally both have to be taken into account, but TOUGHREACT may simplify the calculations and assume gaseous water as a passive bystander.

The basis for all the calculations in TOUGH2 in general form is the basic mass balance equation, which in an unsaturated porous medium for water can be written in the form [28]:

$$\frac{d}{dt}\int_{\Omega} G_w \, dV = -\int_{\partial\Omega} \overrightarrow{f} \cdot \vec{n} \, dS + \int_{\Omega} Q \, dV \tag{1}$$

where G_w is the water accumulation term (mass per volume), and ϕ is the porosity of material. The integral is over an arbitrary domain Ω in the water flow system, $\overrightarrow{f}$ is mass flux and Q is a sink or source term. The system is surrounded by a closed surface $\partial\Omega$. $\vec{n}$ is a normal vector on boundary $\partial\Omega$ pointing outward from Ω. The water accumulation term G_w in general form is:

$$G_w = \phi S_l \rho_l X_{wl} + \phi S_g \rho_g X_{wg} \tag{2}$$

where X_{wl} and X_{wg} are mass fractions of liquid and gaseous phases from total water, S_l and S_g are the liquid and gaseous phase saturations, ρ_l and ρ_g are respectively liquid and gaseous phase densities, and ϕ is porosity.

Mass flux $\overrightarrow{f}$ can be written as:

$$\overrightarrow{f} = X_{wg}\overrightarrow{f_l} + X_{wg}\overrightarrow{f_g} \tag{3}$$

$\overrightarrow{f_l}$ and $\overrightarrow{f_g}$ are uniform and for example $\overrightarrow{f_l}$ can be written as:

$$\overrightarrow{f_l} = \rho_l \overrightarrow{u_l} \tag{4}$$

ρ_l is density of water, and $\overrightarrow{u_l}$ is the Darcy velocity (volume flux) in the liquid phase. For a fully saturated case, equation one simplifies to:

$$\frac{d}{dt}\int_{\Omega} \phi\rho_l \, dV = -\int_{\partial\Omega} \overrightarrow{f_l} \cdot \vec{n} \, dS + \int_{\Omega} Q \, dV \tag{5}$$

By using Gauss' divergence theorem ($\int_{\partial\Omega} \overline{f_l} \cdot \vec{n}\, dS = \int_{\Omega} div\ \overline{f_l}\ dV = \int_{\Omega} \nabla \cdot \overline{f_l}\ dV$) in equation (1), we can get the continuity equation for mass balance law:

$$\frac{d}{dt}\int_{\Omega} G_w\ dV = -\int_{\Omega} div\ \overline{f_l}\ dV + \int_{\Omega} Q\ dV \tag{6}$$

Moving all the equations to the same side we get the condition:

$$\int_{\Omega} \left(\frac{\partial}{\partial t} G_w + div\ \vec{f} - Q \right) dV = 0\ \forall\Omega \tag{7}$$

Thus, we can say that the integrand has to be 0 too, that the conditions are fulfilled and we get the continuity equation:

$$\frac{\partial G_w}{\partial t} + div\ \vec{f} = Q \tag{8}$$

which is a basic equation form used as the starting point for calculating finite difference or finite element discretization approaches for conservative water flow in unsaturated porous media. In saturated conditions the equation is formed equally. G_w in the equation is the water accumulation term, $\overline{f_l}$ is a flux function of water accumulation and Q describes the generation or removal rate.

2.2.1 Saturated flow

Several concepts have been used to describe the flow of water. A gradient in water content has been, for example, used to describe the flow of water through unsaturated soils; other concepts are matric suction gradient and hydraulic head (see for example [12]).

The most appropriate one of the three concepts is the hydraulic head gradient for each phase. In a case where the air pressure gradient is zero, the matric suction gradient is equal to the pressure gradient in the water. This is a normal situation in nature and a reason why the matric suction version has been proposed for water flow; however, the elevation head component has then been left out.

In saturated soils, in most cases the flow of water through a porous medium is commonly described with Darcy's Law (Darcy velocity). According to Darcy's Law, the volumetric flux of water ($m^3_{fluid}/m^2_{medium}/s$) $\vec{u}$ is a vector proportional to the hydraulic head gradient ∇h:

$$\vec{u} = \phi\vec{v} = -\mathbf{K}\nabla h \tag{9}$$

where **K** is the hydraulic conductivity tensor (m/s), and $\vec{v}$ is average water velocity and h is the hydraulic head. Darcy's Law can also be written in terms of fluid pressure:

$$h = z + \frac{P}{\rho g} \tag{10}$$

where z is the depth, P is fluid pressure in the liquid phase, ρ is the density of water and g is the gravitational acceleration. The hydraulic conductivity **K** is defined as:

$$\mathbf{K} = \frac{\kappa\rho g}{\mu} \tag{11}$$

κ is the intrinsic permeability and μ is the dynamic viscosity. By inserting equations (11) and (12) in to equation (10) we get (see for example [9]):

$$\vec{u} = -\frac{\boldsymbol{\kappa}}{\mu}(\nabla P - \rho\vec{g}) \tag{12}$$

where $\vec{u}$ is the flow rate of water (Darcy's velocity), P is the fluid pressure, $\vec{g}$ is the vector of gravitational acceleration, and $\boldsymbol{\kappa}$ is the intrinsic permeability tensor, which in an unsaturated case is the same as absolute permeability.

2.2.2 Unsaturated flow

In this section the difference between saturated and unsaturated flow is discussed and all the parameters and equations needed for unsaturated flow are introduced.

In an unsaturated flow, the void space (pore volume) is partly filled by water and partly by air. There are two important variables used to define the relative quantity of water in the porous medium:

$$\theta_w = \frac{\text{Volume of water in porous medium}}{\text{Bulk volume of porous medium}}; 0 \le \theta_w \le \phi \tag{13}$$

$$S_w = \frac{\text{Volume of water in porous medium}}{\text{Volume of void in porous medium}}; 0 \le S_w \le 1 \tag{14}$$

θ_w is the moisture content and S_w is the water saturation. These are related to each other as:

$$\theta_w = \phi S_w \tag{15}$$

where ϕ is the porosity. These two parameters are important in defining the unsaturated version of Darcy's law. Saturation is used in this thesis to define the relative permeability and capillary pressure functions.
The Darcy velocity in unsaturated flow is defined equally as in a saturated case with a few differences. This is sometimes also called the extended Darcy's Law. The Darcy velocity was defined as (in equations (9) and (12)):

$$\vec{u} = -\mathbf{K}\nabla h = -\frac{\boldsymbol{\kappa}}{\mu}(\nabla P - \rho\vec{g}) \tag{16}$$

The difference between saturated and unsaturated flow is that in an unsaturated case the intrinsic permeability tensor $\boldsymbol{\kappa}$ is dependent on the relative permeability, and is defined as:

$$\boldsymbol{\kappa} = \kappa_{r\beta}\boldsymbol{\kappa}_{\mathbf{a}} \tag{17}$$

where $\kappa_{r\beta}$ is the relative permeability for liquid (l) and gas (g) phase β and $\boldsymbol{\kappa}_{\mathbf{a}}$ is the absolute permeability tensor and permeability for single-phase flow. κ_r is equal to 1 in saturated conditions (this case) and below 1 under partially saturated conditions. The relative permeability in bentonite is then represented as a function of saturation according to van Genuchten [40]:

$$\kappa_{rl}\left(S^*\right) = \begin{cases} \sqrt{S^*}\left[1-\left(1-\left[S^*\right]^{1/\lambda}\right)^{\lambda}\right]^2 & if\ S_l < S_{ls} \\ 1 & if\ S_l \geq S_{ls} \end{cases} \tag{18}$$

where λ is a van Genuchten model parameter called pore-size distribution index, S_l is the liquid saturation degree, S_{ls} is saturation in a fully saturated state (normally 1) and S^* is dimensionless water content:

$$S^* = \frac{S_l - S_{lr}}{S_{ls} - S_{lr}} \tag{19}$$

where S_{lr} is the liquid residual saturation in a porous medium at the beginning

$$\kappa_{rg}\left(S^{\#}\right) = \begin{cases} 1-\kappa_{rl} & if\ S_{gr} = 0 \\ \left(1-S^{\#}\right)^2\left(1-S^{\#}\right)^2 & if\ S_{gr} > 0 \end{cases} \tag{20}$$

where S_{gr} is the gas residual saturation, and $S^{\#}$ is defined as:

$$S^{\#} = \frac{S_l - S_{lr}}{1 - S_{lr} - S_{gr}} \tag{21}$$

An other difference between saturated and unsaturated flow is that, in the unsaturated case, the fluid pressure P is defined as:

$$P = P_r + P_c \tag{22}$$

where P is the fluid pressure of the phase in question, P_r is the pressure of a reference phase (usually gas phase), and P_c is the capillary pressure of the phase in question(≤ 0).

When two immiscible fluids have a mutual interface, there exists a discontinuity of pressure at this interface. The magnitude of this pressure difference depends on the interface curvature and saturation. This pressure difference is called capillary pressure P_c. In a general two-phase system, P_c is the difference between the pressure on the non-wetting side of the interface and that on the wetting one (see for example [6]). The capillary pressure represents also the tendency of the partially saturated porous medium to suck in water (suction). In this work, capillary pressure is approximated with the help of the van Genuchten function [40]:

$$P_c = -P_0 \left(\left[S^* \right]^{-1/\lambda} - 1 \right)^{1-\lambda} \tag{23}$$

with restriction $-P_{\max} \leq P_c \leq 0$. Here $P_0 = \frac{\rho_w g}{\alpha}$ and α is the van Genuchten capillary strength parameter. Sometimes P_0 is also given in literature. $-P_{\max}$ is the minimum pressure value for capillary pressure.

Thus, the motion equations for the liquid (wetting phase l) and the gas (non-wetting phase g) in an unsaturated flow in an isotropic porous medium can be written with the help of equations (16), (18) and (20) as:

$$\vec{u}_l = -\boldsymbol{\kappa}_a \frac{\kappa_{rl}(S^*)}{\mu_l} (\nabla P_l - \rho_l \vec{g}) \tag{24}$$

$$\vec{u}_g = -\boldsymbol{\kappa}_a \frac{\kappa_{rg}(S^{\#})}{\mu_g} (\nabla P_g - \rho_g \vec{g})$$

Here P_l and P_g are the pressures in two phases (liquid and gaseous), κ_{rl} and κ_{rg} are the relative permeabilities of these phases as a function of saturation, and ρ_l and ρ_g are the densities of the phases.

One can assume in some cases that there are no sources or sinks or phase changes, that the gas phase is a passive bystander, and that the gas pressure does not change much, and therefore simplify equation (8) by inserting equations (16) and (17) to obtain:

$$\frac{\partial}{\partial t}\phi S_l \rho_l = -div\left[\mathbf{\kappa_a}\frac{\kappa_{rl}}{\mu_l}\rho_l \nabla(P_l + \rho_l g z)\right] \tag{25}$$

By inserting equations (10) and (11) in to equation (25) and assuming liquid density as a constant, which is appropriate at nearly isothermal conditions, we get the Richards' equation:

$$\frac{\partial}{\partial t}\phi S_l = -div\left[K\nabla h\right] \tag{26}$$

where $\mathbf{K} = \frac{\mathbf{\kappa_a}\kappa_r \rho_l g}{\mu_l}$ and $h = z + \frac{P_l}{\rho_l g}$.

Richards' equation represents the movement of water in unsaturated soils.

2.2.3 Simultaneous air and water flow

The air motion equation and continuity equations can be formed for air just as for water above (see for example [31]). It is possible to consider the simultaneous flow of both the water and the air in the unsaturated zone. Here. the gaseous water is assumed to be a passive bystander as in Richard's equation and therefore it is omitted from these equations. In addition, the liquid air effects are ignored (the error is small, but this is only a simplified version of the real equations that TOUGHREACT calculates). In this case, the program has to solve the continuity equations for air (a) and for water (w) simultaneously and obtain (the source term in this thesis is 0):

$$\left.\begin{aligned} &\frac{\partial \rho_{\mathrm{w}}\phi S_{\mathrm{w}}}{\partial t} + div\left(\rho_{\mathrm{w}}\overrightarrow{u_{\mathrm{w}}}\right) = 0 \\ &\frac{\partial \rho_{\mathrm{a}}\phi S_{\mathrm{a}}}{\partial t} + div\left(\rho_{\mathrm{a}}\overrightarrow{u_{\mathrm{a}}}\right) = 0 \\ &S_{\mathrm{a}} + S_{\mathrm{w}} = 1 \end{aligned}\right\} \tag{27}$$

If we assume that ϕ and ρ_{w} are constant we obtain the form:

$$\begin{aligned}\phi\frac{\partial}{\partial t}S_{\mathrm{w}}+div\left(\overrightarrow{u_{\mathrm{w}}}\right)&=0\\ \phi\frac{\partial\rho_{\mathrm{a}}S_{\mathrm{a}}}{\partial t}+div\left(\rho_{\mathrm{a}}\overrightarrow{u_{\mathrm{a}}}\right)&=0\end{aligned}\qquad(28)$$

Here, liquid phase is water and the gaseous phase is air. If we would like to take into account the water vapour we would replace the first equation in the system of equations (27) by equation (8) without the source term.

2.3 Mass and heat transport processes

The general mass balance equation can be written as:

$$\frac{d}{dt}\int_{\Omega}C^{i}\,dV=-\int_{\partial\Omega}\vec{b}^{\,i}\cdot\vec{n}\,dS+\int_{\Omega}s^{i}\,dV\qquad(29)$$

The integral is over an arbitrary domain Ω in the flow system in question, C^{i} is the accumulation term mass per volume (concentration), $\vec{b}^{\,\mathrm{i}}$ is the mass flux and s^{i} is a sink or source term. The system is surrounded by a closed surface $\partial\Omega$. $\vec{n}$ is a normal vector on boundary $\partial\Omega$ pointing outward from Ω. i=1,2,…,n labelling the mass components (Na^{+}, H_2…) The mass flux $\vec{b}$ can be written in a general form as Fick's Law + convection term (advection):

$$\vec{b}=-D_i\nabla c+\vec{u}c\qquad(30)$$

where D_i is the effective diffusion coefficient specific to component i, c is the concentration of component and $\vec{u}$ is Darcy velocity. For a chemical component in water the effective diffusion coefficient is defined as:

$$D_i=\tau\phi S_l d\qquad(31)$$

where τ is tortuosity, ϕ is porosity, S_l is liquid saturation and d is the diffusion coefficient in water (constant in PetraSim for all components). The gaseous species diffusion coefficient D in TOUGHREACT is calculated as:

$$D=\frac{RT}{3\sqrt{2}\pi PN_A d_m^2}\sqrt{\frac{8RT}{\pi M}}\qquad(32)$$

where R is the molar gas constant, T is temperature in Kelvins, P is pressure [Pa], N_A is Avogadro's number, d_m is molecular diameter [m], and M is molecular weight.

The third basic equation is the energy balance equation which states:

$$\frac{d}{dt}\int_{\Omega} e\, dV = -\int_{\partial\Omega} \vec{q}\cdot\vec{n}\, dS + \int_{\Omega} \mathrm{H}\, dV \tag{33}$$

where e is the energy density, $\vec{q}$ is the heat flux component, H is the source term. Heat flux $\vec{q}$ can be written in a general form as Fourier's law of heat conduction + convection term:

$$\vec{q} = -k\nabla T + CT\rho\vec{u} \tag{34}$$

where k is the coefficient of thermal conductivity, which is a property of a particular substance, T is temperature, C is the specific heat capacity and ρ is density.

The mass accumulation term C for a certain component i can be written as:

$$C^i = \phi\sum_{\beta} S_\beta \rho_\beta X_\beta \tag{35}$$

where ϕ is the porosity of material, β is the fluid phase (liquid, gas), S_β is the saturation of a certain phase (the fraction of pore volume), ρ_β is the density of the phase, and X_β is the mass fraction of the component present in phase β. In many cases there are no volatile chemical components in the gaseous phase of water, and equation (35) simplifies to:

$$C^i = \phi S_l c_l \tag{36}$$

where S_l is liquid saturation and c_l is concentration of aqueous species in the liquid phase.

The heat accumulation term e can be written as:

$$e = (1-\phi)\rho_{\mathrm{R}} C_{\mathrm{R}} T + \phi\sum_{\beta} S_\beta \rho_\beta u_\beta \tag{37}$$

where ρ_{R} is grain density (in TOUGH2 terminology), C_{R} is specific heat of the rock, T is temperature, and u_β is specific internal energy in phase β. [28]

2.3.1 Advection

The easiest of mass transport processes to understand is called advection (or convection), where the mass flow of dissolved species is carried along the bulk fluid phase. The advective flux J_{adv} in porous media can be described as:

$$J_{\text{adv}} = \phi v c_i \tag{38}$$

where ϕ is porosity, v is the average linear velocity of water and c_i is the concentration of the i:th species. The real water velocity v is obtained by dividing the Darcy velocity with the porosity.

2.3.2 Diffusion

Molecular diffusion may easily become a significant and even dominant mechanism for mass transport when advective velocity is small. Fick's First Law describes the molecular diffusion, which states that the diffusive flux is proportional to the concentration gradient (see for example [10]), and can be written:

$$J_i = -D_i \nabla c_i \tag{39}$$

where D_i is effective diffusivity for chemical component i in a certain phase, and c_i is the concentration of the component in question. Effective diffusivity depends on the diffusing component, the pore fluid and the porous medium. Fick's First Law is sufficient, but it is only true in the case of diffusion of uncharged species in dilute solutions. Thus when there are multiple components diffusing in a multiphase system, complications may occur. Additional problems arise between coupling of advective and diffusive transport and between gaseous and aqueous phases (see for example [9]).

Because of the difficulties mentioned above TOUGH2 uses an approach where the diffusive flux g of component i in phase β is described as:

$$g_\beta^i = -\phi \tau_0 \tau_\beta \rho_\beta D_\beta^i \nabla X_\beta^i \tag{40}$$

where ϕ is porosity, $\tau_0\tau_\beta$ is tortuosity (can be fixed as constant) where there is a porous medium dependent factor τ_0 and phase saturation dependent factor τ_β ($\tau_\beta = \tau_\beta S_\beta$), ρ_β is density, D_β^i is diffusion coefficient in bulk fluid phase β, X is the mass fraction. If we mark the diffusion coefficient as d_β^i and write:

$$d_\beta^i = \phi \tau_0 \tau_\beta \rho_\beta D_\beta^i \tag{41}$$

the total diffusive flux can be represented in two-phase conditions as:

$$f^i = -d_l^i \nabla X_l^i - d_g^i \nabla X_g^i \tag{42}$$

The saturation dependence of tortuosity is not well known. If a zero value for porosity is given, the model uses the Millington and Quirk [21] equation, which implies that the diffusive flux should vanish when phase saturation goes to zero, because the wetting fluid becomes discontinuous throughout the flow domain and cannot flow anymore. It can be written as:

$$\tau_0 \tau_\beta = \phi^{1/3} S_\beta^{10/3} \tag{43}$$

There is third kind of mass transport called dispersion, but dispersion is only included in special versions of TOUGH2 and in this 1-D model it is excluded and thus it is not discussed in this thesis.

2.4 Summary of flow and transport laws

All flow and transport equations have the same form. The equations discussed above in the two sections are summarized in Table 3.1. The meaning of the symbols is discussed above and can be found in the beginning of this thesis.

Table 3.1. The governing equations in Equations of State 3 (EOS3) for fluid and heat flow used in this thesis.

General continuity equation: $\dfrac{\partial G^i}{\partial t} = -div\, f^i + q^i$

Water: $G_w = \phi(S_l \rho_l \mathrm{X}_{wl} + S_g \rho_g \mathrm{X}_{wg})$	$\overrightarrow{f_w} = \mathrm{X}_{wl} \rho_l \overrightarrow{u_l} + \mathrm{X}_{wg} \rho_g \overrightarrow{u_g}$	$q_w = q_{wl} + q_{wg}$
Air : $G_a = \phi(S_l \rho_l \mathrm{X}_{al} + S_g \rho_g \mathrm{X}_{ag})$	$\overrightarrow{f_a} = \mathrm{X}_{al} \rho_l \overrightarrow{u_l} + \mathrm{X}_{ag} \rho_g \overrightarrow{u_g}$	$q_a = q_{al} + q_{ag} + q_{ar}$
Heat : $e = (1-\phi)\rho_R C_R T + \phi \sum_{\beta=l,g} S_\beta \rho_\beta u_\beta$	$\vec{q} = -k\nabla T + \sum_{\beta=l,g} C_\beta T \rho_\beta \vec{u}$	q_h

Chemical Components in liquid phase:

$C^i = \phi\, S_l c_{il}$	$\overrightarrow{b_i} = -D_i \nabla c_{il} + \overrightarrow{u_l} c_{il}$	$q_i = q_{il} + q_{is} + q_{ig}$

2.5 Discretization

The continuum equations (1), (29) and (33) are discretized using the Integral Finite Difference Method (IFDM) [23], which gives a flexible discretization and allows using irregular grids. The mass transport equations are solved for each chemical component independently, but the reaction equations are solved on a

grid block basis using Newton-Raphson iteration. IFDM is a variant of the Finite Volume Method (FVM).

The continuum equation (1) can be written in form:

$$\frac{d}{dt}G_m V_m = -\sum_n A_{mn} f_{mn} + Q_m V_m \tag{44}$$

where G_m is the average value of G over V_m. G is a volume normalized extensive quantity, A_{mn} is the area of interface between cells m and n, f_{mn} is the average value of the (outward) normal component of f over the surface segment A_{mn} between volume elements V_m and V_n. f_{mn} is the discretized flux and for the basic Darcy flux term, equations (3) and (12) can be written as:

$$f_{\beta,mn} = -\boldsymbol{\kappa}_{\mathbf{a},mn}\left[\frac{\kappa_{r\beta}\rho_\beta}{\mu_\beta}\right]_{mn}\left[\frac{P_{\beta,m}-P_{\beta,n}}{D_{mn}} - \rho_{\beta,mn}g_{mn}\right] \tag{45}$$

where β denotes the fluid phase, subscript mn is an averaging at the interface between blocks m and n (upstream weighting). D_{mn} is the distance between the nodal points m and n, g_{mn} is the gravitational acceleration in the direction from n to m. The pressure approximation is accurate in the cases where the common edge of cells m and n is perpendicular to the line that connects the centres of these cells. Figure 2.5 illustrates the discretization approach and geometric parameters of the IFDM.

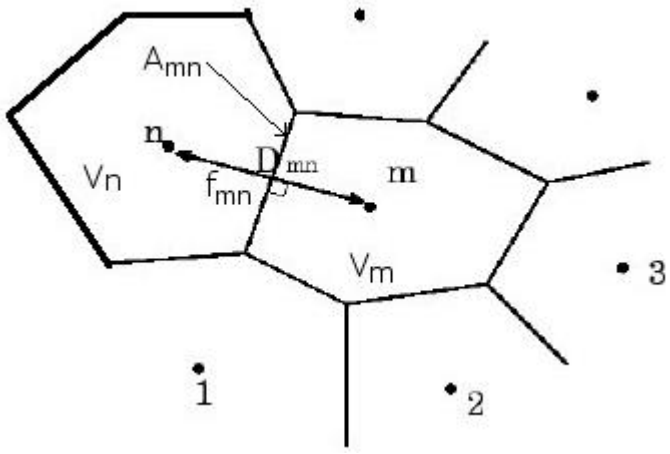

Figure 2.5. Space discretization and geometry data in IFDM.

The time discretization is made as a first-order finite difference where the flux and the source terms are evaluated at the new time level t^{k+1} fully implicitly. As a result we get the following coupled non-linear equation, which in fact has to be calculated independently for every mass component and every-time step:

$$R_m^{k+1} = G_m^{k+1} - G_m^k - \frac{\Delta t}{V_m}\left(\sum_n A_{mn} f_{mn}^{k+1} + V_m Q_m^{k+1} \right) = 0 \tag{46}$$

Newton-Raphson iteration is used to solve these equations but the iteration method is not discussed in this thesis. For further information about the time discretization, iteration, and convergence criterion see the TOUGH2 manual [28] and, for example [36].

2.6 Formulation of chemical reactions in TOUGHREACT

2.6.1 Mathematical formulation of chemical reactions

To describe a geochemical system, it is necessary to select a certain group of aqueous species as building blocks for all other species or substances. This subset is normally called the primary or basis species. In the chemical sense, the primary species is a set of chemical entities such that all the other species which include minerals, aqueous complexes, gaseous species, etc., can be represented as the product of reaction involving only these primary species. The so formed components are called secondary or auxiliary species (see for example [44] or [36]).

From these primary species, the modeller has to choose the ones which will describe the composition of all aqueous species, gases and minerals in a particular system, so that the modelling program has all the primary species necessary for certain minerals. For example, the component Na^+ describes the total amount of sodium in the system and species Na^+ represents the sodium actually present as the univalent sodium ion.

The number of auxiliary species is equal to the number of independent reactions. The secondary species can be represented as a combination of the set of primary species (reversible reaction):

$$L_i = \sum_{j=1}^{N_C} \nu_{ij} L_j \qquad i = 1, ..., N_R \tag{47}$$

where L represents the chemical species (secondary species or components), j is the primary species index, N_C is the total number of primary species needed in the secondary species (set of primary species), i is the secondary species index,

N_R is the number of reactions (or secondary species) and υ_{ij} is the stoichiometric coefficient of the *j*:th master species in the *i*-th secondary species. If, for example, anhydrite $CaSO_4$ is a mineral and a secondary species composed of Ca^{2+} and SO_4^{2-} primary species, υ_{SO4-} and υ_{Ca2+} are both 1.

Aqueous complexes are assumed to be at local equilibrium at the beginning. This local equilibrium assumption is not discussed in detail in this thesis (see for example [18] for further information). However, according to this assumption the concentration of aqueous complexes can be calculated.

Fundamental to any description of equilibrium states in water is the law of mass action. For a generalized reaction it can be written (see for example [1] or [2]):

$$aA + bB \rightleftharpoons cC + dD \tag{48}$$

where *A* and *B* are reactants and *C* and *D* are products, and *a*, *b*, *c* and *d* are stoichiometric coefficients.

The partition of the species at equilibrium is given by:

$$K = \frac{[C]^c [D]^d}{[A]^a [B]^b} \tag{49}$$

where K is the equilibrium constant and the letters in brackets are activities. Simplifications can be made for dilute solution where the activities are nearly same as concentrations and thus the activities can be replaced by the concentrations. Normally the activity is related to the molal concentration by an activity coefficient γ which is a correction term from ideal to non-ideal behaviour. For aqueous species the next relation applies:

$$a_i = \gamma_i \frac{m_i}{m_i^0} = \gamma_i m_i \tag{50}$$

where a is the activity of ion *i*, γ_i is the activity coefficient and m_i is the molality or molal concentration [mol/kg H_2O] and m_i^0 is the standard state [1 mol/kg H_2O]. Thus activity is dimensionless.

The activity coefficient for a charged aqueous species is calculated using the extended Debye-Hückel equation and parameters found from [14]. The equation assumes that the dominant cation and anion in solution are sodium and chloride and accordingly the equation is as follows:

$$\log(\gamma_j) = -\frac{A_\gamma z_j^2 I^{0.5}}{\Lambda} + \log(1 + 0.0180153 m^*) - \left[\omega_j b_{NaCl} + b_{Na^+,Cl^-} - 0.19(|z_j| - 1)\right] I \tag{51}$$

Here

$$\Lambda = 1 + \mathring{a} B_\gamma \bar{I}^{0.5} \tag{52}$$

and

$$\omega_j = \eta \frac{z_j^2}{r_{e,j}} \tag{53}$$

Above subscript j denotes each ion, γ is the activity coefficient, b_{NaCl}, b_{Na+Cl-}, A_γ, and B_γ are Debye-Hückel parameters, z is the ion electric charge, I is the true ionic strength of the solution, ω is the Born coefficient, η is 1.66027 [Åcal/mol], $r_{e,j}$ is the effective radius of the ion given in [18]. The Debye-Hückel parameters were regressed as a function of temperature and the resulting functions are built into TOUGHREACT. The D-H parameter $\mathring{a}$ is calculated in TOUGHREACT using effective ionic radii $r_{e,j}$ and making the assumption that NaCl is the dominant electrolyte as follows:

$$\begin{aligned} \mathring{a}_j &= \frac{2\left(r_{e,j} + 1.91|z_j|\right)}{|z_j| + 1} \qquad \text{for anions} \\ \mathring{a}_j &= \frac{2\left(r_{e,j} + 1.81|z_j|\right)}{|z_j| + 1} \qquad \text{for cations} \end{aligned} \tag{54}$$

Here j means ion. The values 1.91 and 1.81 are the values for Na^+ and Cl^- defined in the database of TOUGHREACT and they can be changed. The values for different ionic charges are estimated in the database using different methods. The method applicability depends on how dominant NaCl is in the solution. However, it is still a simplification and may cause errors to ion activity coefficients at high ionic strength. The model is not recommended to be used at ionic strengths higher than 3 [43]. Ionic strength I (dimensionless) can be defined as:

$$I = \tfrac{1}{2} \sum m_i z_i^2 \tag{55}$$

where m_i is the molality and z_i is the electrical charge of species i. The summation is over all aqueous species.

In general, mass-action equations can be written as:

$$K_i = a_i \prod_{j=1}^{N_C} a_j^{-\nu_{ij}} \tag{56}$$

where K_i is the equilibrium constant, a_i is the activity of secondary species and a_j is the activity of the master species.

After defining how to calculate the ion activity coefficients and the general mass-action equation we can calculate the molal concentrations of the aqueous species.

However, in TOUGHREACT the reactions are written vice versa so that from products one obtains reactants. Thus we can write:

$$K_i = a_i^{-1} \prod_{j=1}^{N_C} a_j^{\nu_{ij}} \tag{57}$$

from which it follows that:

$$m_i = K_i^{-1} \gamma_i^{-1} \prod_{j=1}^{N_C} m_j^{\nu_{ij}} \gamma_j \tag{58}$$

where m_i is the molal concentration of the i:th aqueous complex, and m_j is molal concentration of the j:th primary species.

One can choose for minerals based on whether they are in equilibrium or whether they follow kinetics. Equilibrium mineral dissolution/precipitation ratio can be described as:

$$\Omega_m = X_m^{-1} \lambda_m^{-1} K_m^{-1} \prod_{j=1}^{N_C} c_j^{\nu_{mj}} \gamma_j^{\nu_{mj}} \tag{59}$$

where m is the equilibrated mineral index, X_m is the mole fraction of the m:th mineral phase and λ_m is the mineral thermodynamic activity coefficient. At equilibrium the mineral saturation index is 0 which means that $\log_{10} \Omega_m = 0$.

The kinetics is, however, more complicated. The mineral dissolution/precipitation rate law used is an expression from Lasaga *et al*. (1994) [19] and is written:

$$r_n = \pm k_n A_n \left| 1 - \Omega_n^{\theta} \right|^{\eta} \qquad n = 1 \ldots N_q \tag{60}$$

where negative values of r_n mean precipitation and positive dissolution, k_n is the rate constant, A_n is the specific reactive surface area/kg(H_2O), Ω_n is the kinetic mineral saturation ratio (see equation (59)), and the parameters η and θ are from experiments and usually taken to be 1. Reaction rates are normally described in 25 ^{o}C. Thus they are temperature-dependent and the dependence is easily expressed with the Arrhenius equation, which approximates the temperature-dependence of the rate constant. It can be written as:

$$k = k_{25} \exp\left[\frac{-E_a}{R} \left(\frac{1}{T} - \frac{1}{298.15} \right) \right] \tag{61}$$

where E_a is the activation energy and k_{25} is the rate constant at 25°C, R is gas constant and T is temperature in reaction.

The pH-dependence of mineral reaction rates is expressed as follows:

$$k_{\text{adj}} = k\left(10^{-pH_c}/10^{-pH_1}\right)^{slope1} \quad \text{if } pH_c < pH_1$$
$$k_{\text{adj}} = k\left(10^{-pH_c}/10^{-pH_2}\right)^{-slope2} \quad \text{if } pH_c > pH_2 \tag{62}$$

where k_{adj} is the pH adjuster rate, k is the original rate, pH_c is the current pH_1 is the pH which under the rate is adjusted by *slope1* and pH_2 is the pH which above the rate is adjusted by *slope2*. The slopes are positive numbers which adjust the rate constant and between pH_1 and pH_2 the rate is assumed to remain independent of pH.

The rate constant in equations (60) and (61) only takes into account the mechanism in pure H_2O (neutral pH). These precipitation and dissolution reactions may often be catalyzed by H^+ or OH^- in acid or basic mechanism or it can be dependent on other species as well. The kinetic rate constant can be expressed as a sum of these mechanisms (see for example [19] or [25]:

$$k = k_{25}^{n}\exp\left[\frac{-E_a^n}{R}\left(\frac{1}{T}-\frac{1}{298.15}\right)\right]+\sum_i k_{25}^{H}\exp\left[\frac{-E_a^H}{R}\left(\frac{1}{T}-\frac{1}{298.15}\right)\right]\prod_j a_{ij}^{d_{ij}} \tag{63}$$

where superscript n indicates neutral, a is activity coefficient and d is a power term (constant), subscript i is the additional mechanism index, and j is the species index in one mechanism. In TOUGHREACT it is possible to add up to five additional mechanisms and five species for each mechanism. There is also a possibility to add a special supersaturation condition, which means that below a certain $\log_{10}\Omega_m$ value the mineral does not precipitate (for further information see [43]).

Reactions involving aqueous and gaseous phases are normally assumed to be at equilibrium. From Mass-Action Law one gets:

$$p_f \Gamma_f K_f = \prod_{j=1}^{N_C} c_j^{\nu_{fj}} \gamma_j^{\nu_{fi}} \tag{64}$$

where f is gas index, p is the partial pressure in bars, Γ is the gas fugacity coefficient, for low-pressure gas fugacity is equal to one but for higher temperature and pressures it will have to be corrected according to temperature and pressures implemented in the TOUGHREACT database (see [43]). For further information about the fugacity coefficients and activity coefficients for liquid-gas mixtures see [43] or [35].

The solution of the reaction systems in TOUGHREACT requires information about the initial total concentrations of primary species in the equilibrium

system (aqueous) and mineral volume fractions. In addition, if ion exchanger is present, ion exchange coefficients are needed. For kinetic systems, kinetic parameters for minerals are needed (activation energy, surface areas, etc.). Once the concentrations of the primary species are obtained, all other secondary variables can be computed.

2.6.2 Mineral precipitation/dissolution effects on hydrological properties

The mineral precipitation/dissolution directly affects porosity and thus they may lead to smaller porosity which can also directly affect permeability. However, in this model the mineral dissolution/precipitation effects on fluid flow are ignored. It is assumed that the mineral dissolution/precipitation effects on fluid flow in such a short time period are negligible.

Fracture permeability changes are approximated using the cubic law where the modified permeability k is written as [36]:

$$k = k_i \left(\frac{\phi}{\phi_i} \right)^3 \tag{65}$$

where k_i and ϕ_i are the initial permeability and porosity. Zero permeability occurs only when the porosity goes to zero.

The matrix permeability changes are calculated using the Carmen-Kozeny relation [5]:

$$k = k_i \frac{\left(1-\phi_i\right)^2}{\left(1-\phi\right)^2} \left(\frac{\phi}{\phi_i} \right)^3 \tag{66}$$

Here grain size, tortuosity and surface area are assumed to be constant.

The Leverett Scaling for capillary pressure was used to couple the capillary pressure to porosity and permeability changes. Changes to unsaturated flow are approximated using this scaled method:

$$P_c^{'} = P_c \sqrt{\frac{k_i \phi}{k \phi_i}} \tag{67}$$

In our model, the porosity is constant and consequently these equations become meaningless. However, if we would like to take porosity changes into account, we would need equations (65) to (67). In this model permeability changes, but it is due to saturation, not due to porosity changes, and so the capillary pressure is only a function of saturation too.

2.6.3 Cation exchange

Cation exchange occurs when free cations in porewater exchange with interlayer cations in exchange sites. This reaction also tends to go to equilibrium. In this case the equilibrium constant is called exchange coefficient. In this thesis the Gaines-Thomas convention for cation-exchange reaction was used (see [2]):

$$\frac{1}{v_i}B_i + \frac{1}{v_j}\left(B_j - X_{v_j}\right) \rightleftharpoons \frac{1}{v_i}\left(B_i - X_{v_i}\right) + \frac{1}{v_j}B_j \tag{68}$$

where v_i and v_j denotes the stoichiometric coefficients for cations which are equal to their charges, B_i and B_j are dissolved cationic species, and X_{vi} and X_{vj} are exchange sites where the cations are attached. The equilibrium constant for cation exchange is obtained from (47):

$$K^*_{i/j} = \frac{w_i^{1/v_i} \cdot a_j^{1/v_j}}{w_j^{1/v_j} \cdot a_i^{1/v_i}} \tag{69}$$

where $K^*_{i/j}$ is selectivity coefficient, a_j and a_i are the activities of the *i*:th and *j*:th dissolved species and *w* denotes the activity of the exchanged species. Activities for dissolved cations are calculated as mentioned before in equations (50) to (54). The activities for interlayer cations *w* are assumed to equal their equivalent fraction β_i (for small ionic strengths activity can be assumed to be equal to concentration). The Gaines-Thomas convention uses the equivalent fractions of the exchangeable cations for the calculation of the selectivity coefficient. The equivalent fraction is defined as:

$$\beta_i = \frac{c_i}{\sum_{i=1}^{N_c} c_i} \tag{70}$$

where c_i is the concentration of the *i*:th interlayer cation and N_c is the total number of these cations. The sum of the concentrations of these interlayer cations is called Cation Exchange Capacity (CEC). Inserting equation (50) to (69) we obtain the general equation for cation exchange:

$$K^*_{i/j} = \frac{\beta_i^{1/v_i} \cdot \left(c_j \gamma_j\right)^{1/v_j}}{\beta_j^{1/v_j} \cdot \left(c_i \gamma_i\right)^{1/v_i}} \tag{71}$$

From this equation one can solve the equivalent fraction of the *j*:th interlayer (exchange site) cation by raising both sides to a power of v_j and obtain:

$$\beta_j = (K^*_{i/j})^{-\nu_j} c_j \gamma_j \left(\frac{\beta_i}{c_i \gamma_i} \right)^{\nu_j/\nu_i} \qquad j = 1, 2, ..., N_C \tag{72}$$

From equation (72) and from the definition of equivalent fraction (70) the equation can be derived:

$$\sum_{j=1}^{N_c} (K^*_{i/j})^{-\nu_j} c_j \gamma_j \left(\frac{\beta_i}{c_i \gamma_i} \right)^{\nu_j/\nu_i} = 1 \tag{73}$$

which for given dissolved concentrations can be solved for the equivalent fraction β_i. Once this equivalent fraction is known, all the other equivalent fractions can be solved from equation (69). The concentration of the *i*:th exchanged cation c_j [kg/l] can be solved from the j:th equivalent fraction with the equation:

$$c_j = \beta_j \cdot CEC \cdot \rho_s \frac{(1-\phi)}{100 \phi z_j} \tag{74}$$

where *CEC* is the cation-exchange capacity [meq/100g], ϕ is porosity, ρ_s is the density of solid [kg/dm^3] and z_j is the charge of the *j*:th cation.

2.6.4 Reactive surface areas of minerals

The reactive surface area is used in the rate law expression. However, in the rock matrix or porous medium mineral surface areas are input parameters. Thus, in this model the fracture equations are not used. The mineral surface areas of grains in contact with the open pore space can be calculated with the help of initial grain diameter. The abundance of secondary mineral phases, which are formed as alteration products, can be used to reduce the free surface area of the framework grains. For further information about the surface areas see [43].

It is, however, clear that the amount of reactive surface area in a real geological system is a complex function of the particular rock properties (permeability, grain size, etc.). The reactive surface areas have to be determined experimentally for each case and are at the moment a large uncertainty factor in THC-modelling.

2.7 Preliminary calculations

Preliminary calculations are needed for the chemistry input for TOUGHREACT and TOUGH to get as realistic results as possible. This section explains what needs to be calculated in order to make a final repository model for PetraSim.

According to Tanhua-Tyrkkö [37], CEC in TOUGHREACT is calculated so that the material density should be 2.65 g/cm^3. Thus, if it is something else (2.75 g/cm^3 in this work), there has to be a correlation according to the next equation:

$$CEC_{\text{input}} = CEC_{\text{experiment}} \frac{\rho_{\text{material}}}{\rho_{\text{default}}} = 75 \, {}^{meq}\!/\!_{100g} * \frac{2.75 \, {}^{g}\!/\!_{cm^3}}{2.65 \, {}^{g}\!/\!_{cm^3}} \approx 77.8 \, {}^{meq}\!/\!_{100g} \tag{75}$$

where the CEC_{input} is the cation-exchange capacity put in PetraSim, $CEC_{\text{experiment}}$ is the CEC from the experiment (see Table 5.1) and ρ_{material} is the density of the material in question, and ρ_{default} is the original fixed density.

One other important factor is the diffusion tortuosity for bentonite, which can be calculated with the help of effective diffusivity, and which according to Ochs and Talerico p.88 [24] can be calculated as:

$$D_e = 6.7785E-9 \times e^{-2.5671E-3 \times \rho_d} = 1.21217 \cdot 10^{-10} \ m^2/s \tag{76}$$

where ρ_d is dry density which can be calculated as:

$$\rho_d = (1-\phi) \times \rho_r = (1-0.43) \times 2750 kg/m^3 = 1567.5 kg/m^3 \tag{77}$$

where ϕ is porosity and ρ_r is grain density (from Table 5.1). In TOUGHREACT [28] the effective diffusivity is as follows:

$$D_e = \phi \tau d_w \tag{78}$$

where τ is tortuosity, d_w is free water diffusivity (=2.27E-9 m^2/s). From equation (4) we can obtain tortuosity as:

$$\tau = \frac{D_e}{\phi d_w} = \frac{1.21217 \cdot 10^{-10}}{0.43 \times 2.27 \cdot 10^{-9}} \approx 0.124 \tag{79}$$

Cation exchanger composition

In this thesis montmorillonite is the inert cation exchanger and is composed of Mg^{2+}, Ca^{2+}, K^+ and mainly from Na^+. The TOUGHREACT is given the concentration of the initial solution which it uses to calculate the ion exchanger composition. The initial solution concentration has to be calculated beforehand. The exchange reactions are written backwards as other reactions and can be written as follows:

$$\begin{aligned} &Na^+ + KX \rightleftharpoons K^+ + NaX \\ &Na^+ + ½CaX_2 \rightleftharpoons ½Ca^{2+} + NaX \\ &Na^+ + ½MgX_2 \rightleftharpoons ½Mg^{2+} + NaX \end{aligned} \tag{80}$$

where X represents one mole of exchanger. If the exchanger compositions are known (equivalent fractions), the equivalent concentrations of cations are equal to the sum of the equivalent concentrations of SO_4^{2-} and Cl^- and if the exchanger selectivities are given we can obtain the concentrations of the cations. According to Gaines-Thomas mentioned above and using equation (69) we obtain exchange reaction coefficients for cations:

$$\begin{aligned} K^*_{K^+/Na^+} &= \frac{\beta_{NaX}}{\beta_{KX}} \times \frac{a_K}{a_{Na^+}} \\ K^*_{Ca^{2+}/Na^+} &= \frac{\beta_{NaX}}{\beta^{½}_{CaX_2}} \times \frac{a^{½}_{Ca^{2+}}}{a_{Na^+}} \\ K^*_{Mg^{2+}/Na^+} &= \frac{\beta_{NaX}}{\beta^{½}_{MgX_2}} \times \frac{a^{½}_{Mg^{2+}}}{a_{Na^+}} \end{aligned} \tag{81}$$

where β denotes the equivalent fraction of the interlayer cations and a the activity of the dissolved species. The concentrations of each solution species as a function of Na^+ can then be written as:

$$\begin{aligned} \left[K^+\right] &= \frac{\beta_{KX}}{\beta_{NaX}} \times \frac{\gamma_{Na^+}}{\gamma_{K^+}} \times \left[Na^+\right] \times K^*_{K^+/Na^+} \\ \left[Ca^{2+}\right] &= \left(\frac{\beta^{½}_{CaX_2}}{\beta_{NaX}} \times \frac{\gamma_{Na^+}}{\gamma^{½}_{Ca^{2+}}} \times \left[Na^+\right] \times K^*_{Ca^{2+}/Na^+} \right)^2 \\ \left[Mg^{2+}\right] &= \left(\frac{\beta^{½}_{MgX_2}}{\beta_{NaX}} \times \frac{\gamma_{Na^+}}{\gamma^{½}_{Mg^{2+}}} \times \left[Na^+\right] \times K^*_{Mg^{2+}/Na^+} \right)^2 \end{aligned} \tag{82}$$

with electroneutrality relationship:

$$\left[Cl^-\right] + 2 \times \left[SO_4^{2-}\right] = 2 \times \left[Ca^{2+}\right] + 2 \times \left[Mg^{2+}\right] + \left[Na^+\right] + \left[K^+\right] \tag{83}$$

and inserting equations (82) in to equation (83) we get:

$$\frac{2\gamma_{Na^+}^2}{\beta_{NaX}^2}\left(\frac{\beta_{CaX_2}K_{Ca^{2+}/Na^+}^{*2}}{\gamma_{Ca^{2+}}}+\frac{\beta_{MgX_2}K_{Mg^{2+}/Na^+}^{*2}}{\gamma_{Mg^{2+}}}\right)\left[Na^+\right]^2+$$
$$\left(1+\frac{\beta_{KX}\gamma_{Na^+}K_{K^+/Na^+}^{*}}{\beta_{NaX}\gamma_{K^+}}\right)\left[Na\right]^+-\left[Cl^-\right]-2\left[SO_4^{2-}\right] \quad (84)$$

where the concentration of Na^+ has to be solved. This equation can be solved with the quadratic equation ($ax^2+bx+c=0$):

$$\left[\mathrm{Na}^+\right]=\frac{b\pm\sqrt{b^2-4ac}}{a^2} \quad (85)$$

where

$$a=\frac{2\gamma_{\mathrm{Na}^+}^2}{\beta_{\mathrm{NaX}}^2}\left(\frac{\beta_{\mathrm{CaX_2}}K_{\mathrm{Ca}^{2+}/\mathrm{Na}^+}^{*2}}{\gamma_{\mathrm{Ca}^{2+}}}+\frac{\beta_{\mathrm{MgX_2}}K_{\mathrm{Mg}^{2+}/\mathrm{Na}^+}^{*2}}{\gamma_{\mathrm{Mg}^{2+}}}\right)$$
$$b=\left(1+\frac{\beta_{\mathrm{KX}}\gamma_{\mathrm{Na}^+}K_{\mathrm{K}^+/\mathrm{Na}^+}^{*}}{\beta_{\mathrm{NaX}}\gamma_{\mathrm{K}^+}}\right) \quad (86)$$
$$c=-\left[\mathrm{Cl}^-\right]-2\left[\mathrm{SO}_4^{2-}\right]$$

With this concentration of natrium we can solve equations (82) and keeping electron neutrality define the initial water concentrations for these cations and anions to get the right ion exchanger composition at the beginning. For low ionic strength, which in this case is $\left[\mathrm{Cl}^-\right]+2\times\left[\mathrm{SO}_4^{2-}\right]$ (for example 1E-5), the activity coefficient is approximately 1 and equation (72) can be simplified.

The values for exchange coefficients are given, for example, in [42]. However, these are for direct reaction and the relationship for *K* given in [42] and for PetraSim *K* is shown below:

$$\begin{cases} K^*=\dfrac{1}{K} & \text{for monovalent cations} \\ K^*=\dfrac{1}{\sqrt{K}} & \text{for divalent cations} \end{cases} \quad (87)$$

These *K* and K^* values are given and calculated in Table 2.1.

Table 2.1. Cation-exchange coefficients for MX-80 [42].

Log selectivity		**K**		**PetraSim K***	
log $K_{Na/K}$	0.60	$K_{Na/K}$	3.981	$K_{K/Na}$	0.251
log $K_{Na/Ca}$	0.41	$K_{Na/Ca}$	2.570	$K_{Ca/Na}$	0.624
log $K_{Na/Mg}$	0.34	$K_{Na/Mg}$	2.188	$K_{Mg/Na}$	0.676

3. Experimental concept

The LOT test experiment A2 parcel and its results were used in this Master of Science thesis as reference data. In the LOT experiments, relatively small test parcels are exposed to field conditions at Äspö HRL. Figure 3.1 is a conceptual figure of the KBS-3V disposal concept for spent fuel, the behaviour of which the LOT experiment is supposed to simulate. The LOT test series includes three test parcels with similar conditions to those in a Kärnbränslesäkerhet-3 (KBS-3V) repository and four test parcels with adverse conditions [17].

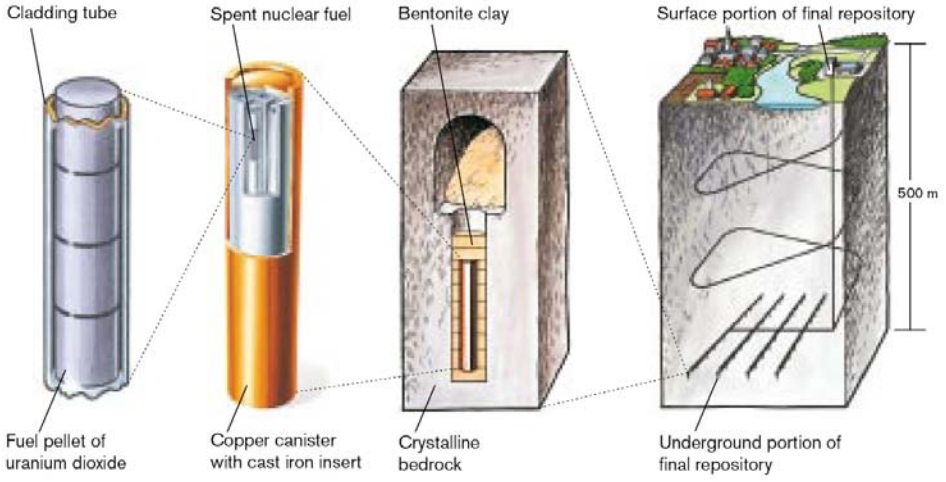

Figure 3.1. The KBS-3V disposal concept for spent nuclear fuel of nuclear wastes. [20].

The A2 parcel is an adverse conditions parcel. Adverse in this case refers to conditions that accelerate alteration processes (higher temperature and higher temperature gradient). The A2 parcel was placed in a vertical borehole in granitic rock. After approximately five to six years' exposure, the test parcel was

lifted and partitioned for examination. The results of these examinations were used as a reference for the modelling in this work. The test parcel dimensions were smaller compared to the KBS-3V deposition hole in order to shorten the water saturation period, to achieve a higher temperature gradient over the buffer material and to ease lifting of the test parcel. [17]

Adverse conditions were used because the alteration processes in bentonite buffer are predicted to be very slow under KBS-3 repository conditions. Adverse conditions in this case mean higher temperature and higher temperature gradient. The standard maximum temperature limit for final disposal repositories is 90°C. In the A2 test, the maximum temperature was set to 120–150°C. A 5-year period in these conditions covers a significant proportion of the thermal load in a KBS-3V repository. The higher temperature conditions also accelerate kinetically controlled, slow processes. The temperature evolution in the A2 test is shown in Figure 3.2.

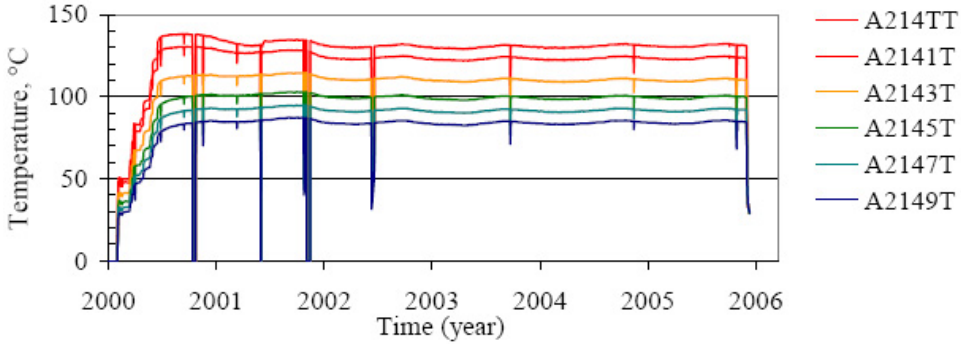

Figure 3.2. Temperature results from the thermocouples in LOT A2 test. Uppermost curve shows the temperature at the copper tube surface, and the underlying curves show the temperatures of points successively 2 cm closer to the rock. The lowest curve represents a point approximately 1 cm from the rock [17, p. 25].

Test site description

The test site depth was around 450 m from the surface. The rock consists mainly of Äspö diorite. The A2 hole was 8 meters deep and was situated 33 meters from the tunnel entrance. The water pressure was kept higher than the vapour pressure at the test temperature and the water inflow rate low enough to prevent piping erosion. As this rate of water inflow was too low, it was decided to introduce external water via a supply hole. The water pressure in the hole was about 1.2

MPa. The water was injected into the test hole through titanium tubes. This pressure was kept constant throughout the test period. [17]

The test hole diameter was 300 mm and it was measured to exceed 300 mm by up to 10 mm in some parts. The central tube was made of copper in order to simulate the KBS-3V test parcel and keep as realistic chemical conditions as possible. The copper tube had a length of 4700 mm, an inner diameter of 100 mm and a wall thickness of 4mm. The bentonite cylinder diameter was 280 mm and height 100 mm when installed. Thus the bentonite thickness was approximately 96 mm ± 10 mm after swelling. The test parcel was situated at 450 m depth from the surface and the hole was 4 m deep. The test parcel is illustrated in Figure 3.3. [17]

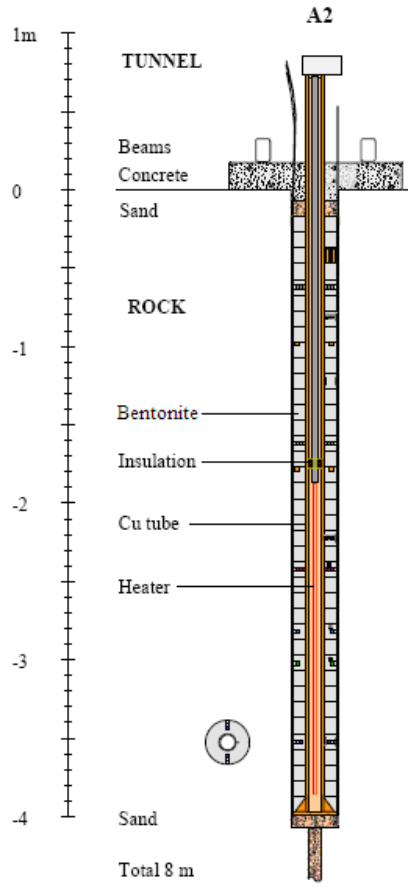

Figure 3.3. Scaled schematic drawing of the A2 test parcel [17, p. 21].

4. Modelling concept

The chemical phenomena occurring in the bentonite barrier in a spent fuel repository depend on numerous factors, such as the rate of iron corrosion, the reaction temperature, the composition of the interaction fluid, the diffusion coefficients of the solutes, and the reactive surface area of minerals, etc.

Owing to the complexity of their estimation and mutual couplings, consideration of all of these parameters within a single model remains highly challenging. Certain simplifications must, therefore, be made. The model presented in this section is a simplified model, and its limitations as such must be recognized.

It is assumed that three phases (solid, liquid and gas) are present in the modelled porous medium. The basic component of the solid montmorillonite is assumed to be insoluble but able to absorb ions and exchange them with solution. Precipitated minerals are assumed to be part of the solid phase. The gas phase consists of water vapour and air, while the liquid phase consists of water, dissolved air and other dissolved species. Local equilibrium is assumed for all the chemical reactions excluding mineral reactions with kinetics. Equilibrium is a limiting case for kinetics when mass transport is slow compared to reaction rates.

The model was created using the PetraSim user interface of the TOUGH2 and TOUHGREACT programs. The applied model is a coupled thermo-hydro-chemical model, meaning no mechanical alterations and effects are considered. The purpose of the model was to match the results as closely to the experimental results as possible, and thus the time frame was limited to 10 years (the LOT A2 parcel test duration was approximately 6 years). A conceptual figure of the model in this thesis can be seen in Figure 4.1. BC in the figure means boundary condition and IC initial condition.

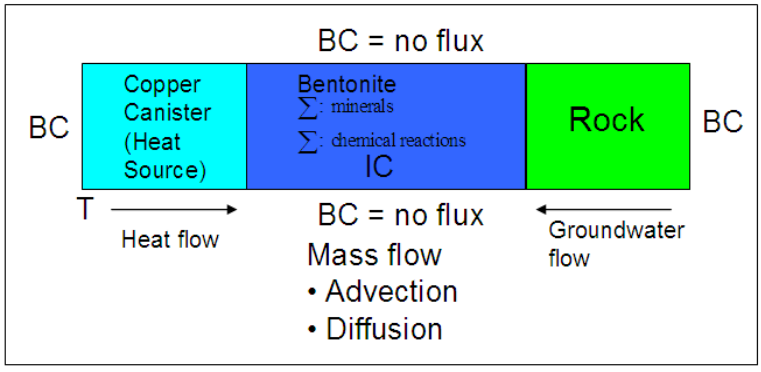

Figure 4.1. Conceptual model of THC modelling in the thesis.

4.1 Model purpose

The experimental part of this thesis was the modelling of the LOT parcel test A2. The goal was to obtain results as near as possible compared to the results of the parcel test A2. After getting a sufficient match between the test and the model the results could be compared and analyzed. Thus, a glimpse could be seen of what the thermal evolution of minerals and chemistry will look like in a repository. The model also serves as a database for comparing more complex models and their results to each other.

The final purpose in the future is to continue to model the real repository for up to thousands of years. Thus we could see the chemical evolution during the thermal phase of the final repository and how temperature, chemistry and water affect each other and the bentonite during this stage. This will be useful information for modellers continuing the modelling of glacial erosion, as well as for the SKB and POSIVA which are soon preparing disposal of the highly active waste in the bedrock.

4.2 Model construction

TOUGHREACT was used to model the reactive unsaturated mass transport processes in 1-D, and the grid was pitched at uniform intervals. The model constructed was a simplified one. The idea was to simplify the real 3-D model in which the copper canister producing heat is surrounded by bentonite and the rock matrix in which there is an intersecting water-conducting fracture. Figure 4.2 shows a fracture cutting the bentonite-copper canister system in the SKB-3 repository and a more detailed figure of the bentonite surrounding the canister.

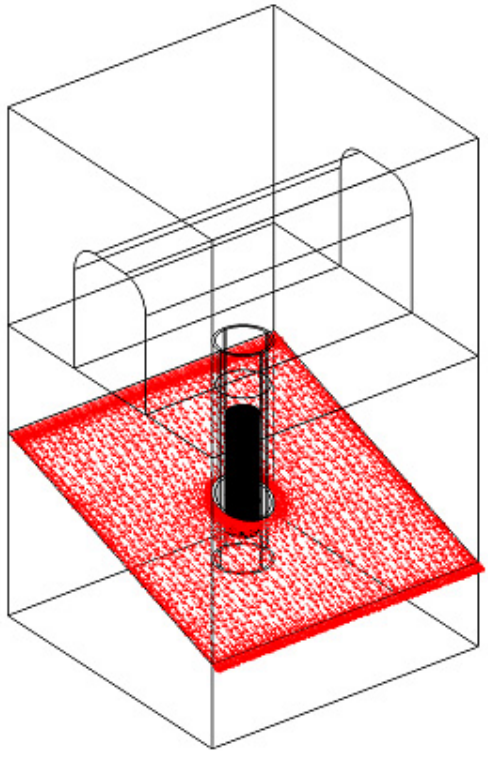

Figure 4.2. 3-D model of the disposal site with zoom in. The water velocity field is represented by red arrows. The dimensions of the system are: copper canister: radius = 0.53 m, height 4.8 m; bentonite: thickness = 0.35 m, height = 1 + 4.8 + 1 m; rock block: 10 m x 10 x 8 m.

Figure 4.3 shows a 2-D model of the bentonite, copper canister and the fracture. The model can be simplified to two dimensions because the changes in the bentonite are highest at the location of the fracture and become smaller further away. Thus the worst possible scenario is along the fracture surface.

The two black lines in the middle of the picture describe the next simplification. The model used in this thesis is a 1-D model and it is simplified from the 2-D model. The diffusion gradient and the water flow affecting the bentonite are highest in the fracture location and diminish with increasing distance. Thus the worst possible scenario is at the position in which the water coming from the fracture meets the bentonite interface. Figure 4.4 shows the constructed model and the mesh created with PetraSim.

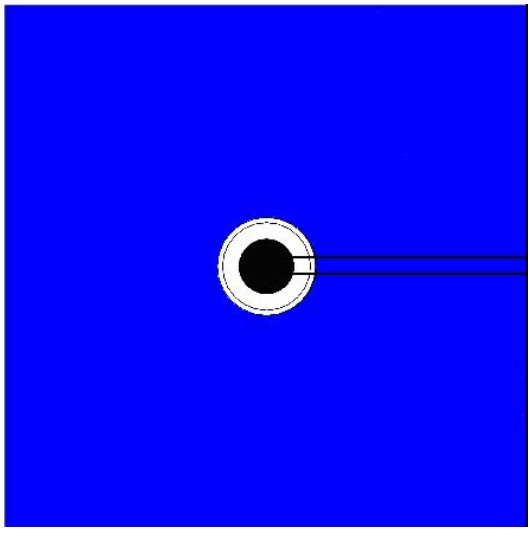

Figure 4.3. 2-D picture along the fracture cutting the granite matrix and surrounding the bentonite-copper canister system.

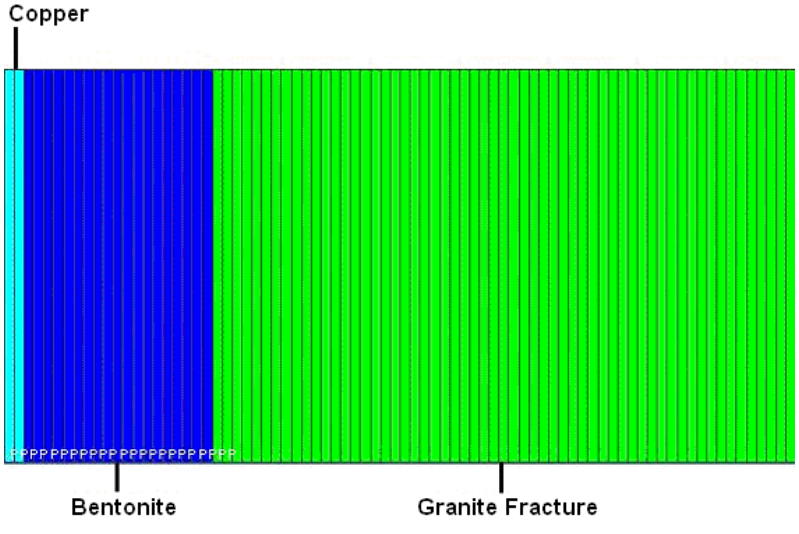

Figure 4.4. 1-D grid with 80 pitched cells at uniform intervals.

Whereas the grid is simple, the phenomena at play within an actual system of this type are complex. The light blue cell on the left represents the heat source, i.e. the heat coming from the decay of spent fuel and the inert copper canister (1 cm). The green zone is granitic rock (29.5 cm) containing relatively free mov-

ing water. The dark blue zone is the bentonite (9.5 cm), which is initially partially saturated or virtually dry. The rightmost cell is a magnified water source. As such, the chemistry and water concentration in that cell remains constant. The bentonite has an initial water, mineral content and cation-exchange capacity, and it interacts with the granitic Äspö groundwater outside the bentonite block. The copper canister is inert, excluding its heat production. A simplified figure from Fig. 4.4 describes the model which is represented in Figure 4.5.

In the model the bentonite was dry at the beginning and saturation took place during one year (this was the case in the A2 test). Step to step instructions for all the choices and making this kind of model with PetraSim are given in Appendix A.

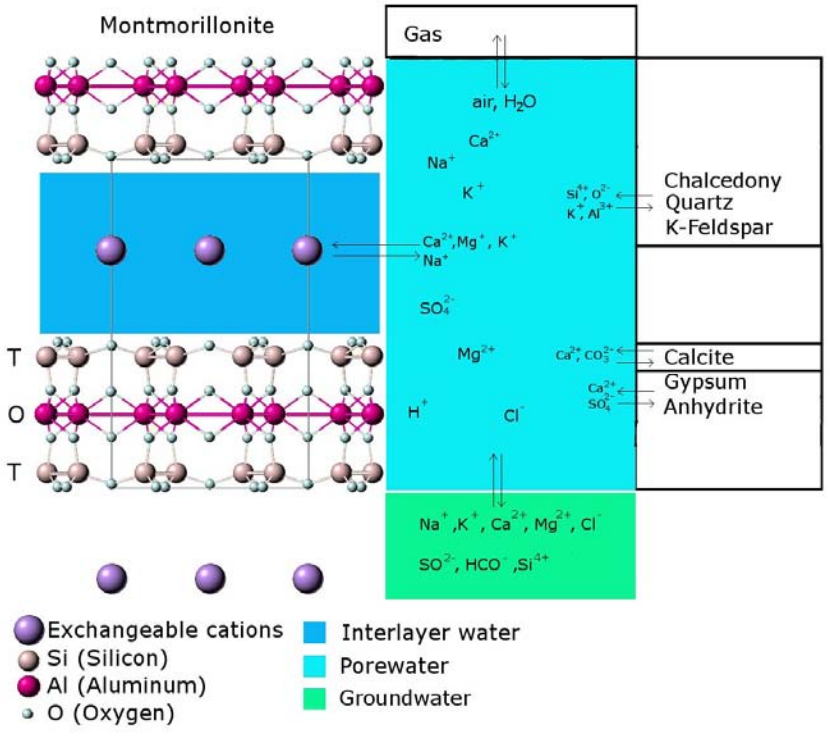

Figure 4.5. Schematic illustration of geochemical equilibrium processes in bentonite-water system in the model used.

4.3 Model parameters

The model parameters for these models were taken from different sources. Some of the parameters were approximated according to the data. There are a lot of parameters that have to be taken into account. In Table 4.1 the material parame-

ters are given, and in Table 4.2 the wetting parameters needed for the model. The water retention parameters for the fracture were set for constant saturation of the rock. The calculation methods are not discussed in this chapter, only the data used in the model.

Table 4.1. Material parameters used in the model for bentonite, granitic crack and copper [4, 15, 17, 38].

Parameter	**Bentonite**	**Granite fracture**	**Copper**
Pressure [Pa]	NTP	$1.20 \cdot 10^{6}$	NTP
Cation-exchange capacity [meq/100g]	75		
Grain density [kg/m^3]	2750	2650	8960
Diffusion coefficient m^2/s	$2 \cdot 10^{-9}$		
Wet Heat Conductivity [W/(mC)]	1.3	2	2
Dry Heat Conductivity [W/(mC)]	0.3		
Porosity	0.43	0.14	0.01
Intrinsic Permeability [m^2]	$3.00 \cdot 10^{-21}$	$5.00 \cdot 10^{-11}$	0
Tortuosity	0.124	0.2	
Specific Heat [J/(kgC)]	2500	784	385

Table 4.2. Water retention parameters: van Genuchten for the bentonite and Fatt&Klikoff for the granite fracture [15].

	Bentonite	**Granite Crack**
λ	0.338	
S_{lr}	0.1	0.999
S_{ls}	1	
S_{gr}	0	
P_0	14.12 MPa	
P_{max}	140 MPa	

Besides the material parameters, chemical data was needed for the model. Table 4.3 shows the bentonite mineral volume fractions in the model. Siderite and Pyrite are omitted for simplicity from the final model and their volume fractions are added to montmorillonite. In other words, the bolded minerals are assumed

to be montmorillonite. The mineral kinetics data are represented in Table 4.4. Reaction order n is given with respect to H^+.

Table 4.3. Mineral data: mass fractions, densities, masses, volumes and volume fractions in the bentonite. [3]

Minerals	**Mass fraction [%]**	**Density [g/cm^3]**	**Mass [g]**	**Volume [cm^3]**	**Volume fraction**
Gypsum $CaSO_4 \cdot 2(H_2O)$	0.17	2.30	1.335	0.580	0.0012
Anhydrite CaSO4	0.17	2.97	1.335	0.449	0.0009
Quartz SiO2	15.00	2.62	117.751	44.943	0.0897
Montmorillonite $Na_{0.2}Ca_{0.1}Al_2Si_4O_{10}(OH)_2(H_2O)_{10}$	75.00	2.80	588.753	210.269	0.4199
K-Feldspar $KAlSi_3O_8$	7.00	2.57	54.950	21.381	0.0427
Calcite $CaCO_3$	0.70	2.71	5.495	2.028	0.0040
Siderite $FeCO_3$	0.70	3.96	5.495	1.388	0.0028
Pyrite FeS^2	0.30	5.01	2.355	0.470	0.0009
Chalcedony SiO_2 (crystalline)	0.96	2.62	7.536	2.876	0.0057
Sum	100		785	284.385	0.568

Table 4.4. Mineral kinetics, rate parameters, activation energies for neutral, acidic and alkaline conditions, surface areas and grain radius used in the model [25; 38].

Minerals	**$K_{neutral}$**	**$E_a^{neutral}$ [kJ/mol]**	**K_{acid}**	**E_a^{acid} [kJ/mol]**	**n_{acid}**	**$K_{alkaline}$**	**$E_a^{alkaline}$ [kJ/mol]**	**$n_{alkaline}$**	**Surface areas (cm^2/g)**	**Grain radius**
Gypsum	0.0016218	0							9.8	0.001
Anhydrite	0.0006457	14.3							9.8	0.001
Quartz	3.981E-14	90.9							9.8	0.001
Chalce-dony	equilibrium								9.8	0.001
K-Feldspar	3.89E-13	38	8.71E-11	51.7	0.5	6.31E-22	94.1	-0.823	9.8	0.001
Calcite	1.549E-06	23.5	0.5	14.4	1	0.0003			9.8	0.001

The bentonite porewater and granitic groundwater compositions were also needed for the initial state and these values are given in Table 4.5. The cation

exchanger composition is given as equivalent fractions. The bentonite porewater was chosen so that the ion exchanger was initially filled correctly [39].

Table 4.5. Granitic groundwater composition, bentonite porewater composition and ion exchanger composition [17, 39, 42].

Variable	Groundwater composition [mmol/l]	Bentonite porewater composition [mmol/l]	Cation exchanger composition (equivalent fractions/[meq/100g])
pH	6.9	8.62	
Na^+	100	$9.972 \cdot 10^{-4}$	0.808/60.6
K^+	0.28	$2{,}79 \cdot 10^{-7}$	0.009/0.675
Ca^{2+}	47.3	$7.603 \cdot 10^{-11}$	0.128/9.6
Mg^{2+}	2.4	$3{,}838 \cdot 10^{-11}$	0.055/4.125
Cl^-	178	$1 \cdot 10^{-3}$	
$SO4_2^-$	4.6	traces	
HCO_3^-	0.44	traces	
Al^{3+}	traces	traces	
H_4SiO_4(aq)	traces	traces	
O_2(aq)	traces	traces	

4.4 Modelling Program

The modelling program used was PetraSim v. 4.1.0219. PetraSim is a user interface that is an interactive pre/post-processor for the TOUGH2, T2VOC, TMVOC, TOUGHREACT, TOUGH-Fx/HYDRATE and TETRAD simulators. PetraSim helps users to develop models and view results of models based on (TOUGH2) non-isothermal flows of multi-component/-phase fluids in one, two, and three-dimensional porous and fractured media. T2VOC and TMVOC include three-phase flows of water, air and volatile organic chemicals. The TOUGHREACT adds chemical reactions to PetraSim and the TOUGH-Fx/HYDRATE the capability to represent methane hydrates. [38]

Only two of the mentioned programs were used. The TOUGH2 was used for non-isothermal flows and TOUGHREACT was used to handle chemical reactions in a simplified system. PetraSim is a capable tool for simulating the final reposi-

tory but the code is sometimes unstable and the user manual is unfocused and very brief. In addition it lacks the tools to construct realistic and modern geometries.

A newer version of the PetraSim (4.2.1118) user interface, which uses newer versions of TOUGH2 and TOUGHREACT, is also available, but we were unable to produce consistent results with this version. The newer version produced a number of anomalous results and the cation exchanger compositions were also calculated apparently incorrectly. The reasons for this are being studied.

4.5 Equation of state modules

Equation of State Modules (EOS) are different modules in TOUGH2 and TOUGHREACT. These modules specify the governing mass- and energy-balance equations for the fluid mixtures. Besides this these modules describe the fluid system and its variables. Different fluid mixtures are described by different EOS modules [28]. The ones used in this thesis are described below. Only one EOS was used in this thesis, which was EOS 3 (water, air). EOS 3 can model both air and unsaturated water flow together.

EOS 3 was used for the unsaturated model in this thesis. In this module air is supposed to behave like an ideal gas and additivity is assumed for air and vapour partial pressures in the gas phase ($P_g = P_{air} + P_{vapour}$). The solubility of air in water is represented by Henry's law [28]:

$$P_g = k_H c \tag{88}$$

where k_H is Henry's constant and in TOUGH2 it is assumed to be constant 10^{10} Pa. P_g is gas pressure and c is concentration.

EOS 3 differs from other EOS mainly by choice of primary thermodynamic variables. Normally in TOUGH for single-phase we have (P, T, X) and for two-phase (P_g, S_g, T). Here in EOS 3 for single-phase it is (P, X, T) and for two-phase (P_g, S_g+10, T). This is the choice because both X and S_g vary over the range (0,1) and thus we could not separate the distinction between single and two-phase conditions, but by setting the S_g value between 10 and 11 the two can be separated from each other. [28]

4.6 Limitations and simplifications

This section describes the limitations applied to the creation of the model.

4.6.1 Chosen limitations

1. The calculation time of the model was limited to 10 years as the principal aim was to obtain calculated results that were as close as possible to the measured values, and because the LOT A2-parcel test duration was approximately 6 years.
2. Montmorillonite was chosen as the insoluble solid phase with constant ion-exchange capacity.
3. The calculations were carried out in one dimension to simplify the system. The grid was thus created with one cell only in the y and z directions and multiple cells in the x direction.
4. It was assumed that the bentonite was already swelled to fill the hole completely at the beginning and that the saturation did not cause swelling anymore.

4.6.2 Model limitations

Many physical and chemical phenomena cannot be taken into account in the PetraSim model.

1. A major source of uncertainty is the fact that the model does not take into account the three different water types present in bentonite: the interlayer water, double layer water and free water. The model assumes that all water content is accessible to solutes for mass transport and geochemical reactions.
2. THC predicted concentrations systematically overestimate the measured values near the heater and show probably sharper gradients than those of the measured data. This is because the model does not take into account bentonite swelling/shrinkage (or water evapouration near the copper-bentonite interface).
3. TOUGHREACT does not include surface complexation, which consists of protonation/deprotonation of surface edge sites.

4. Even though THC processes are expected to alter the capillary strength parameter (1/α), this effect has not been included in these models.
5. The diffusion coefficient is assumed constant for all ions and neutral molecules.
6. Swelling and rock mechanics are not included.
7. All material parameters are constant, and functions such as temperature cannot be added.
8. The model was 1-D, whereas a realistic model should be 3-D.

4.6.3 Data limitations

There are also lots of data needed which is not yet thoroughly studied.

1. General lack of kinetic data for environmental and geochemical processes is a major drawback. Laboratory-based values are not necessarily applicable to the field situation.
2. It is not well understood how to handle the lack of equilibrium among redox couples [44].
3. Reactive surface areas and grain radii of minerals are highly uncertain owing to lack of data.
4. Uncertainties in thermodynamic data, especially at higher temperatures, may exist.
5. Van Genuchten function parameters for partial saturation in rock and bentonite are not well known, and no data is given for different temperatures.

5. Results

The results obtained were fairly realistic and there was a clear similarity between the model and experimental results. The obtained results were so numerous that they can be addressed here in part only. The figures in this chapter are made from tables constructed by TOUGHREACT. The results are shown in figures in this chapter as a function of distance over time. The tables would have been added to the Appendices, but the table sizes are so enormous that they would take tens of pages. There are 12 different time steps taken from the 10-year period. We should remember here that the first 9.5 cm is bentonite and after that the material is rock.

5.1 Properties

This section deals with the evolution of the bentonite properties and partly rock properties. A number of key properties were given special attention. The bentonite pressure with evolving capillary pressure generates suction so that the bentonite remains saturated. The bentonite pressure evolution is tabulated in Appendix B.

The bentonite was shown to saturate 96% within approximately a 1-year period, which correlates closely with the LOT test report [17, p. 25], in which the bentonite was fully water saturated after less than 2 years. There is also water vapour near the copper surface. The initial saturation in bentonite is 40% of porosity and in the granitic fracture part 100%. Figure 5.1 shows the modelled movement of the saturating water front.

Figure 5.2 shows the modelled (compare to Figure 3.2) temperature and temperature gradient in the bentonite and part of the rock matrix. As can be seen, the temperature gradient is approximately 4.7 ^{o}C/cm and the temperature 130–85 ^{o}C in the bentonite. Temperature is after a certain time balanced to 130 ^{o}C near the heater (copper canister) and to 85 ^{o}C near the cold granitic rock surface.

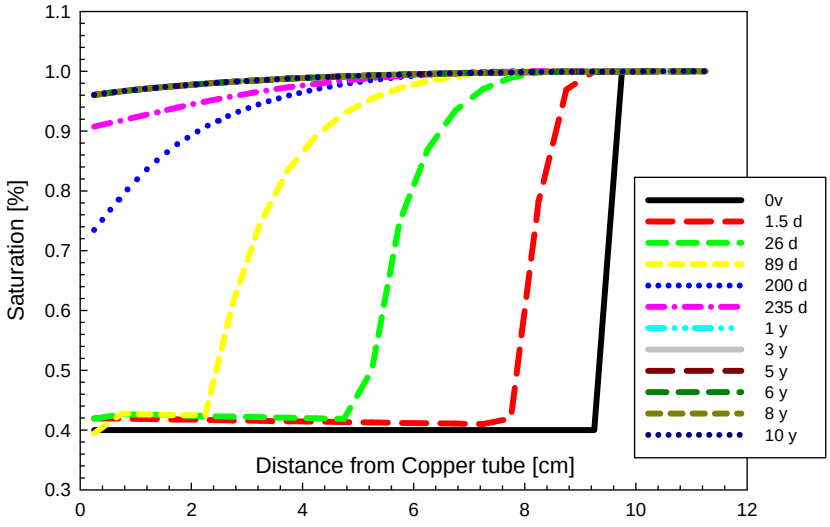

Figure 5.1. Saturation as a function of distance from the copper tube, over time.

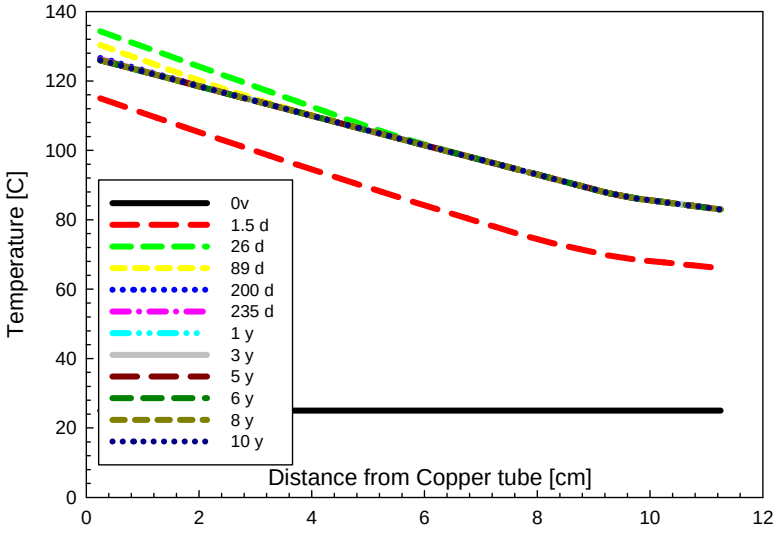

Figure 5.2. Temperature evolution as a function of distance from the copper tube, over time.

At the beginning the pH is 8.3 (Figure 5.3) in bentonite and 7.7 in the granitic crack. However after the temperature rises the water ionic product gets bigger which lowers the pH. Also it seems that the pH in bentonite balances with the granitic water pH. The bentonite should buffer the pH changes, however surface complexation is excluded from the model and it does not do so.

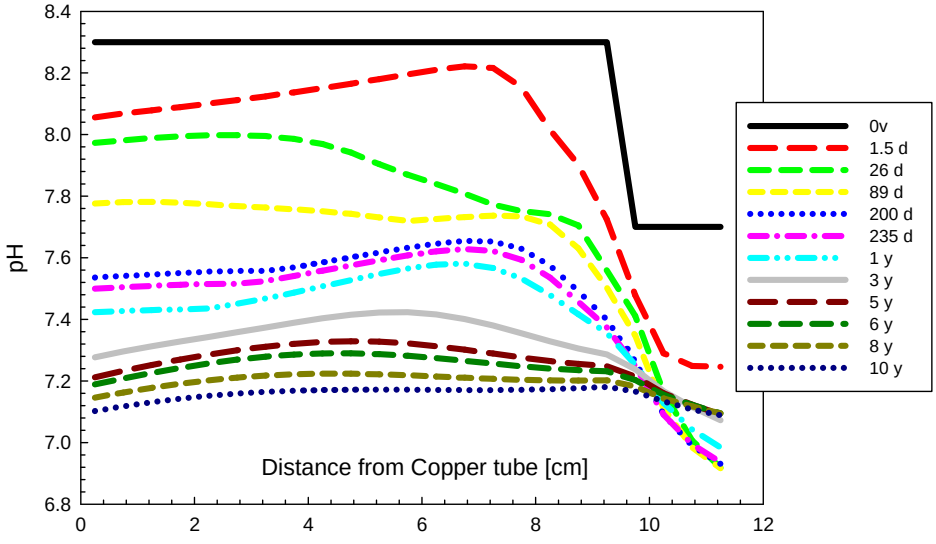

Figure 5.3. Evolution of pH as a function of distance from the copper tube, over time.

The porosity changes are shown in Figure 5.4. As can be seen, the porosity changes are highest near the heater surface but very small even there. The porosity changes are only 0.1% even near the heater and thus the induced changes effects on flow are also minimal. The porosity is defined as the porous volume/bentonite volume.as the porous volume/bentonite volume.

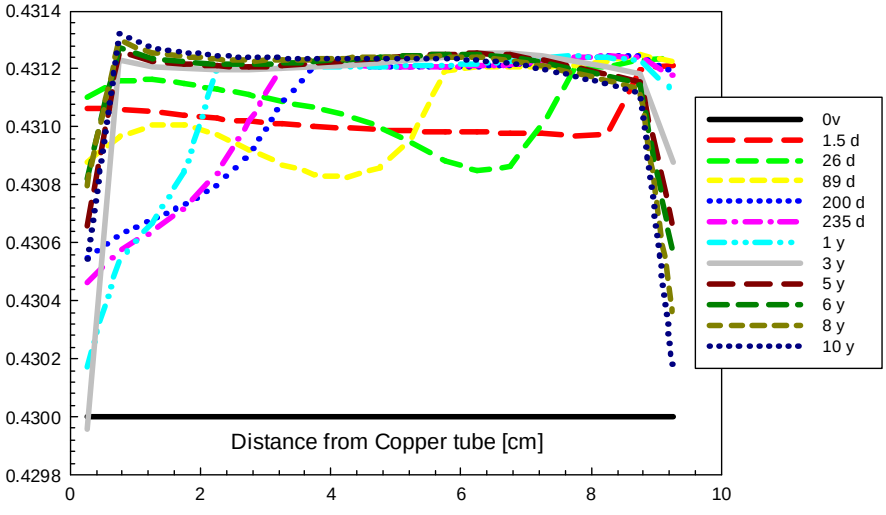

Figure 5.4. Porosity changes as a function of distance from the copper tube, over time.

5.2 Minerals

Chalcedony (SiO_4) (Figure 5.5) is in equilibrium and some equilibrium processes occur with H_4SiO_4(aq), which increases towards the heater where chalcedony is dissolving. Minor precipitation also occurs near the rock surface. Some calcite (Figure 5.6) appears to dissolve near the copper (heat source) surface, thus affecting the concentrations of calcium and carbonate ions. Gypsum (Figure 5.7) dissolves within a couple of days. Quartz and K-feldspar are almost stable during the whole test period. The kinetics of quartz and K-feldspar are slow and thus they would need a lot longer time period to be dissolved/precipitated. The results of these minerals can be seen in the tables in Appendix B, where the minor precipitation of quartz both in the bentonite and the rock side near the bentonite/rock surface can be seen.

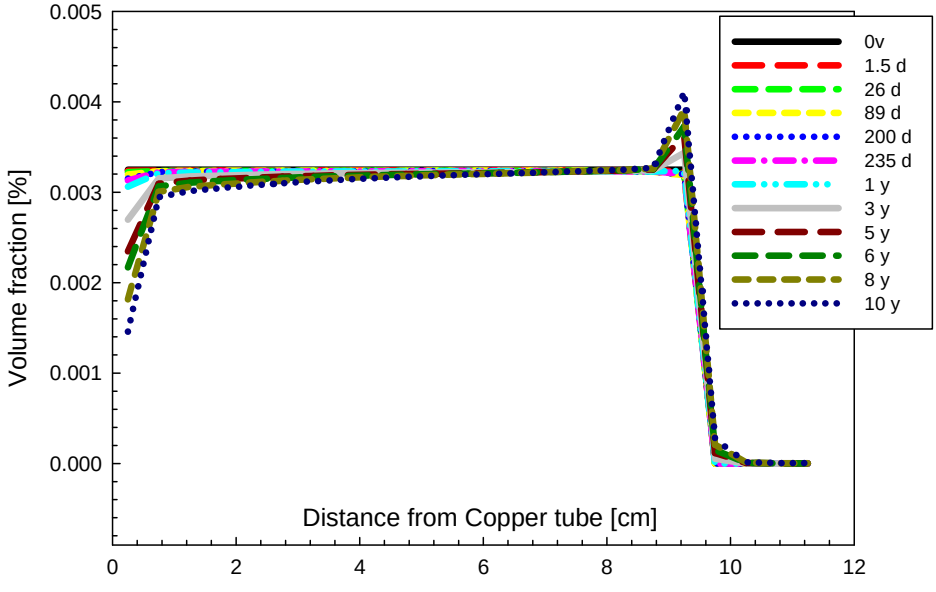

Figure 5.5. Chalcedony volume fractions as a function of distance from the copper tube, over time.

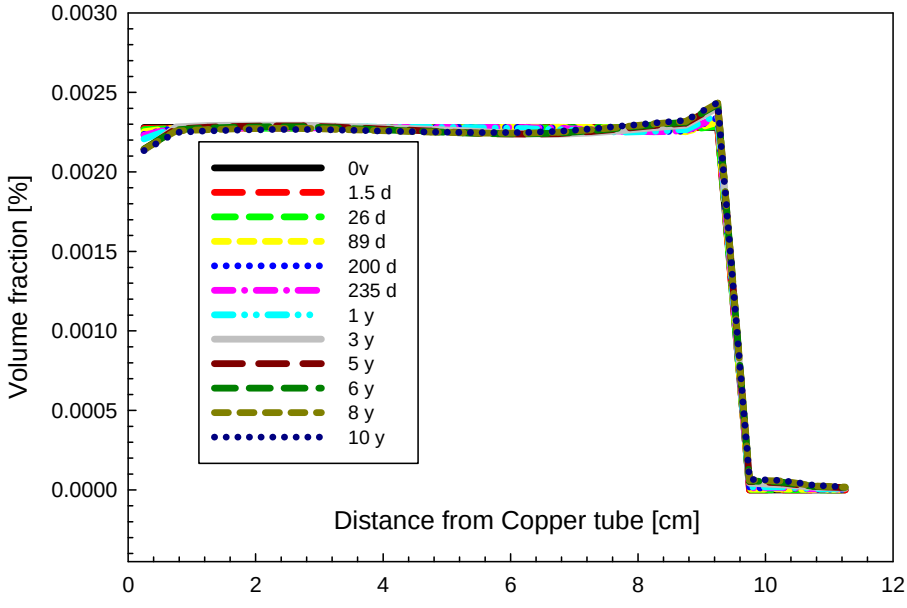

Figure 5.6. Calcite volume fractions as a function of distance from the copper tube, over time.

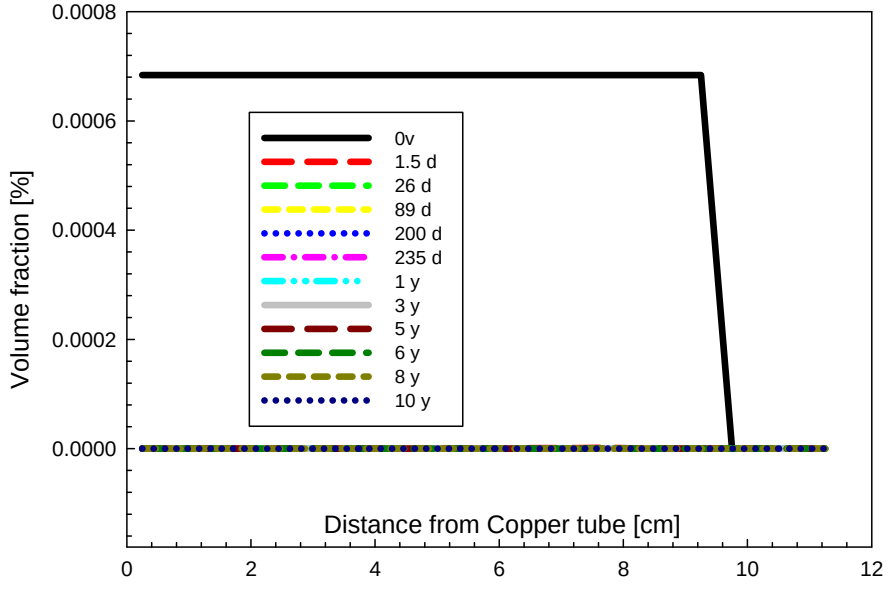

Figure 5.7. Gypsum volume fractions as a function of distance from the copper tube, over time.

The most interesting of the minerals was, however, anhydrite. Figure 5.8 shows the anhydrite profile. It appears that when sulphate is diffusing out and calcium is coming in anhydrite precipitates near the rock surface. Anhydrite also starts to precipitate near the copper surface due to high temperature.

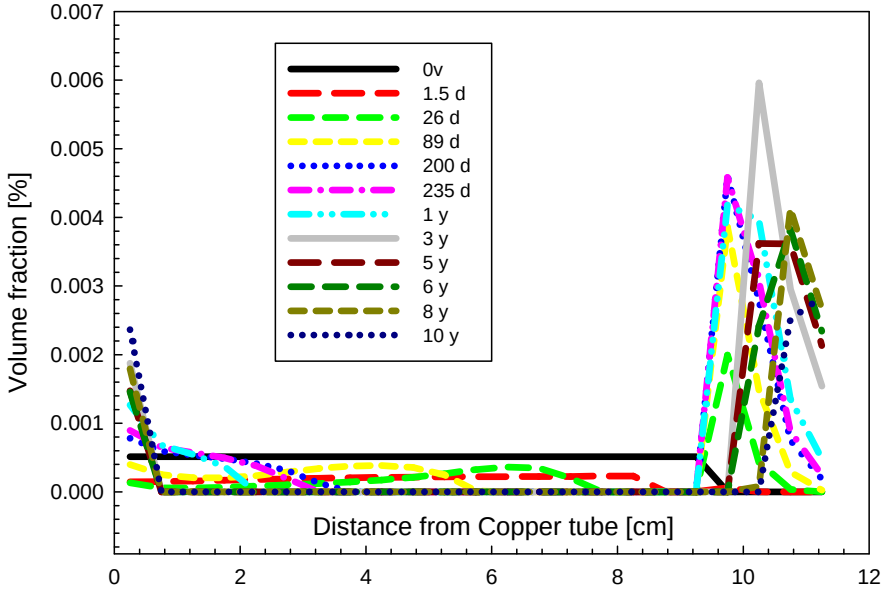

Figure 5.8. Anhydrite volume fractions as a function of distance from the copper tube, over time.

5.3 Primary species

This section covers the species concentration evolution in bentonite and part of the granitic rock part during 10 years. These concentrations are total aqueous component concentrations including all the dissolved components like $CaCl_2$ (aq), $CaSO_4$(aq) etc., where these primary species are included. The main primary species affecting the system were: Na^+, Mg^{2+}, Ca^{2+}, K^+, Cl^-, SO_4^{2-} and HCO_3^-. Other species present are only traces and are not discussed here, but are shown in Appendix B.

Figure 5.9 shows the total sulphate (SO_4^{2-}) ion concentration evolution in the bentonite and granitic rock. Here, total means that even sulphate-containing minerals (gypsum and anhydrite) are included in these concentrations proportioned to water amount in fully saturated bentonite. This figure appears to follow the precipitation of anhydrite. After a few days a rise in concentration appears but this is due to dissolved gypsum and the trend is balanced later on.

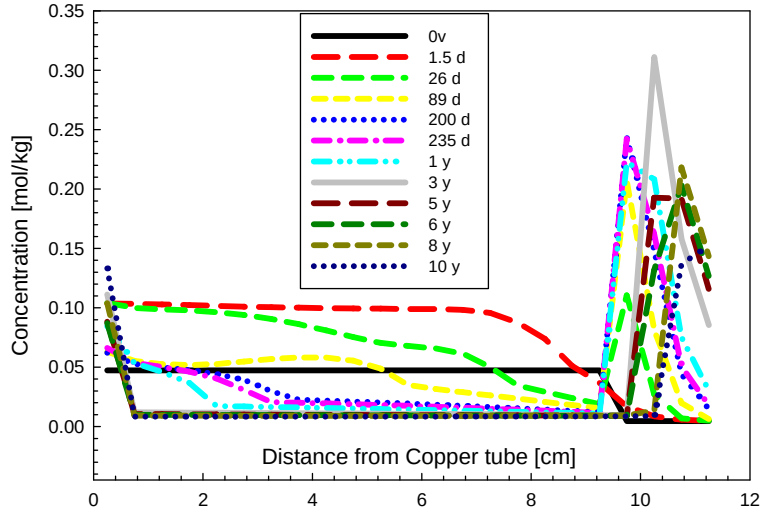

Figure 5.9. Total sulphate concentrations as a function of distance from copper tube, over time.

The calcium profile (Figure 5.10) shows calcium diffusing from groundwater to the bentonite. However, the diffusion has not yet reached equilibrium and would continue even after 10 years.

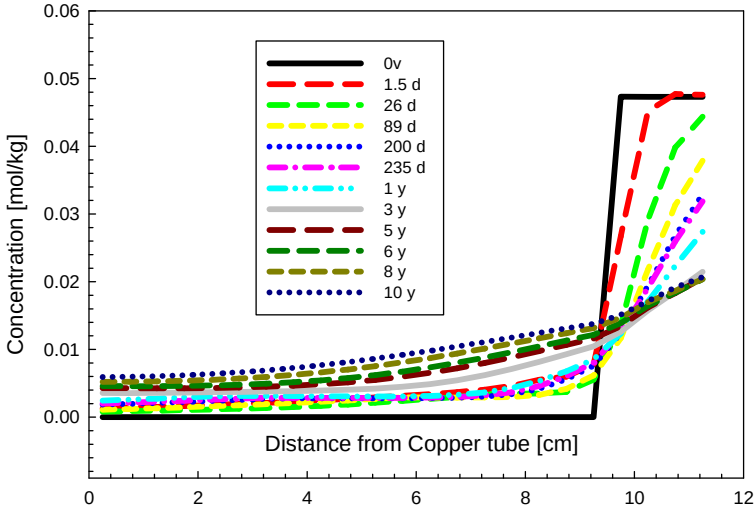

Figure 5.10. Total aqueous calcium component concentrations as a function of distance from the copper tube, over time.

Chloride concentration (Figure 5.11) increases with saturation and diffusion continues, although the diffusion profile is slightly anomalous compared to the boundary conditions.

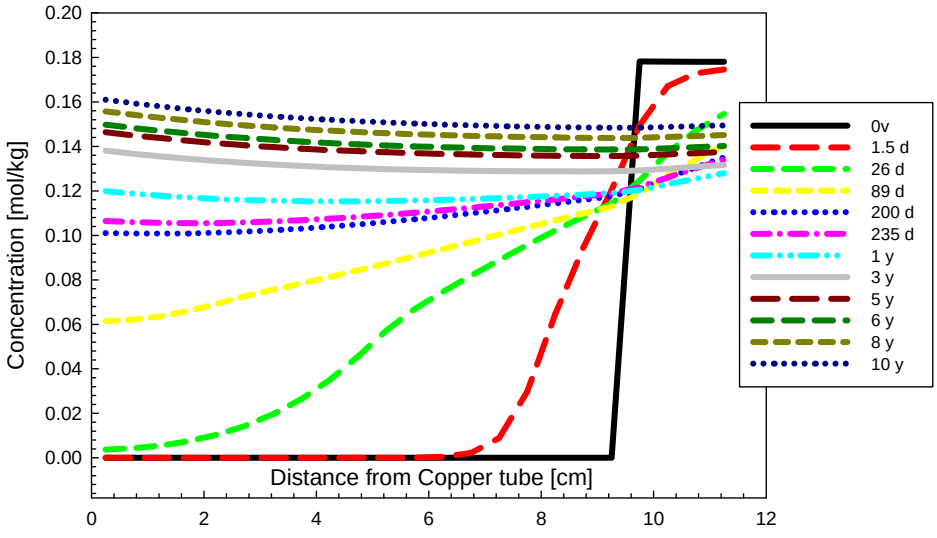

Figure 5.11. Total aqueous chloride component concentrations as a function of distance from the copper tube, over time.

The H_4SiO_4(aq) concentration (Figure 5.12) rises soon after the start of the modelling time and this is because chalcedony dissolves near the heater and begins to diffuse towards the rock surface. See mineral section 5.2.

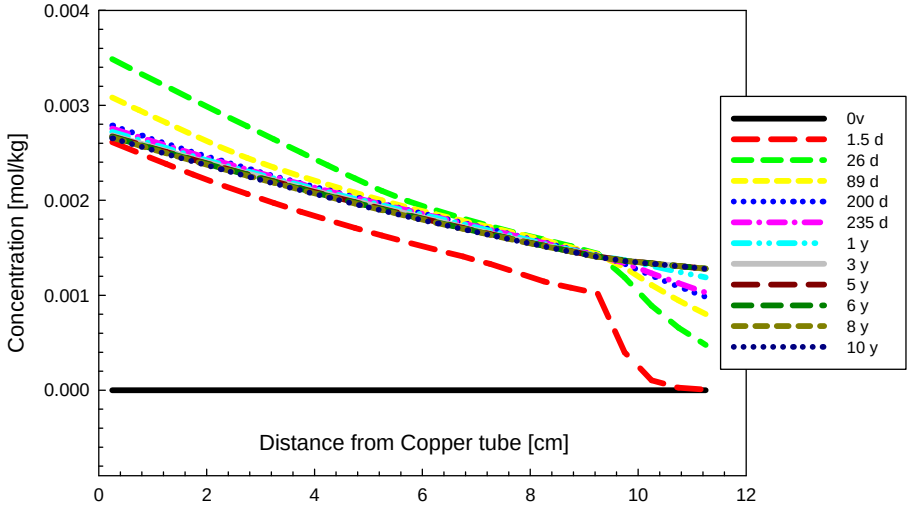

Figure 5.12. H_4SiO_4(aq) species concentrations as a function of distance from the copper tube, over time.

HCO_3^- rises (Figure 5.13) as saturation proceeds. Also the calcite dissolution near the heater increases in concentration at the beginning. However, over time the diffusion balances the concentration even when the dissolution of calcite continues and the diffusion flux is outwards from bentonite. Result is near the experiment (see Appendix C).

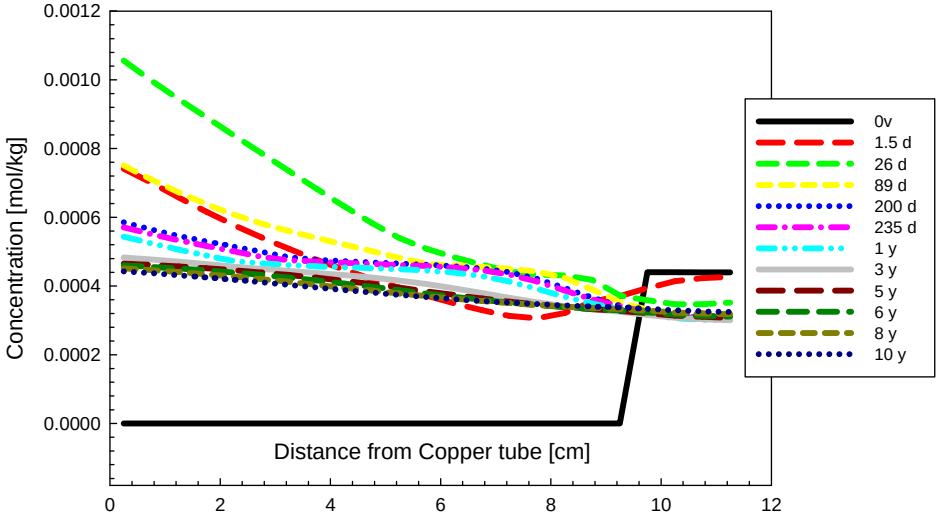

Figure 5.13. HCO3- species concentration as a function of distance from copper tube, over time.

Magnesium and potassium concentrations (Figures 5.14 and 5.15) in the bentonite increase due to saturation and cation exchange. The diffusion is at first from groundwater to porewater, but later the direction of diffusion changes outwards to the rock matrix as the concentration in the bentonite exceeds that of the groundwater due to cation exchange. These values are very near to the experimental values (see Appendix C).

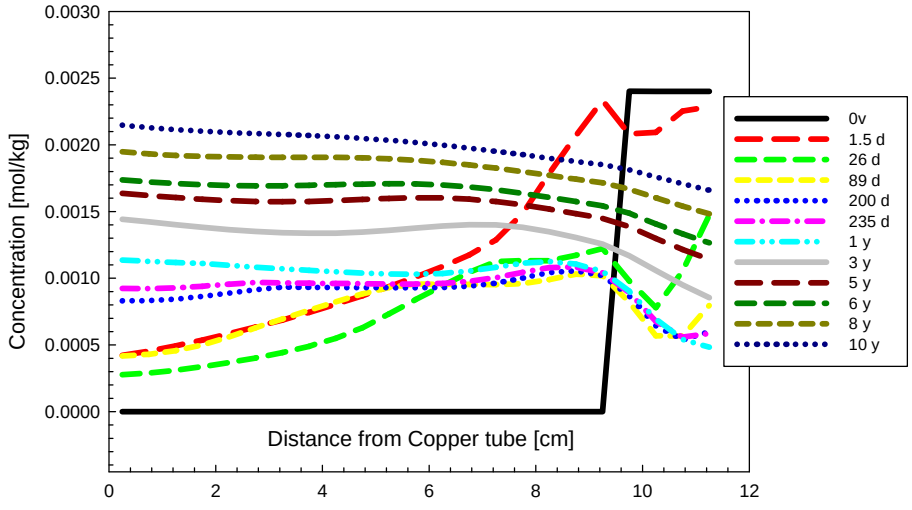

Figure 5.14. Total aqueous magnesium component concentrations as a function of distance from the copper tube, over time.

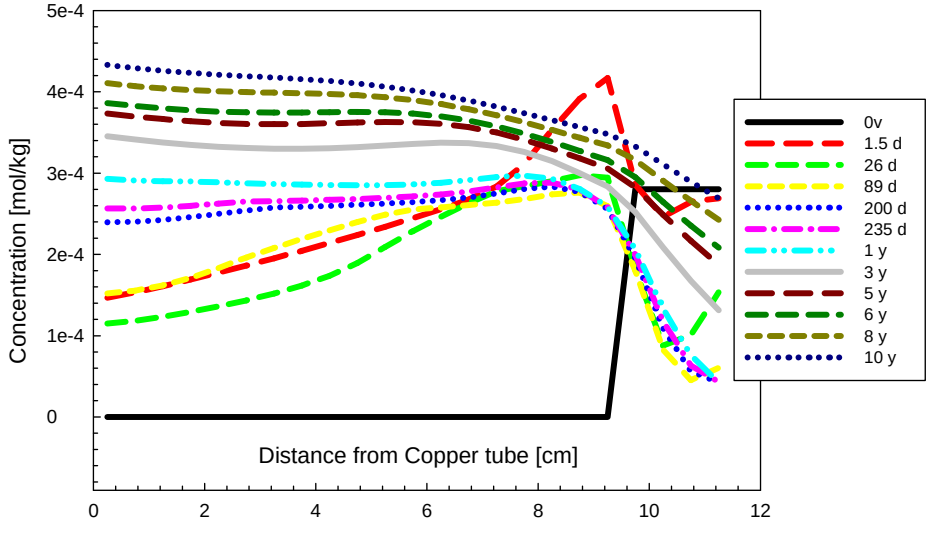

Figure 5.15. Total aqueous potassium component concentrations as a function of distance from the copper tube, over time.

Both sodium and sulphate ions diffuse out from the bentonite. This is due to increasing sodium concentrations in the bentonite resulting from cation-exchange reactions (Figures 5.16 and 5.17) and an initial increase in sulphate concentrations owing to the dissolution of gypsum (Figures 5–7). Both sulphate and sodium show similarity with the experimental results (see Appendix C).

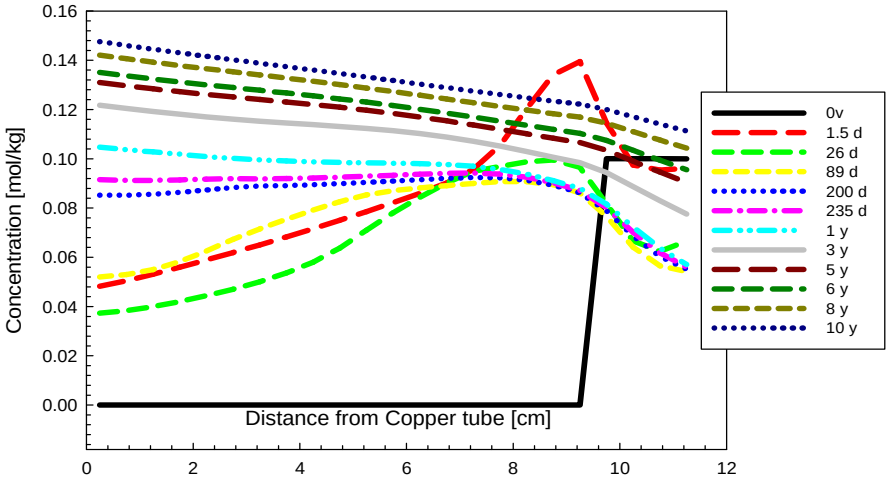

Figure 5.16. Total aqueous sodium component concentrations as a function of distance from the copper tube, over time.

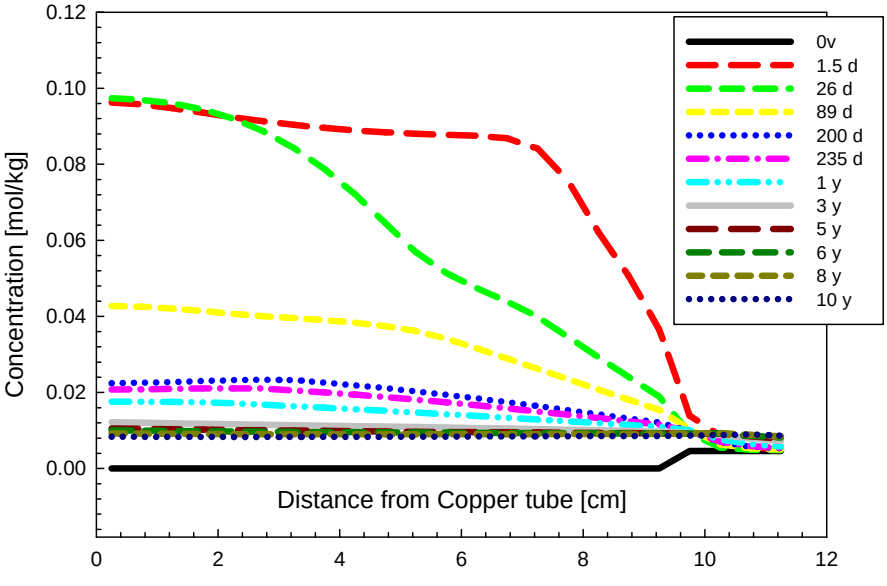

Figure 6.17. Total aqueous sulphate component concentration as a function of distance from copper tube, over time.

5.4 Exchangeable cations

The cation exchanger composition changes are shown in the figures below as meq/100g bentonite. It appears that calcium enters the cation exchanger and

sodium exits (Figures 5.18 and 5.19). The calcium levels are, however, higher near the bentonite-rock interface owing to anhydrite precipitation near both interfaces (copper and rock) and incoming calcium from the groundwater. Thus, the concentrations are not balanced equally and equilibrium is not reached within the modelled time. The cation exchanger changes to calcium type, and because there is more calcium in incoming groundwater than in bentonite porewater the cation exchanger takes more calcium from the bentonite-rock interface. Consequently, not so much calcium reaches the other end, which is the main reason for the disequilibrium. The sodium content decreases with the changes highest near the rock surface. The cation exchanger acts differently than in the experiment (Appendix C). This can be attributable to the model boundary conditions and bentonite porewater differing from the experiment. Even the temperature behaviour of the cation exchanger coefficients are unknown and not thoroughly studied for compacted bentonite.

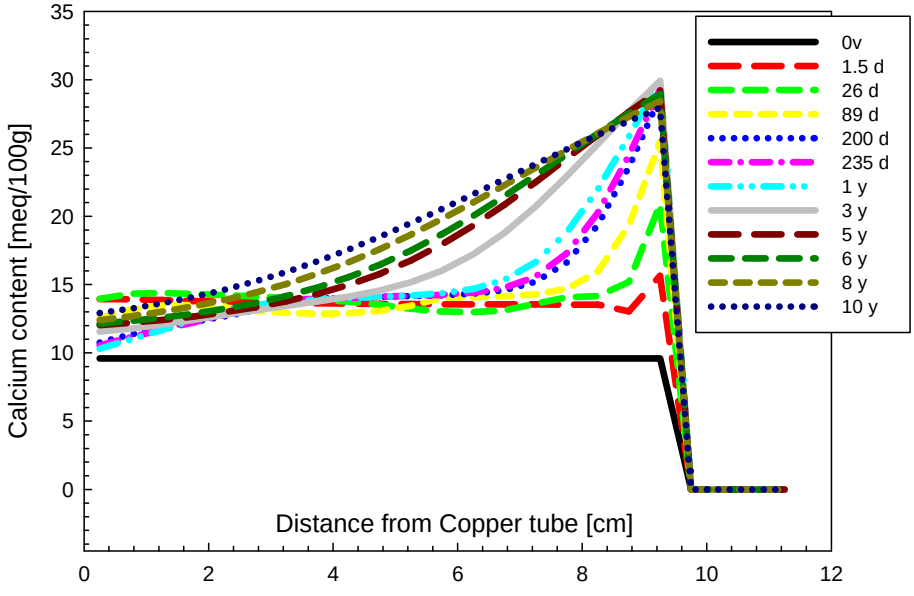

Figure 5.18. Calcium content [meq/100g] in the cation exchanger as a function of distance from the copper tube, over time.

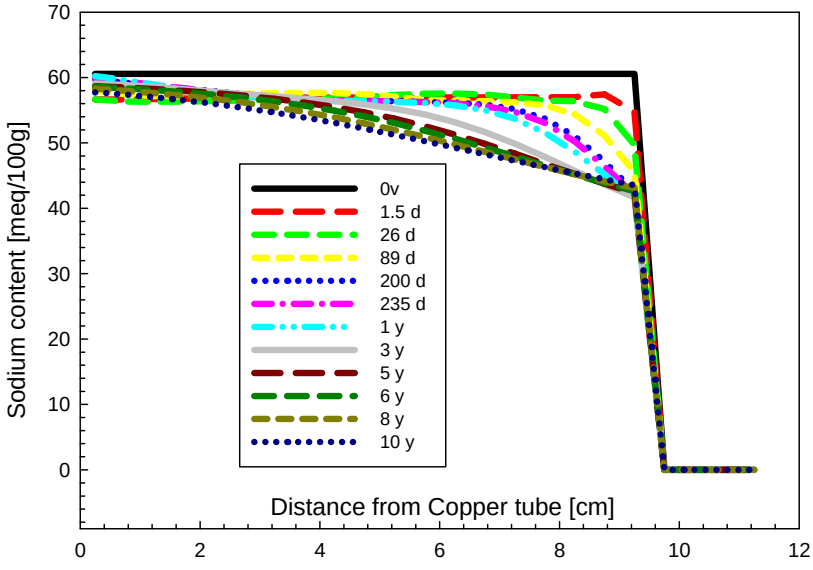

Figure 5.19. Sodium content [meq/100g] in the cation exchanger as a function of distance from the copper tube, over time.

Potassium and magnesium also exit the exchanger and are replaced by calcium (Figures 5.20 and 5.21). These changes are also highest near the rock interface.

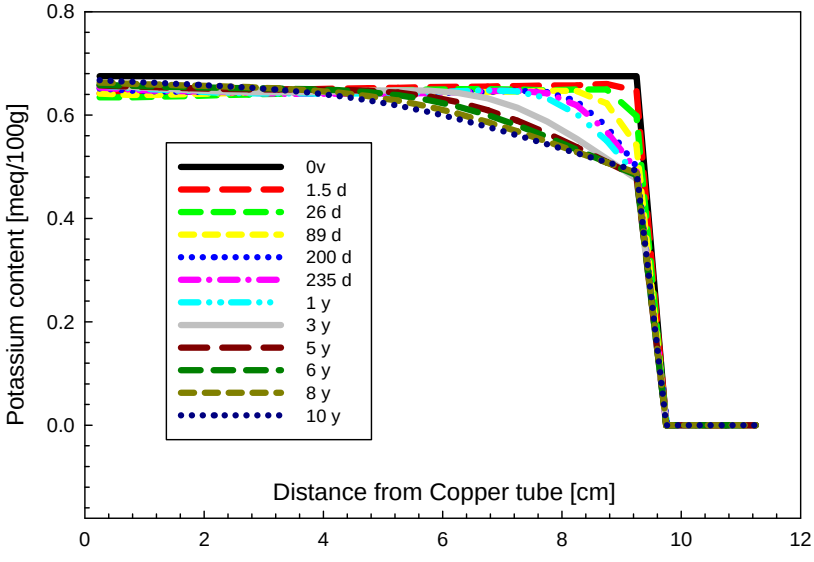

Figure 5.20. Potassium content [meq/100g] in the cation exchanger as a function of distance from the copper tube, over time.

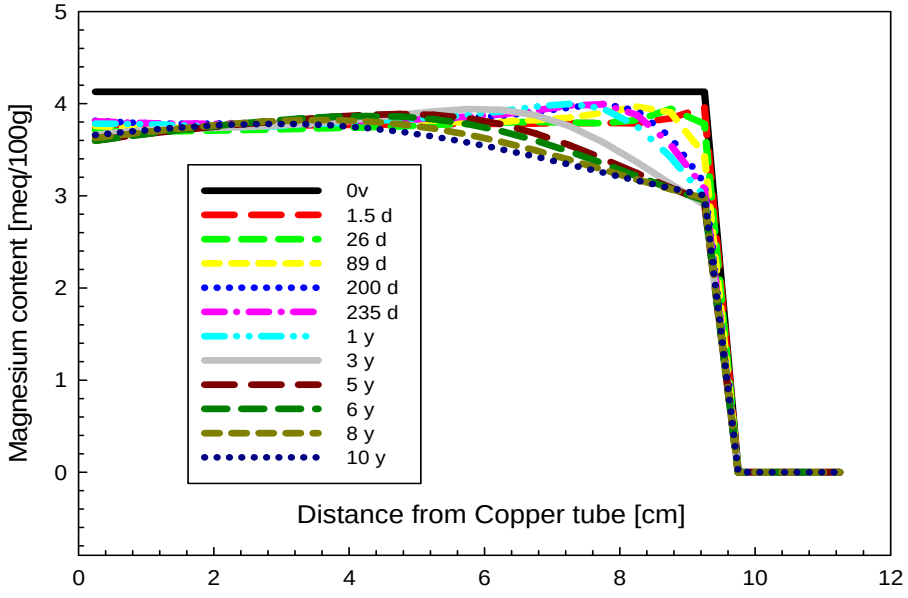

Figure 5.21. Magnesium content [meq/100g] in the cation exchanger as a function of distance from the copper tube, over time.

6. Discussion of results

Whereas the majority of the results appear to be qualitatively correct, their validity is open to a number of questions. Some of these limitations were already discussed in Section 4.5. However, even the experimental results can be questioned. There are different methods to measure, for example, cation exchange, which yield different results. There could be many factors that cause uncertainty in the experiments, such as calibration of sensors, transportation of bentonite block, air affecting the bentonite after lifting, and splitting of bentonite blocks, etc. Even if the experimental results are all correct, we could get very different results with the model. The reason can for instance be the parameters, the inbuilt model formulas, or the difference between the model and the real system.

The bentonite structure and waters affecting the system are under large uncertainty, for example, because the bentonite molecular structure and behaviour are not well known. Our model also assumes that the bentonite is at the beginning swelled, which is not the case in a real experiment. When the water contacts the bentonite, the bentonite near the waterfront starts to get wet and loses its density. Thus, there will be a soft mass at the beginning where different behaviour can occur. This can affect the bentonite saturation and accelerate it. When the bentonite is saturated enough and swells, this soft mass comes in to contact the rock interface and the exterior of the bentonite block starts to tighten again. However, if we would like to take this into account, we would need to include mechanical phenomena in the model, which would also include density distribution during saturation in the parcel bentonite mass [9, p.33].

Additionally, based on the results of chloride compared to [22], we could assume that more of the water goes in as water vapour in the experiment than in the model, because the chloride ion should be quite inert and thus it should be carried along with the liquid water. The experimental results are shown in Ap-

pendix C. The sulphate concentrations, however, in the experiment and in the model seem to indicate that anhydrite precipitates somewhere near the heater.

According to the modelling results, the bentonite changes more to the calcium form. When the bentonite changes more to calcium form, it means that the stability of bentonite improves but the swelling pressure gets smaller. This means that, in dilute waters, bentonite does not dissolve so easily, which is a good factor when it happens in the outer parts of the bentonite near the bentonite-rock interface.

The model is also designed such that the water in the bentonite is very dilute and that the ion exchanger is filled correctly. This is not, however, the case in real bentonite porewater, where there is, for example, more sulphate in bentonite porewater than in groundwater. This can cause some difference in the results in short-time calculations when the equilibrium is not fully reached.

7. Conclusions

The results show similarity with experimental data. However, the results are open to question and further study is needed to confirm their validity. The parameters used should be applied to other modelling programs and the results compared with the results of TOUGHREACT.

Furthermore, more experimental data is needed (see Section 5.6 for details). Constructing surface complexation in TOUGHREACT would be of key importance with respect to modelling a final repository for nuclear waste.

THC models could be improved by incorporating mechanical and geochemical coupling to account for porosity changes caused by swelling phenomena. This would lead to fully coupled THMC models (where M = mechanical). According to the FEBEX study this would also improve the geochemical results of the models [30].

To understand better how the saturation of bentonite affects the chemistry we should subsequently compare initially partially saturated and saturated states and their results with each other. We should also consult the model developers to understand the difference between the results of version 4.2 and 4.1 of PetraSim.

The experiment is not so easily applied to models because the water surrounds the bentonite block first and then the swelling starts. However, our model cannot take that into account but we have to assume that the bentonite is swelled at the beginning. To model this correctly, we would need a fully coupled THMC model in 3-D. We have to also remember that the changes in a real repository would take longer because the changes in the bentonite are lesser elsewhere than in the fracture position after the swelling seals the repository hole. This is probably the case in the experimental results. As one can see there is not much change in cation exchanger (see Appendix C).

The terminology is very indistinct and inconsistent in the literature of the research area. This may lead to many misunderstandings. For example physicists

and geologists can use the same word for different purpose or different words for same purpose. This inconsistency should be clarified and terminology made uniform.

Finally, dramatic changes in bentonite do not occur, but there is still need for further modelling and more thorough research of partially saturated modelling, especially since very little is known about this topic and the model will be applied to KBS-3V conditions later on. This thesis has given the author the knowledge to further study and model the final repository of spent nuclear fuel. It can take several years to create a model accurate enough to model the partial saturation of the final repository and this project will be a long-term one.

References

[1] Anderson, G.M. Thermodynamics of Natural Systems, 2nd Edition. New York 2005, Cambridge University Press. 648 p.

[2] Appelo, C.A.J., Postma, D. Geochemistry, groundwater and pollution, 2nd edition. Leiden 2007, A.A. Balkema Publishers. 649 p.

[3] Arcos, D., Bruno, J. & Karnland, O. Geochemical model of the granite-bentonite-groundwater interaction at Äspö HRL (LOT experiment). Applied Clay Science 23(2003)1–4, pp. 219–228.

[4] Arthur, R. & Zhou, W. Reactive-Transport Model of Buffer Cementation. Stockholm 2005, SKI report 2005:59. 36 p.

[5] Bear, J. Dynamics of Fluid in Porous Media. New York 1972, Dover Publication, Inc. 764 p.

[6] Bear, J. Hydraulics of Groundwater. Israel 1979, McGraw-Hill Inc. 567 p.

[7] Bolt, G.H. & van Riemsdijk, W.H. Surface chemical processes in soil. In: Stumm, W. Aquatic Surface Chemistry. Chemical Processes at the Particle-Water Interface. United States 1987, John Wiley & Sons, Inc. pp. 127–164.

[8] Bradbury, M.H. & Baeyens, B. Porewater Chemistry in Compacted Re-Saturated MX-80 Bentonite: Physico-Chemical Characterisation and Geochemical Modelling. Villigen 2002, PSI Bericht Nr. 02-10. 42 p.

[9] Brantley, S.L., Kubicki, J.D. & White, A.F. Kinetics of Water-Rock Interaction. New York 2008, Springer Sicence+Business Media, LLC. 830 p.

[10] de Marsily, G. Quantative Hydrogeology. Groundwater Hydrology for Engineers. London 1986, Acedemis Press, Inc. 464 p.

[11] Elden, L., Wittmeyer-Koch, L. & Nielsen, H.B. Introduction to Numerical computation – analysis and MATLAB illustrations. Lund 2004, The Authors and Studentlitteratur. 375 p.

[12] Fredlun, D.G. & Rahardjo, H. Soil Mechanics For Unsaturated Soils. New York 1993, A Wiley-Interscience Publication, John Wiley & Sons, Inc.

[13] Grauer, R. Bentonite as a backfill material in the high-level waste repository: Chemical aspects. Villigen 1986, Nagra Technical Report NTB 86-12E. 130 p.

[14] Helgeson, H.C., Kirkham, C.H. & Flower, D.C. Theoretical prediction of the thermodynamic behaviour of aqueous electrolytes at high pressures and tempera-

tures: IV. Calculation of activity coefficients, osmotic coefficients, and apparent molal and standard and relative partial molal properties to 600C and 5kb. American Journal of Science 281(1981), pp. 1249–1516.

[15] Jacinto, A.C., Villar, M.C., Gomez-Espina, R. & Ledesma, A. Adaptation of the van Genuchten expression to the effects of temperature and density for compacted Bentonites. Applied Clay Science 42(2009), pp. 572582.

[16] Karnland, O., Olsson, S. & Nilsson, U. Mineralogy and sealing properties of various bentonites and smectite-rich clay materials. Stockholm 2006. SKB Technical Report 06-30, 117 p.

[17] Karnland, O., Olsson, S., Dueck, A., Birgersson, M., Nilsson, U. & Herman-Håkansson, T. LOT project. Long Term Test of Buffer Material. Lund 2009, Clay Technology AB, Parcel A2 field and laboratory draft report. 117 p. + app. 218 p.

[18] Knapp, R.A. Spatial and temporal scales of local equilibrium in dynamic fluid-rock systems. Geochimica et Cosmochimica Acta 53(1989)8, pp. 1955–1964.

[19] Lasaga, A.C., Soler, J.M., Ganor, J., Burch, T.E. & Nagy, K.L. Chemical wathering rate laws and global geochemical cycles. Goechimica et Cosmochimica Acta 58(1994)10, pp. 2361–2386.

[20] Longterm safety for KBS3 repositories at Forsmark and Laxemar a first evaluation. Main report of the SR-Can project. Stockholm 2006, SKB Technical Report 06-09. 620 p.

[21] Millington, R.J. & Quirk, J.P. Permeability of Porous Solids. Transactions of Faraday Society 57(1961), pp. 1200–1207.

[22] Muurinen, A. Chemical Conditions in the A2 Parcel of the Long-term Test of Buffer Material in Äspö (LOT). Olkiluoto 2006, Posiva Working Report 2006-83. 23 p.

[23] Narasimhan, T.N. & Witherspoon, P.A. An integrated finite difference method for analyzing fluid flow in porous media. Water Resources Research 12(1976)1, pp. 57–64.

[24] Ochs, M. & Talerico, C. Data and uncertainty assessment. Migration parameters for the bentonite buffer in the KBS-3 concept. Stockholm 2004, SKB Technical Report 04-18. 165 p.

[25] Palandri, J.L. & Kharaka Y.K. A compilation of rate parameters of water-mineral interaction kinetics for application to geochemical modelling. Menlo Park, California 2004, U.S. Geological Survey, Open File Report 2007-1068. 64 p.

[26] Pastina, B. & Hellä, P. Expected Evolution of a Spent Nuclear Fuel Repository at Olkiluoto. Olkiluoto 2006, Posiva Working Report 2006–05. 405 p.

[27] Prost, R., Koutit, T., Benchar, A. & Huard, E. State and location of water Adsorbed on clay minerals: Consequences of the hydration and swelling-shrinkage phenomena. Clays and Clay Minerals 46(1998)2, pp. 117–131.

[28] Pruess, K., Oldenburg, C. & Moridis, G. TOUGH2 User's guide. Version 2.0. Berkeley 1999, Earth Sciences Division, Lawrence Berkeley National Laboratory, University of California. 198 p.

[29] Pusch, R., Karnland, O. & Hokmark, H. GMM – A general microstructural model for qualitative and quantitative studies of smectite clays. Stockholm 1990, SKB Technical Report 90-43, 99 p.

[30] Samper, J., Zheng, L., Montenegro, L., Fernandez, A.M. & Rivas, P. Coupled thermo-hydro-chemical models of compacted bentonite after FEBEX in situ test. Applied Geochemistry 23(2008)5, pp. 1186–1201.

[31] Seetharam, S.C. An investigation of the thermo/hydro/chemical/mechanical behaviour of unsaturated soils. PhD. thesis. Cardiff 2003. Geoenvironmental Research Centre, Cardiff School of Engineering, Cardiff University.

[32] Smellie, J. Wyoming Bentonites. Evidence from the geological record to evaluate the suitability of bentonite as a buffer material during the long-term underground containment of radioactive wastes. Stockholm 2001, SKB Technical Report 01-26. 24 p.

[33] Soldatov, V.S. Application of basic concepts of chemical thermodynamics to ion exchange equilibria. Reactive & Functional Polymers 27(1995)2, pp. 95–106.

[34] Sonnenthal, E., Ito, A., Spycher, N., Yui, M., Apps, J., Sugita, Y., Conrad, M. & Kawakami, S. Approaches to modelling coupled thermal, hydrological, and chemical processes in the drift scale heater test at Yucca Mountain. International Journal of Rock Mechanics & Mining Sciences 42(2005)5–6, pp. 698–719.

[35] Spycher, N. F. & Reed, M.H. Fugacity coefficients of H_2, CO_2, CH_4, H_2O and of H_2O-CO_2-CH_4 mixtures: A virial equation treatment for moderate pressures and temperatures applicable to calculations of hydrothermal boiling. Geochimica et Cosmochimica Acta 52(1988)3, pp. 739–749.

[36] Steefel, C.I. & Lasaga, A.C. A coupled model for transport of multiple precipitation/dissolution reaction with application to reactive flow in single phase hydrothermal systems. American Journal of Science 294(1994), pp. 529–592.

[37] Tanhua-Tyrkkö, M. Modelling hydrological and chemical phenomena during interaction of bentonite and high pH plume. Espoo, 2009, VTT, Technical Research Centre of Finland, Unpublished Master's thesis. 71 p.

[38] PetraSim user manual. Manhattan 2008, Thunderhead Engineering. 96 p.

[39] Tournassat, C., Gailhanou, H. & Crouzet, C. Two cation exchange models for direct and inverse modelling of solution major cation composition in equilibrium with illite surfaces. Geochimica et Cosmochimica Acta 71(2007)5, pp. 1098–1114.

[40] van Genuchten, M.A. Closed-form Equation for Predicting the Hydraulic Conductivity of Unsaturated Soils. Soil Science Society of American Journal 44(1980), pp. 892–898.

[41] van Olphen, H. An Introduction to clay clolloid chemistry. For Clay Technologists, Geologists, and Soil Scientists New York 1967, John Wiley & Sons, Inc. 301 p.

[42] Wersin, J. Geochemical modelling of bentonite porewater in high-level waste repositories. Journal of Contaminant Hydrology 61(2003), pp. 405–422.

[43] Xu, T., Sonnenthal, E., Spycher, N. & Pruess, K. TOUGHREACT User's Guide: A Simulation Program for Non-isothermal Multiphase Reactive Geochemical Transport in Variably Saturated Geologic Media. Version 1.2.1. Berkeley 2008, Earth Sciences Division, Lawrence Berkeley National Laboratory, University of California. 195 p.

[44] Zhu, C. & Anderson, G. Environmental Applications of Geochemical Modeling. Cambridge 2002, Cambridge University Press. p. 284.

Appendix A: Construction of the model

This Appendix defines the model in this thesis and its creation with PetraSim.

Specify the Equation of State (EOS)

To ensure that PetraSim uses TOUGHREACT and EOS3, edit the preferences.

1. On the **File** menu, click **preferences**.
2. In the **Simulator Mode** list, select **TOUGHREACT**.
3. In the **Default Equation of State (EOS)** list, select **EOS3**.
4. Click **OK**.
5. On the **File** menu, click **New**.

Create the Model Boundary

To create the boundary for the model, use the **Define Boundary** on the **model** menu. To create the model boundary use the parameters shown in table below.

Axis	Min (m)	Max (m)
x	0	0.4
y	0	0.2
z	0	0.1

Create Grid

To create the grid:

1. On the **Model** menu, click **Create grid**.
2. In the **Division Method** box, select **Regular**.
3. In the **X Cells box**, type 80, choose **X Factor** to be 1.
4. In the **Y Cells box**, type 1, choose **Y Factor** to be 1.
5. In the **Z Cells box**, type 1, choose **Z Factor** to be 1.
6. Click **OK** to create the grid.

Global Properties

Global properties apply to entire model. Choose **Properties** menu and click **Global Properties**.

1. In the **Analysis** tab choose **Enable Reactive Transport**.
2. In **EOS** tab under **EOS3: Water and Air**, choose **Non-Isothermal** and **Molecular diffusion**.
3. Click **Edit CoEFs**… and Write Gaseous **Water** and **Air** diffusion coefficients to be **$2.13 \cdot 10^{-5}$**. Click **OK**.
4. In **Initialization Options – MOP (19)**. Choose **Standard: (P,X,T) and (Pg, Sg+10, T)**.
5. Do not do anything to MINC and Misc tabs.

Material Properties

To specify the material properties, use the **Material Data** dialog in **properties** menu. This model requires three materials. Click **Materials** on **Properties** menu.

Material Data

1. In the **Materials** list, select **ROCK1**. Change the name to **BENTO**.
2. In **Density** box write 2750.0.
3. In **Porosity** box write 0.43.
4. In all three **Permeability** boxes (X, Y, and Z), type 3.0E-21.
5. In the **Wet Heat Conductivity** box, type 1.3.
6. In the Specific Heat box, type 952.9.
7. Click Apply to save changes.
8. Click **New** under **Materials** and type ROCK in the **name** box, choose BENTO on **Based on** box.
9. Do this to add COPPE material for copper canister also.
10. Insert the values given in Table 3.2 for these materials as above.

Relative Permeability

To specify the relative permeability function:

1. Click the **Relative Perm** tab for BENTO.
2. In the **Relative Permeability** list, select **van Genuchten-Mualem Model**.

3. In the **λ** box, type 0.338.
4. In the **S_{lr}** box , type 0.4.
5. In the **S_{ls}** box, type 1.0.
6. In the **S_{gr}** box, type 0.0.

Capillary Pressure

To specify the capillary pressure function:

1. Click the **Capillary Press** tab.
2. In the **Capillary Pressure** list, select **van Genuchten Function**.
3. In the **λ** box, type 0.338.
4. In the **$1/P_0$** box , type 7.08E-8.
5. In the **P_{max}** box, type 1.4E8.
6. In the **S_{ls}** box, type 1.0.
7. Click the **Misc** tab.
8. Select **Dry heat Conductivity** to be **User Defined** and write 0.3 in the box.
9. In the **Tortuosity Factor** box, type 0.123.

Click **OK** to exit the **Additional Material Data** dialog. Do **Relative Permeability** and **Misc** changes to Rock. Leave COPPE material **Additional Material Data** to default. Change Rock **Relative Permeability** to **Fatt&Klikoff**, type 0.999 to **S_{lr}** box and 0.2 to **Tortuosity Factor** box. Click **OK** to save and exit **Material Data** dialog.

Initial Conditions

The initial state of each cell in the model must be defined. To edit the **Default Initial Conditions** dialog: On the Properties menu, click **Initial Conditions…**.

1. In list, select **Two-Phase**.
2. In the **Pressure** box, type 101300.
3. In the **Temperature** box, type 25.
4. In the **Gas Saturation** box, type 0.6.

Click Ok to exit.

Solution Controls

On the Analysis menu, click Solution Controls…

Times

1. In the Solution Controls dialog, click the **Times** tab.
2. In the **End Time box**, type 3,1536E8.
3. In the **Time Step** box, type 1.
4. In the **Max Num Time Steps** list, type 9999.
5. In the **Max Time Step** list, select **User Defined** and type 2000.

Weighting

1. In the **Solution Controls** dialog, click the **Weighting** tab.
2. As the **Density at Interface** option, select **Average of Adjacent Elements**.

Output Controls

We can change the resolution of the output in the **Output Controls** dialog.

1. On the **Analysis** menu, click **Output Controls...**.
2. In the **Print and Plot Every # Steps** box, type 2000.
3. In the **Additional Output Data** group, select **Fluxes and Velocities**.

In addition to printing output every 2000 steps, we can also specify times for which we want to view data in the **Additional Print Times** dialog.

To specify additional times for output:

1. On the **Output Controls** dialog, click the **Edit** button to open the **Additional Print Times** dialog.
2. In the **Times** table, type 100, 1.29E5, 2.26E6, 7.7E6, 1.73E7, 2,03E7, 3.154E7, 9.46E7, 1.576E8, 1.892E8, 2.522E8, 3.154E8.
3. Click **OK** two times.

TOUGHREACT Solution Parameters

We will now set the TOUGHREACT parameters. If one wishes to change the model grid, it would be easier to do this before the grid. To open the **Solution Parameters** dialog: on the **Tough React** menu, click **Solution Parameters...**.

1. Select **Standard** from the list and select **Enable Gaseous Species Transport**.
2. Select **Advanced** from the list on the left and select Use **Leverett Scaling for Capillary Pressure**, **Ignore Mineral Dissolution/Precipitation Effects on Flow** and **Print Porosity, Permeability, Capillary Pressure Changes on Flow**.
3. Select **Diffusion Coefficients** from the list, type 2.0E-9 to **Aqueous Species Diffusion Coefficient** box.
4. Do not change other parameters.

TOUGHREACT Output Options

TOUGHREACT output options can be changed on the **Output Options** dialog.

1. On the **Tough React** menu, click **Output Options...**.
2. In the **Grid Block Output Frequency(s)** box, type 2000.
3. For **Aqueous Concentration Output**, select **Write Total Aqueous Component Concentrations**.
4. live the other tabs as default.

Click **OK** to exit the **Output Options** dialog.

TOUGHREACT Chemical Components

On the **Tough React** menu, select **Chemical Components...**. The database used for chemical modelling was taken from the website for 0-300^{o}C: http://thermoddem.brgm.fr/index.asp?langue=GB

To define the primary species:

1. In the list on the left of the **Chemical Components** dialog, select **Primary Species**.
2. In the **Thermodynamic Database** list in the middle of the dialog, select **Al+**, **Ca++**, **Cl-**, **H+**, **H2O** , **H4SiO4(aq)**, **HCO3-**, **K+**, **Mg++, Na+**, **O2(aq)**, **SO4--**.
3. Click the **-→** button to move the selected species into the **Current Simulation** list on the right.
4. Click **Apply** to add the selected species to the analysis.

The parameters specific to each type can be viewed and changed by clicking on that type in the subtree under **Primary Species** in the list on the left.

To edit parameters for na+ :

1. Select **Na+** in the list under **Primary Species**.
2. In the panel on the right, select **Output Concentration History at Selected Cells**.
3. Select **Enable Cation exchange**, type 1.0 to **Specify Coefficient Relative to Reference Cation** and click **Apply**. Then click **This is the Reference Cation** tab.
4. Repeat the Step 2 for every primary species
5. Enable Cation Exchange to Ca++, Mg++ and K+ and specify coefficients according to Table 5.1.

To define the minerals:

1. In the list on the left of the **Chemical Components** dialog, select **Minerals**.
2. In the **Thermodynamic Database** list in the middle of the dialog, select **Anhydrite**, **Calcite**, **Chalcedony**, **Gypsum**, **K-Feldspar**, **Quartz**.
3. Click the **-→** button to move the selected species into the **Current Simulation** list on the right.
4. Click **Apply** to add the selected species to the analysis.

The parameters specific to each type can be viewed and changed by clicking on that type in the subtree under **Minerals** in the list on the left.

1. Select Anhydrite in the list under **Minerals**.
2. In the panel on the right, select **Output Abundance History at Selected Cells**.
3. Repeat the steps 1 and 2 for other minerals.
4. Specify kinetic Constraints and Rate Constant Dependences on pH under Specify Additional Mechanisms tab according to Table 3.5.

To define Aqueous Complexes. In the list on the left of the **Chemical Components** dialog, select **Aq. Complexes** and Select **Enable All** tab.

TOUGHREACT Zone Data

On the **Tough React** menu, click **Zone Data...**. To Create the initial water zones:

1. Select **Water (Initial)** in the list on the left.
2. Click **Add**.

3. In the **Create a New Zone** dialog, type Bentowater and click **OK**.
4. Click **Add**.
5. In the **Create a New Zone** dialog, type Groundwater and click **OK**.
6. Click **Apply**.
7. In the list on the left, click **+** beside **Water (Initial)** to expand the subtree.
8. In the subtree under **Water (Initial)**, click **Bentowater** to display the zone parameters to the right of the list.
9. Enter the data that is shown in Table 3.6.
10. Repeat step 7-9 to Groundwater.
11. The H+ concentration have to be selected as **fixed**.

To Create the initial Mineral Zones:

1. Select **Mineral** in the list on the left.
2. Click **Add**.
3. In the **Create a New Zone** dialog, type Bentominerals and click **OK**.
4. Click **Add**.
5. In the **Create a New Zone** dialog, type Rockminerals and click **OK**.
6. Click **Apply**.
7. Specify the **Grain Radius**es and **Surface area**s for both zones according to Table 3.5 and initial **Volume fraction**s for Bentominerals according to Table 3.4.

To create the **Permeability Porosity** zones. Do as above and create zones for Bento and Rock. and select **Simplified Carmen-Kozeny** for **Permeability Law**.

To create **Cation Exchange** zone. Do as above for Bento, type 77.8 for **Exchange Capacity** box. Click **OK** to save changes.

Define Boundary Conditions and Associate Zones

To edit cells, you can use the **Grid Editor**. To open the **Grid Editor**: on the **Model** menu, click **Edit Grid**.

Copper

Click on the first cell on the left. To edit the properties of this cell, on the **Edit** menu, click **Properties**.

1. Click the **Material** box and select COPPE from the list.
2. Click the **Sources/Sinks** tab.
3. Select Heat In as **Constant**, and type 11 to **Rate** box.
4. Select **Initial Conditions** tab.
5. Select **Single-Phase** from the **Specify Initial Condition by Cell** list.
6. Type 101300 to **Pressure**, 25 to **Temperature** and 1 to **Air Mass Fraction**
7. Select **Zones** tab.
8. Select **Specify Zones by Cell** and select bentowater from the **Initial Water Zone list.**
9. Click **OK**.
10. Repeat this to second cell from the right except don't add Heat Source.

Bentonite

Select cells from 3-21 from the left. and click **Properties** from **Edit** menu. The material is already defined as BENTO and the initial conditions were defined before.

1. Click the **Zones** tab.
2. Select **Specify Zones by Cell** and select bentowater from the **Initial Water Zone list**, Bentomineral for **Mineral Zone**, Bento for **Permeability/Porosity Zone** and Bento for **CationExchange Zone**.
3. Select **Print Options** tab.
4. Mark **Print Cell Time Dependent Data**.
5. Click **OK**.

Granitic Crack

Select the last cell from left and click **Properties** from **Edit** menu.

1. Click the **Material** box and select ROCK from the list.
2. Type 1.0E30 to **Volume Factor** box.
3. Select **Initial Conditions** tab.
4. Select **Single-Phase** from the **Specify Initial Condition by Cell** list.
5. Type 101300 to **Pressure**, 25 to **Temperature** and 0.0 to **Air Mass Fraction**.

6. Select **Specify Zones by Cell** and select groundwater from the **Initial Water Zone list**, rockmineral for **Mineral Zone**, Rock for **Permeability/Porosity Zone**.
7. Click **OK**.
8. Repeat this to cells 22-79 from the left except do not change the volume fractions for these cells.

Save and Run

On the **File** menu, click **Save As** and on the **Analysis** menu, click **Run T2REACT**.

Appendix B: Data tables

Pressure Table

Pressure [bars]

Cell	Distance [cm]	0 d	1.5 d	26 d	89 d	200 d	235 d	1 y	3 y	5 y	6 y	8 y	10 y
3	0.25	1.01	4.43	6.45	7.47	16.40	27.39	41.74	41.74	41.74	41.74	41.74	41.74
4	0.75	1.01	4.03	5.91	6.84	15.26	25.68	39.56	39.56	39.56	39.56	39.56	39.56
5	1.25	1.01	3.67	5.42	6.25	14.21	24.06	37.45	37.45	37.45	37.45	37.45	37.45
6	1.75	1.01	3.34	4.96	5.71	13.23	22.52	35.40	35.40	35.40	35.40	35.40	35.40
7	2.25	1.01	3.03	4.53	5.21	12.33	21.06	33.41	33.41	33.41	33.41	33.41	33.41
8	2.75	1.01	2.76	4.13	4.77	11.48	19.68	31.49	31.49	31.49	31.49	31.49	31.49
9	3.25	1.01	2.50	3.76	4.40	10.69	18.38	29.64	29.64	29.64	29.64	29.64	29.64
10	3.75	1.01	2.27	3.42	4.07	9.95	17.14	27.85	27.85	27.85	27.85	27.85	27.85
11	4.25	1.01	2.06	3.11	3.77	9.25	15.97	26.13	26.13	26.13	26.13	26.13	26.13
12	4.75	1.01	1.87	2.82	3.50	8.60	14.87	24.48	24.48	24.48	24.48	24.48	24.48
13	5.25	1.01	1.69	2.56	3.25	7.99	13.83	22.90	22.90	22.90	22.90	22.90	22.90
14	5.75	1.01	1.53	2.34	3.01	7.41	12.85	21.39	21.39	21.39	21.39	21.39	21.39
15	6.25	1.01	1.39	2.15	2.79	6.87	11.93	19.96	19.96	19.96	19.96	19.96	19.96
16	6.75	1.01	1.25	1.99	2.58	6.37	11.06	18.58	18.58	18.58	18.58	18.58	18.58
17	7.25	1.01	1.13	1.84	2.39	5.89	10.25	17.28	17.28	17.28	17.28	17.28	17.28
18	7.75	1.01	1.02	1.70	2.21	5.45	9.48	16.05	16.05	16.05	16.05	16.05	16.05
19	8.25	1.01	0.93	1.57	3.28	6.97	8.79	14.88	14.88	14.88	14.88	14.88	14.88
20	8.75	1.01	0.86	3.56	7.59	9.45	10.38	13.78	13.78	13.78	13.78	13.78	13.78
21	9.25	1.01	12.00	12.00	12.00	12.00	12.00	12.74	12.74	12.74	12.74	12.74	12.74
22	9.75	0.03	12.00	12.00	12.00	12.00	12.00	12.00	12.00	12.00	12.00	12.00	12.00
23	10.25	5.89	12.00	12.00	12.00	12.00	12.00	12.00	12.00	12.00	12.00	12.00	12.00
24	10.75	8.88	12.00	12.00	12.00	12.00	12.00	12.00	12.00	12.00	12.00	12.00	12.00
25	11.25	10.40	12.00	12.00	12.00	12.00	12.00	12.00	12.00	12.00	12.00	12.00	12.00

Minerals

K-feldspar [volume fractions]

Cell	Dis-tance [cm]	0 d	1.5 d	26 d	89 d	200 d	235 d	1 y	3 y	5 y	6 y	8 y	10 y
3	0.25	2.4E-02	2.4E-02	2.4E-02	2.4E-02	2.4E-02	2.4E-02	2.4E-02	2.4E-02	2.4E-02	2.4E-02	2.4E-02	2.4E-02
4	0.75	2.4E-02	2.4E-02	2.4E-02	2.4E-02	2.4E-02	2.4E-02	2.4E-02	2.4E-02	2.4E-02	2.4E-02	2.4E-02	2.4E-02
5	1.25	2.4E-02	2.4E-02	2.4E-02	2.4E-02	2.4E-02	2.4E-02	2.4E-02	2.4E-02	2.4E-02	2.4E-02	2.4E-02	2.4E-02
6	1.75	2.4E-02	2.4E-02	2.4E-02	2.4E-02	2.4E-02	2.4E-02	2.4E-02	2.4E-02	2.4E-02	2.4E-02	2.4E-02	2.4E-02
7	2.25	2.4E-02	2.4E-02	2.4E-02	2.4E-02	2.4E-02	2.4E-02	2.4E-02	2.4E-02	2.4E-02	2.4E-02	2.4E-02	2.4E-02
8	2.75	2.4E-02	2.4E-02	2.4E-02	2.4E-02	2.4E-02	2.4E-02	2.4E-02	2.4E-02	2.4E-02	2.4E-02	2.4E-02	2.4E-02
9	3.25	2.4E-02	2.4E-02	2.4E-02	2.4E-02	2.4E-02	2.4E-02	2.4E-02	2.4E-02	2.4E-02	2.4E-02	2.4E-02	2.4E-02
10	3.75	2.4E-02	2.4E-02	2.4E-02	2.4E-02	2.4E-02	2.4E-02	2.4E-02	2.4E-02	2.4E-02	2.4E-02	2.4E-02	2.4E-02
11	4.25	2.4E-02	2.4E-02	2.4E-02	2.4E-02	2.4E-02	2.4E-02	2.4E-02	2.4E-02	2.4E-02	2.4E-02	2.4E-02	2.4E-02
12	4.75	2.4E-02	2.4E-02	2.4E-02	2.4E-02	2.4E-02	2.4E-02	2.4E-02	2.4E-02	2.4E-02	2.4E-02	2.4E-02	2.4E-02
13	5.25	2.4E-02	2.4E-02	2.4E-02	2.4E-02	2.4E-02	2.4E-02	2.4E-02	2.4E-02	2.4E-02	2.4E-02	2.4E-02	2.4E-02
14	5.75	2.4E-02	2.4E-02	2.4E-02	2.4E-02	2.4E-02	2.4E-02	2.4E-02	2.4E-02	2.4E-02	2.4E-02	2.4E-02	2.4E-02
15	6.25	2.4E-02	2.4E-02	2.4E-02	2.4E-02	2.4E-02	2.4E-02	2.4E-02	2.4E-02	2.4E-02	2.4E-02	2.4E-02	2.4E-02
16	6.75	2.4E-02	2.4E-02	2.4E-02	2.4E-02	2.4E-02	2.4E-02	2.4E-02	2.4E-02	2.4E-02	2.4E-02	2.4E-02	2.4E-02
17	7.25	2.4E-02	2.4E-02	2.4E-02	2.4E-02	2.4E-02	2.4E-02	2.4E-02	2.4E-02	2.4E-02	2.4E-02	2.4E-02	2.4E-02
18	7.75	2.4E-02	2.4E-02	2.4E-02	2.4E-02	2.4E-02	2.4E-02	2.4E-02	2.4E-02	2.4E-02	2.4E-02	2.4E-02	2.4E-02
19	8.25	2.4E-02	2.4E-02	2.4E-02	2.4E-02	2.4E-02	2.4E-02	2.4E-02	2.4E-02	2.4E-02	2.4E-02	2.4E-02	2.4E-02
20	8.75	2.4E-02	2.4E-02	2.4E-02	2.4E-02	2.4E-02	2.4E-02	2.4E-02	2.4E-02	2.4E-02	2.4E-02	2.4E-02	2.4E-02
21	9.25	2.4E-02	2.4E-02	2.4E-02	2.4E-02	2.4E-02	2.4E-02	2.4E-02	2.4E-02	2.4E-02	2.4E-02	2.4E-02	2.4E-02
22	9.75	0.0E+00	0.0E+00	0.0E+00	0.0E+00	0.0E+00	0.0E+00	0.0E+00	1.9E-12	9.5E-12	1.5E-11	2.6E-11	3.9E-11
23	10.3	0.0E+00	0.0E+00	0.0E+00	0.0E+00	0.0E+00	0.0E+00	0.0E+00	0.0E+00	4.0E-13	2.2E-12	9.1E-12	1.9E-11
24	10.8	0.0E+00	0.0E+00	0.0E+00	0.0E+00	0.0E+00	0.0E+00	0.0E+00	0.0E+00	0.0E+00	0.0E+00	2.6E-12	9.5E-12
25	11.3	0.0E+00	0.0E+00	0.0E+00	0.0E+00	0.0E+00	0.0E+00	0.0E+00	0.0E+00	0.0E+00	0.0E+00	2.5E-13	4.5E-12

Quartz [volume fractions]

Cell	Distance [cm]	0 d	1.5 d	26 d	89 d	200 d	235 d	1 y	3 y	5 y	6 y	8 y	10 y
3	0.25	5.1E-02	5.1E-02	5.1E-02	5.1E-02	5.1E-02	5.1E-02	5.1E-02	5.1E-02	5.1E-02	5.1E-02	5.1E-02	5.1E-02
4	0.75	5.1E-02	5.1E-02	5.1E-02	5.1E-02	5.1E-02	5.1E-02	5.1E-02	5.1E-02	5.1E-02	5.1E-02	5.1E-02	5.1E-02
5	1.25	5.1E-02	5.1E-02	5.1E-02	5.1E-02	5.1E-02	5.1E-02	5.1E-02	5.1E-02	5.1E-02	5.1E-02	5.1E-02	5.1E-02
6	1.75	5.1E-02	5.1E-02	5.1E-02	5.1E-02	5.1E-02	5.1E-02	5.1E-02	5.1E-02	5.1E-02	5.1E-02	5.1E-02	5.1E-02
7	2.25	5.1E-02	5.1E-02	5.1E-02	5.1E-02	5.1E-02	5.1E-02	5.1E-02	5.1E-02	5.1E-02	5.1E-02	5.1E-02	5.1E-02
8	2.75	5.1E-02	5.1E-02	5.1E-02	5.1E-02	5.1E-02	5.1E-02	5.1E-02	5.1E-02	5.1E-02	5.1E-02	5.1E-02	5.1E-02
9	3.25	5.1E-02	5.1E-02	5.1E-02	5.1E-02	5.1E-02	5.1E-02	5.1E-02	5.1E-02	5.1E-02	5.1E-02	5.1E-02	5.1E-02
10	3.75	5.1E-02	5.1E-02	5.1E-02	5.1E-02	5.1E-02	5.1E-02	5.1E-02	5.1E-02	5.1E-02	5.1E-02	5.1E-02	5.1E-02
11	4.25	5.1E-02	5.1E-02	5.1E-02	5.1E-02	5.1E-02	5.1E-02	5.1E-02	5.1E-02	5.1E-02	5.1E-02	5.1E-02	5.1E-02
12	4.75	5.1E-02	5.1E-02	5.1E-02	5.1E-02	5.1E-02	5.1E-02	5.1E-02	5.1E-02	5.1E-02	5.1E-02	5.1E-02	5.1E-02
13	5.25	5.1E-02	5.1E-02	5.1E-02	5.1E-02	5.1E-02	5.1E-02	5.1E-02	5.1E-02	5.1E-02	5.1E-02	5.1E-02	5.1E-02
14	5.75	5.1E-02	5.1E-02	5.1E-02	5.1E-02	5.1E-02	5.1E-02	5.1E-02	5.1E-02	5.1E-02	5.1E-02	5.1E-02	5.1E-02
15	6.25	5.1E-02	5.1E-02	5.1E-02	5.1E-02	5.1E-02	5.1E-02	5.1E-02	5.1E-02	5.1E-02	5.1E-02	5.1E-02	5.1E-02
16	6.75	5.1E-02	5.1E-02	5.1E-02	5.1E-02	5.1E-02	5.1E-02	5.1E-02	5.1E-02	5.1E-02	5.1E-02	5.1E-02	5.1E-02
17	7.25	5.1E-02	5.1E-02	5.1E-02	5.1E-02	5.1E-02	5.1E-02	5.1E-02	5.1E-02	5.1E-02	5.1E-02	5.1E-02	5.1E-02
18	7.75	5.1E-02	5.1E-02	5.1E-02	5.1E-02	5.1E-02	5.1E-02	5.1E-02	5.1E-02	5.1E-02	5.1E-02	5.1E-02	5.1E-02
19	8.25	5.1E-02	5.1E-02	5.1E-02	5.1E-02	5.1E-02	5.1E-02	5.1E-02	5.1E-02	5.1E-02	5.1E-02	5.1E-02	5.1E-02
20	8.75	5.1E-02	5.1E-02	5.1E-02	5.1E-02	5.1E-02	5.1E-02	5.1E-02	5.1E-02	5.1E-02	5.1E-02	5.1E-02	5.1E-02
21	9.25	5.1E-02	5.1E-02	5.1E-02	5.1E-02	5.1E-02	5.1E-02	5.1E-02	5.1E-02	5.1E-02	5.1E-02	5.1E-02	5.1E-02
22	9.75	0.0E+00	0.0E+00	1.4E-12	4.6E-12	1.1E-11	1.3E-11	2.1E-11	6.9E-11	1.2E-10	1.4E-10	1.9E-10	2.3E-10
23	10.3	0.0E+00	0.0E+00	2.0E-13	1.9E-12	6.5E-12	8.1E-12	1.5E-11	5.8E-11	1.0E-10	1.2E-10	1.7E-10	2.1E-10
24	10.8	0.0E+00	0.0E+00	0.0E+00	6.0E-13	3.6E-12	4.8E-12	1.1E-11	4.9E-11	8.9E-11	1.1E-10	1.5E-10	1.9E-10
25	11.3	0.0E+00	0.0E+00	0.0E+00	9.7E-14	1.8E-12	2.7E-12	7.3E-12	4.2E-11	7.8E-11	9.6E-11	1.3E-10	1.7E-10

Primary Species

Al+++ [mol/kg]

Cell	Distance	0 d	1.5 d	26 d	89 d	200 d	235 d	1 y	3 y	5 y	6 y	8 y	10 y
3	0.25	1.0E-09	9.8E-07	8.0E-06	4.1E-06	2.1E-06	1.9E-06	1.7E-06	1.4E-06	1.3E-06	1.3E-06	1.2E-06	1.2E-06
4	0.75	1.0E-09	8.5E-07	7.3E-06	3.6E-06	1.9E-06	1.7E-06	1.5E-06	1.3E-06	1.2E-06	1.2E-06	1.1E-06	1.1E-06
5	1.25	1.0E-09	7.3E-07	6.6E-06	3.2E-06	1.7E-06	1.6E-06	1.4E-06	1.2E-06	1.1E-06	1.1E-06	1.0E-06	9.9E-07
6	1.75	1.0E-09	6.2E-07	5.9E-06	2.7E-06	1.5E-06	1.4E-06	1.3E-06	1.1E-06	1.0E-06	9.9E-07	9.4E-07	9.0E-07
7	2.25	1.0E-09	5.2E-07	5.1E-06	2.2E-06	1.4E-06	1.3E-06	1.2E-06	9.9E-07	9.2E-07	8.9E-07	8.5E-07	8.1E-07
8	2.75	1.0E-09	4.4E-07	4.3E-06	1.8E-06	1.2E-06	1.1E-06	1.0E-06	9.0E-07	8.3E-07	8.0E-07	7.6E-07	7.3E-07
9	3.25	1.0E-09	3.7E-07	3.6E-06	1.5E-06	1.1E-06	1.0E-06	9.3E-07	8.1E-07	7.5E-07	7.2E-07	6.8E-07	6.6E-07
10	3.75	1.0E-09	3.1E-07	3.0E-06	1.3E-06	9.5E-07	9.1E-07	8.3E-07	7.2E-07	6.7E-07	6.5E-07	6.1E-07	5.9E-07
11	4.25	1.0E-09	2.6E-07	2.3E-06	1.1E-06	8.4E-07	8.1E-07	7.5E-07	6.4E-07	5.9E-07	5.8E-07	5.5E-07	5.3E-07
12	4.75	1.0E-09	2.2E-07	1.8E-06	9.2E-07	7.4E-07	7.1E-07	6.6E-07	5.7E-07	5.3E-07	5.1E-07	4.9E-07	4.8E-07
13	5.25	1.0E-09	1.9E-07	1.3E-06	7.8E-07	6.5E-07	6.3E-07	5.9E-07	5.1E-07	4.7E-07	4.6E-07	4.4E-07	4.3E-07
14	5.75	1.0E-09	1.6E-07	9.3E-07	6.6E-07	5.7E-07	5.5E-07	5.2E-07	4.5E-07	4.2E-07	4.1E-07	3.9E-07	3.8E-07
15	6.25	1.0E-09	1.3E-07	7.2E-07	5.7E-07	5.0E-07	4.9E-07	4.6E-07	4.0E-07	3.7E-07	3.7E-07	3.5E-07	3.4E-07
16	6.75	1.0E-09	1.1E-07	5.7E-07	4.9E-07	4.4E-07	4.3E-07	4.0E-07	3.5E-07	3.3E-07	3.3E-07	3.2E-07	3.1E-07
17	7.25	1.0E-09	9.2E-08	4.6E-07	4.2E-07	3.8E-07	3.7E-07	3.6E-07	3.2E-07	3.0E-07	3.0E-07	2.9E-07	2.8E-07
18	7.75	1.0E-09	7.4E-08	3.8E-07	3.6E-07	3.4E-07	3.3E-07	3.2E-07	2.9E-07	2.7E-07	2.7E-07	2.6E-07	2.5E-07
19	8.25	1.0E-09	5.9E-08	3.1E-07	3.1E-07	3.0E-07	2.9E-07	2.8E-07	2.6E-07	2.5E-07	2.5E-07	2.4E-07	2.3E-07
20	8.75	1.0E-09	4.8E-08	2.6E-07	2.8E-07	2.7E-07	2.7E-07	2.6E-07	2.4E-07	2.3E-07	2.3E-07	2.2E-07	2.1E-07
21	9.25	1.0E-09	4.0E-08	2.3E-07	2.5E-07	2.5E-07	2.5E-07	2.5E-07	2.3E-07	2.2E-07	2.2E-07	2.1E-07	2.0E-07
22	9.75	1.0E-09	1.2E-08	1.9E-07	2.3E-07	2.4E-07	2.4E-07	2.4E-07	2.3E-07	2.2E-07	2.1E-07	2.0E-07	2.0E-07
23	10.25	1.0E-09	2.9E-09	1.4E-07	2.0E-07	2.1E-07	2.2E-07	2.3E-07	2.2E-07	2.1E-07	2.1E-07	2.0E-07	1.9E-07
24	10.75	1.0E-09	1.3E-09	1.0E-07	1.7E-07	1.9E-07	2.0E-07	2.2E-07	2.2E-07	2.1E-07	2.1E-07	2.0E-07	1.9E-07
25	11.25	1.0E-09	1.0E-09	7.4E-08	1.4E-07	1.7E-07	1.8E-07	2.1E-07	2.1E-07	2.1E-07	2.0E-07	1.9E-07	1.9E-07

O2(aq) [mol/kg]

Cell	Distance	0 d	1.5 d	26 d	89 d	200 d	235 d	1 y	3 y	5 y	6 y	8 y	10 y
3	0.25	1.0E-09	9.5E-10	9.6E-10	9.9E-10	9.9E-10	1.0E-09	1.0E-09	1.1E-09	1.1E-09	1.1E-09	1.1E-09	1.1E-09
4	0.75	1.0E-09	9.5E-10	9.6E-10	9.8E-10	9.9E-10	1.0E-09	1.0E-09	1.0E-09	1.1E-09	1.1E-09	1.1E-09	1.1E-09
5	1.25	1.0E-09	9.5E-10	9.6E-10	9.8E-10	9.9E-10	9.9E-10	1.0E-09	1.0E-09	1.0E-09	1.1E-09	1.1E-09	1.1E-09
6	1.75	1.0E-09	9.6E-10	9.5E-10	9.8E-10	9.8E-10	9.9E-10	1.0E-09	1.0E-09	1.0E-09	1.0E-09	1.0E-09	1.1E-09
7	2.25	1.0E-09	9.6E-10	9.5E-10	9.7E-10	9.8E-10	9.8E-10	1.0E-09	1.0E-09	1.0E-09	1.0E-09	1.0E-09	1.0E-09
8	2.75	1.0E-09	9.6E-10	9.5E-10	9.7E-10	9.8E-10	9.8E-10	9.9E-10	1.0E-09	1.0E-09	1.0E-09	1.0E-09	1.0E-09
9	3.25	1.0E-09	9.6E-10	9.5E-10	9.7E-10	9.8E-10	9.8E-10	9.9E-10	1.0E-09	1.0E-09	1.0E-09	1.0E-09	1.0E-09
10	3.75	1.0E-09	9.6E-10	9.5E-10	9.7E-10	9.7E-10	9.8E-10	9.8E-10	1.0E-09	1.0E-09	1.0E-09	1.0E-09	1.0E-09
11	4.25	1.0E-09	9.6E-10	9.6E-10	9.7E-10	9.7E-10	9.7E-10	9.8E-10	1.0E-09	1.0E-09	1.0E-09	1.0E-09	1.0E-09
12	4.75	1.0E-09	9.7E-10	9.6E-10	9.7E-10	9.7E-10	9.7E-10	9.8E-10	9.9E-10	1.0E-09	1.0E-09	1.0E-09	1.0E-09
13	5.25	1.0E-09	9.7E-10	9.6E-10	9.7E-10	9.7E-10	9.7E-10	9.7E-10	9.9E-10	1.0E-09	1.0E-09	1.0E-09	1.0E-09
14	5.75	1.0E-09	9.7E-10	9.6E-10	9.7E-10	9.7E-10	9.7E-10	9.7E-10	9.8E-10	9.9E-10	1.0E-09	1.0E-09	1.0E-09
15	6.25	1.0E-09	9.7E-10	9.6E-10	9.7E-10	9.7E-10	9.7E-10	9.7E-10	9.8E-10	9.9E-10	9.9E-10	1.0E-09	1.0E-09
16	6.75	1.0E-09	9.7E-10	9.6E-10	9.6E-10	9.7E-10	9.7E-10	9.6E-10	9.8E-10	9.9E-10	9.9E-10	1.0E-09	1.0E-09
17	7.25	1.0E-09	9.7E-10	9.6E-10	9.6E-10	9.7E-10	9.7E-10	9.6E-10	9.8E-10	9.8E-10	9.9E-10	9.9E-10	1.0E-09
18	7.75	1.0E-09	9.8E-10	9.6E-10	9.6E-10	9.7E-10	9.7E-10	9.6E-10	9.7E-10	9.8E-10	9.9E-10	9.9E-10	1.0E-09
19	8.25	1.0E-09	9.8E-10	9.6E-10	9.6E-10	9.7E-10	9.7E-10	9.6E-10	9.7E-10	9.8E-10	9.8E-10	9.9E-10	1.0E-09
20	8.75	1.0E-09	9.8E-10	9.7E-10	9.6E-10	9.7E-10	9.7E-10	9.6E-10	9.7E-10	9.8E-10	9.8E-10	9.9E-10	9.9E-10
21	9.25	1.0E-09	9.8E-10	9.7E-10	9.6E-10	9.7E-10	9.7E-10	9.6E-10	9.7E-10	9.8E-10	9.8E-10	9.9E-10	9.9E-10
22	9.75	1.0E-09	9.8E-10	9.7E-10	9.7E-10	9.7E-10	9.7E-10	9.6E-10	9.7E-10	9.8E-10	9.8E-10	9.9E-10	9.9E-10
23	10.25	1.0E-09	9.8E-10	9.7E-10	9.7E-10	9.7E-10	9.7E-10	9.6E-10	9.7E-10	9.8E-10	9.8E-10	9.8E-10	9.9E-10
24	10.75	1.0E-09	9.8E-10	9.7E-10	9.7E-10	9.7E-10	9.7E-10	9.6E-10	9.7E-10	9.8E-10	9.8E-10	9.8E-10	9.9E-10
25	11.25	1.0E-09	9.8E-10	9.7E-10	9.7E-10	9.7E-10	9.7E-10	9.6E-10	9.7E-10	9.8E-10	9.8E-10	9.8E-10	9.9E-10

Appendix C: Experimental results

Here are some of the major results that were compared to the model results.

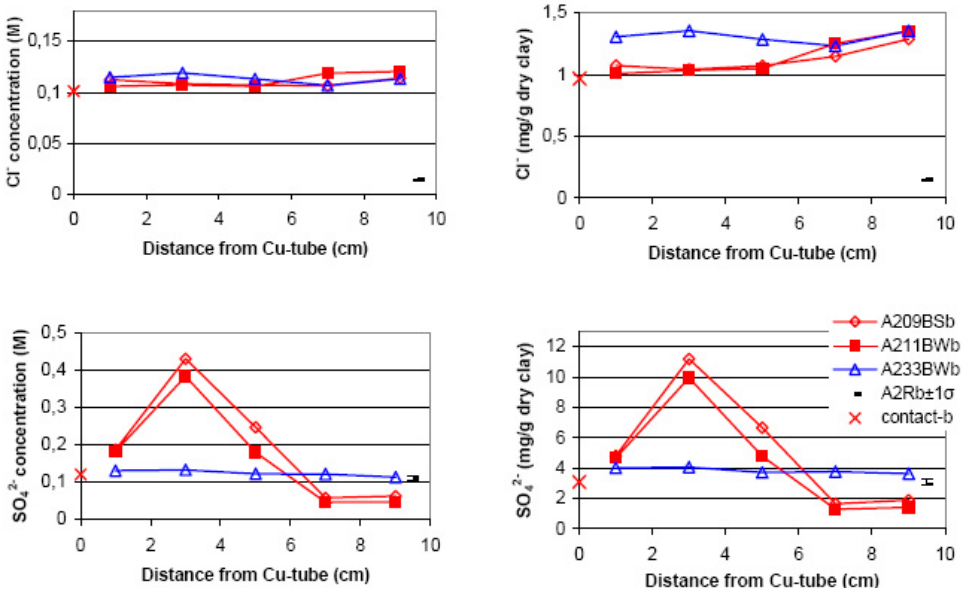

Figure C1. The radial distribution of Cl^- and $SO4^{2-}$ in water extracts of bulk samples from blocks 09, 11 and 33 of the LOT A2 parcel. The concentration of the reference samples (A2Rb) is shown at position 9.5 cm as the mean ±1 standard deviation of five samples [9, p. 66].

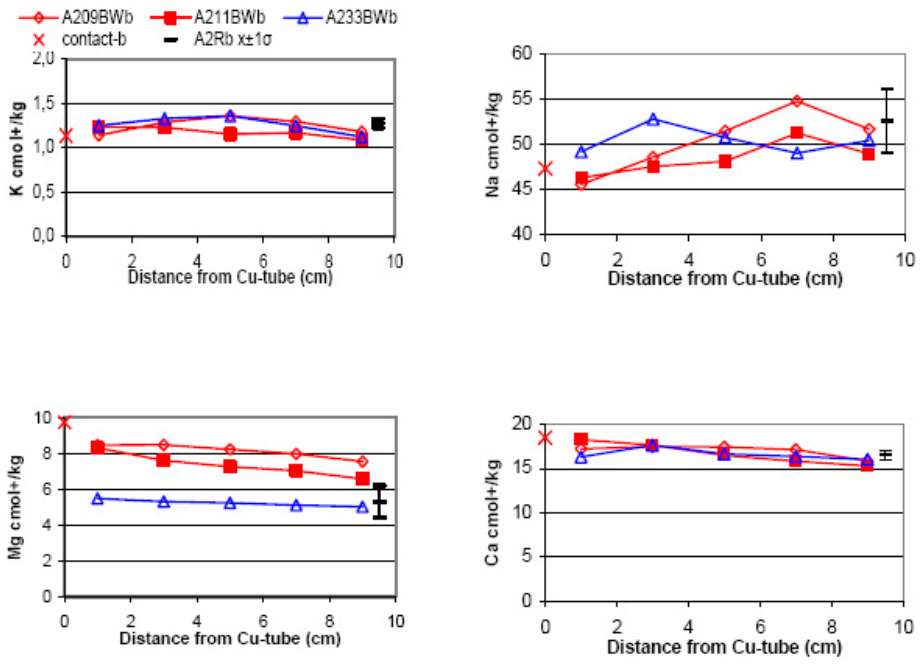

Figure C2. Plots of exchangeable K, Na, Mg and Ca, respectively, versus the distance from the Cu-tube for blocks 09, 11 and 33 of the LOT A2 parcel. Values of the reference samples (A2Rb) are shown at position 9.5 cm as the mean ±1 standard deviation of five samples [9, p. 69].

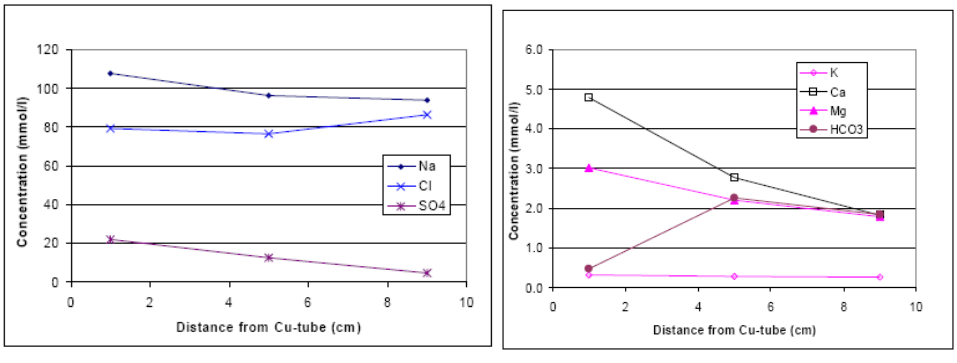

Figure C3. Radial distributions of concentrations of major (left) and minor (right) components in the squeezed porewaters of samples A2 18 B SE [21, p 12].

Series title, number and report code of publication

VTT Publications 721
VTT-PUBS-721

Author(s)
Aku Itälä

Title

Chemical Evolution of Bentonite Buffer in a Final Repository of Spent Nuclear Fuel During the Thermal Phase

Abstract

Finnish spent nuclear fuel disposal is planned to be based on the KBS-3V concept. Within this concept, the role of the bentonite buffer has been considered to be central. The aim was to model the evolution of a final repository during the thermal phase (heat-generating period of spent fuel), when the bentonite is partially saturated at the beginning, and the rock matrix surrounding it is fully saturated. It is essential to study how temperature affects saturation and how both of these affect the chemistry of bentonite.

In order to make the modelling more concrete, an experimental case was adopted: the Long Term Test of Buffer Materials (LOT) A2-parcel test at the Äspö Hard Rock Laboratory (HRL) in Sweden. In the A2-parcel the MX-80 bentonite was exposed to adverse (120–150^{o}C) temperature conditions and high-temperature gradients. The test parcel diameter was smaller than in the KBS-3V concept to speed up the saturation. Different kinds of thermodynamic and kinetic properties of minerals cause a redistribution of phases inside the bentonite. For example, according to laboratory tests, gypsum seems to dissolve and anhydrite seems to precipitate near the heater-bentonite interface. Also incoming groundwater affects the bentonite porewater and its properties. These changes may affect the mechanical properties of bentonite and it has to be clarified if these phenomena have to be taken into account in safety assessment.

The applied model is a coupled thermo-hydro-chemical model, which means that all the mechanical alterations and effects are not considered. The purpose of the model was first to obtain similarity to the results compared to the experiment, and thus, the time frame was limited to 10 years (the LOT A-2 parcel test lasted approximately 6 years). The system is simplified to 1-D in order to reduce the computational work, which is significant mostly due to complex chemical calculations. TOUGH and TOUGHREACT was applied to model the reactive unsaturated transport processes in 1-D and the grid was pitched at uniform intervals. The results may be used to gain knowledge of the bentonite evolution during the thermal phase, and after a good match with experiment the modelling can be continued until the end of the thermal phase for thousands of years.

ISBN
978-951-38-7363-9 (soft back ed.)
978-951-38-7364-6 (URL: http://www.vtt.fi/publications/index.jsp)

Series title and ISSN	Project number
VTT Publications 1235-0621 (soft back ed.) 1455-0849 (URL: http://www.vtt.fi/publications/index.jsp)	32810

Date	Language	Pages
December 2009	English, Finnish abstr.	78 p. + app. 16 p.

Name of project	Commissioned by
PUSKURI/KYT2010	KYT

Keywords	Publisher
THC, temperature dependence, modelling, cation exchange, heat formation, heat transport, bentonite, porewater, montmorillonite	VTT Technical Research Centre of Finland P. O. Box 1000, FI-02044 VTT, Finland Phone internat. +358 20 722 4520 Fax +358 20 722 4374

Julkaisun sarja, numero ja raporttikoodi

VTT Publications 721
VTT-PUBS-721

Tekijä(t)
Aku Itälä

Nimeke

Bentoniittipuskurin kemiallinen evoluutio käytetyn ydinjätteen loppusijoitustilassa termisen vaiheen aikana

Tiivistelmä

Monet maat Euroopassa, Suomi mukaan lukien, suunnittelevat bentoniitin käyttämistä puskurimateriaalina korkea-aktiivisten ydinjätteiden loppusijoitustilassa. Suomalaisen käytetyn polttoaineen loppusijoituksen on suunniteltu perustuvan KBS-3V-konseptiin. Tässä konseptissa bentoniittipuskurin rooli on keskeinen. Tämän työn tarkoituksena oli mallintaa loppusijoitustilaa termisen vaiheen aikana (polttoaineen lämpöä tuottava ajanjakso), jolloin bentoniitti on aluksi osittain kyllästynyt ja kallio sen ympärillä täysin kyllästynyt. On tärkeää tutkia, miten termiset, hydrologiset, mekaaniset ja kemialliset ilmiöt ja prosessit loppusijoitustilassa voivat muokata bentoniitin kemiallisia ja mekaanisia ominaisuuksia. Bentoniitin pitkäaikaiskestävyyden tutkiminen perustuu mallinnukseen, koska kokeellinen tutkimus veisi tuhansia vuosia.

Jotta mallinnuksesta saatiin luotettavampaa, käytettiin vertailupohjana LOT-koetta. Äspön kalliolaboratoriossa Ruotsissa on menossa pitkäaikainen puskurimateriaalin testaus, niin sanottu LOT-koe korkea-aktiivisen ydinjätteen loppusijoitusta varten. Tässä työssä keskitytään yhteen näistä kokeen osista, A2-sylinterikokeeseen. A2-kokeessa suhteellisen pienet testisylinterit altistetaan kohonneelle lämpötilalle. Suunniteltu maksimilämpötila loppusijoitustilassa on 90 ^{o}C, mutta A2-kokeessa se asetettiin 120–150 asteeseen. Noin 5–6 vuoden altistamisen jälkeen testisylinteri nostettiin ja paloiteltiin osiin tutkimuksia varten. Viiden vuoden jakso näissä olosuhteissa kattaa merkittävän osan koko termisestä kuormasta KBS-3V-loppusijoitustilassa.

Malli luotiin käyttämällä PetraSim 4.1.0219 -käyttöliittymää TOUGH2- ja TOUGHREACT-ohjelmille. Sovellettu malli on termo-hydro-kemiallinen (THC) kytketty malli, mikä tarkoittaa sitä, että useat mekaaniset muutokset ja vaikutukset on jätetty huomiotta. Mallin tarkoituksena oli saada aluksi tulokset vastaamaan suhteellisen hyvin kokeellisia tuloksia, joten laskenta-aika rajoitettiin kymmeneen vuoteen. Malli on yksidimensioinen.

ISBN
978-951-38-7363-9 (nid.)
978-951-38-7364-6 (URL: http://www.vtt.fi/publications/index.jsp)

Avainnimeke ja ISSN	Projektinumero
VTT Publications 1235-0621 (nid.) 1455-0849 (URL: http://www.vtt.fi/publications/index.jsp)	32810

Julkaisuaika	Kieli	Sivuja
Joulukuu 2009	Englanti, suom. tiiv.	78 s. + liitt. 16 s.

Projektin nimi	Toimeksiantaja(t)
PUSKURI/KYT2010	KYT

Avainsanat	Julkaisija
THC, temperature dependence, modelling, cation exchange, heat formation, heat transport, bentonite, porewater, montmorillonite	VTT PL 1000, 02044 VTT Puh. 020 722 4520 Faksi 020 722 4374

Finnish spent nuclear fuel disposal is planned to be based on the KBS-3V concept. Within this concept, the role of the bentonite buffer has been considered to be central. The aim was to model the evolution of a final reposi-tory during the thermal phase (heat-generating period of spent fuel), when the bentonite is partially saturated at the beginning, and the rock matrix surrounding it is fully saturated. It is essential to study how temperature af-fects saturation and how both of these affect the chemistry of bentonite.

In order to make the modelling more concrete, an experimental case was adopted: the Long Term Test of Buffer Materials (LOT) A2-parcel test at the Äspö Hard Rock Laboratory (HRL) in Sweden. In the A2-parcel the MX-80 bentonite was exposed to adverse (120–150 °C) temperature conditions and high-temperature gradients. The test parcel diameter was smaller than in the KBS-3V concept to speed up the saturation. Different kinds of ther-modynamic and kinetic properties of minerals cause a redistribution of phases inside the bentonite. For example, according to laboratory tests, gypsum seems to dissolve and anhydrite seems to precipitate near the heater-bentonite interface. Also incoming groundwater affects the bentonite porewater and its properties. These changes may affect the mechanical properties of bentonite and it has to be clarified if these phenomena have to be taken into account in safety assessment. This test case was modelled in a simplified 1D geometry in order to reduce the computational work.

ISBN 978-951-38-7363-9 (soft back ed.)
ISSN 1235-0621 (soft back ed.)

ISBN 978-951-38-7364-6 (URL: http://www.vtt.fi/publications/index.jsp)
ISSN 1455-0849 (URL: http://www.vtt.fi/publications/index.jsp)